Delft University of Technology
Faculty of Civil Engineering
Section Fluid Mechanics

The influence of Mooring Lines on the Damping of Low Frequency Motions of Moored Offshore Structures

by :

René M. Raaijmakers

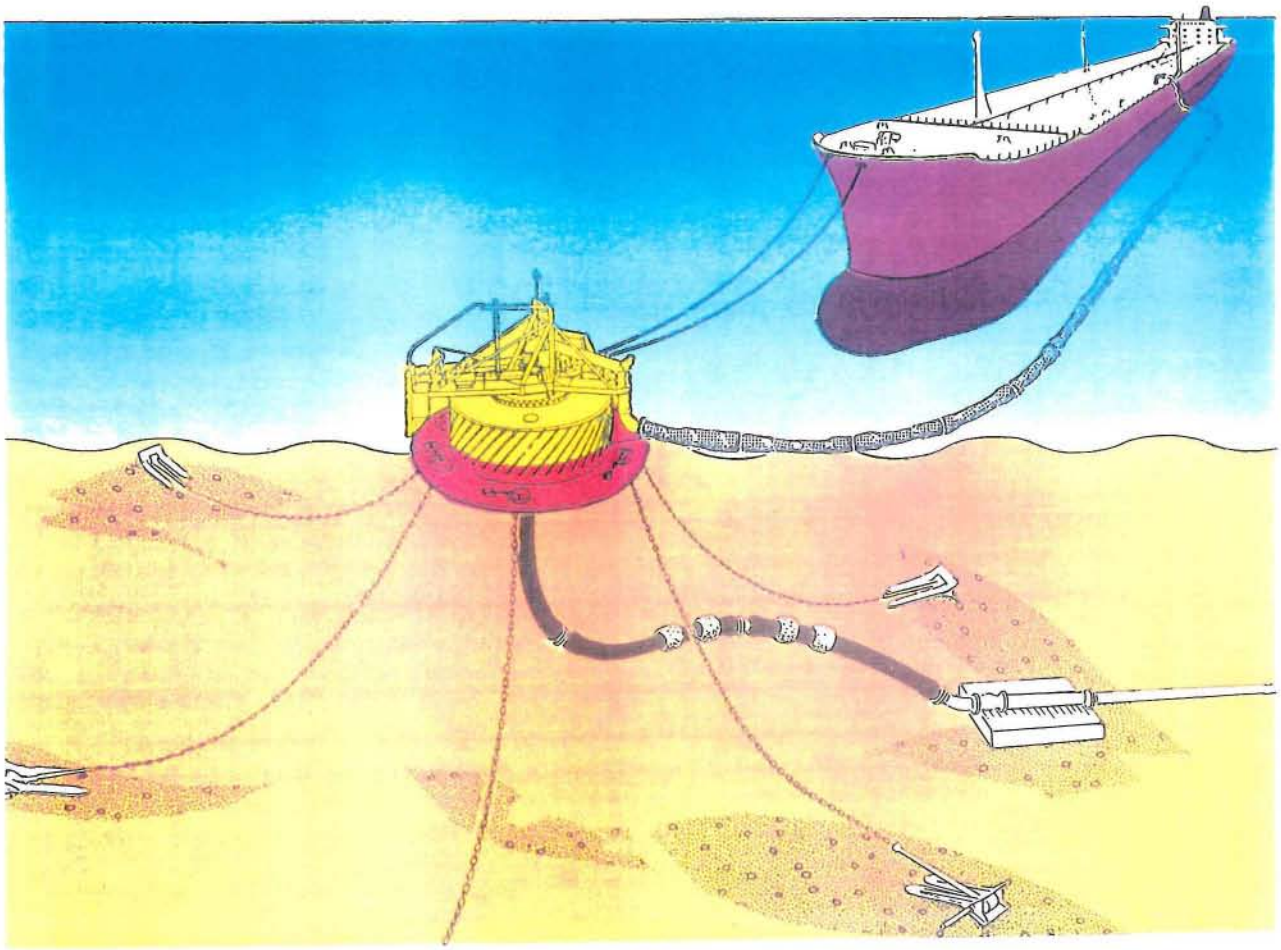

December, 1995

The influence of Mooring Lines on the Damping of Low Frequency Motions of Moored Offshore Structures

by :

René M. Raaijmakers

Preface

The study *"The influence of mooring lines on the damping of the low frequency motions of moored offshore structures"* presented in this report forms the major part of the author's graduation programme at the Faculty of Civil Engineering, Delft University of Technology.

Both the disciplines of fluid mechanics and offshore technology are involved in this study. This combination was the reason why I chose to do this study. I enjoyed designing and executing the laboratory tests very much, even though the scaling analysis seemed difficult. It is most likely that I will not get such an experience again in the near future.

I hope that the investigations on *mooring line damping* will be continued at the faculty of Civil Engineering. A number of interesting and relevant problems still have to be studied. The magnitude and difficulty of the proposed investigations seem ideal for Civil Engineering graduation programmes.

I specifically would like to thank the following people for their support and guidance during the last year(s) :

The graduation committee, for their support, recommendations and expertise during the completion of the performed investigation;
W.W. Massie, for his extraordinary enthusiasm as a teacher and for exciting my curiosity in offshore technology during the last two years;
The staff of the Ship Hydromechanics Laboratory, Delft, for their enthusiasm, skilful help during the execution of the experiment and their delicious ice-creams when things got hot this summer;
My parents, for their support to make this happen;
My dear friend, Chimwemwe, for her patience and unconditional support;

René Raaijmakers.

Amsterdam, 15 December 1995

Graduation Committee:

Prof.dr.ir. J.A. Battjes	(President)
Prof.dr.ir. J.H. Vugts	
Prof.dr.ir. J.A. Pinkster	
W.W. Massie, Msc, PE	(Supervisor)

Abstract

For years it has been customary, in the prediction the Low Frequency (LF) dynamic behaviour of moored offshore structures, to assume that the mooring system only influences the restoring force characteristics. The contribution of the mooring system to the total system damping was neglected. Research and model tests in recent years have shown that mooring line damping can be an important contributor to the total system damping of the LF-surge or sway motions of moored offshore structures and vessels. A number of tests even showed that mooring line damping can be the major part of the total system damping.

In 1986, Huse proposed the following theory. Drag forces normal to the mooring line are assumed to be the main source of energy dissipation due to the motion of the mooring lines through the water. A small offset of the top end of the line (fairlead) can result in large transverse displacements along the mooring line. This is the reason why in some cases considerable drag forces, and thus energy dissipation, can be expected. Given the catenary configuration of the mooring line it is possible to calculate the energy dissipated by the line in the case of a LF-sinusoidal surge motion of the top end of the line. A simplified calculation is possible on the assumption of a quasi-static response, implying that the configuration of the mooring line stays catenary at all times during the oscillation.

In the present study, an analytical model by Huse to calculate the dissipated energy per cycle has been derived. The verification of this model is performed by means of experiments. The experiments have been executed in the towing tank of the Ships Hydromechanical Laboratory, Delft, were the top end of a modelled chain line was forced into a horizontal, LF-sinusoidal oscillation. A wide spectrum of catenary configurations of a single mooring line were tested for a number of top end oscillations at different frequencies. During each test run, the in-line tension fluctuations were measured. By integrating the scalar product of the measured in-line tension with the instantaneous top end velocity over one full period of oscillation, the total dissipated energy per cycle is obtained.

The hydrodynamic model has been verified by comparison with the measured energy dissipations. Two methods for the numerical evaluation of this model are executed. The results of a graphical calculation method, developed by Huse in 1988, and the results of an analytical version of the current investigation, have been verified. The results of Huse's graphs did not agree with the verification test, while the results of the current investigation, which were based on a direct numerical evaluation of Huse's theory, corresponded very well. The source of the apparent errors in the graphical results of Huse are not yet known.

The presented hydrodynamic model for the calculation of the energy dissipation during one surge cycle, due to drag forces normal to the mooring lines, describes the measured dissipated energy very well. This model is especially considered a useful tool in the description of LF-dynamics of moored floating structures, when the WF-motions are very small compared to the LF-motions of the structure. We can conclude that the influence of mooring line damping for moored structures in low sea-states can be analysed very well with the presented model.

Table of Contents

Preface 1

Abstract 2

List of Symbols Used 6

1. Introduction 8

2 Dynamic Behaviour of Moored Floating Structures 10
2.1 Introduction 10
2.2 Dynamics of Moored Floating Structures 11
2.2.1 Types of Mooring Systems Considered 11
2.2.2 Dynamic LF-Model for Moored Floating Structures 12
2.3 Environmental Loads 14
2.3.1 Wind 14
2.3.2 Current 14
2.3.3 Waves 15
2.4 Restoring Force Characteristics of the Mooring System 15
2.5. Damping Mechanisms 17
2.6 Added Mass 17
2.7 Dynamic LF-Model : Equation of Motion 18

3 Mooring Line Damping in the Dynamic LF-model 19
3.1 Introduction 19
3.2 Damping Coefficient in Dynamic LF-model 20
3.2.1 Introduction 20
3.2.2 Wave Drift Damping 20
3.2.3 Current and Viscous Flow Damping 20
3.2.4 Mooring Line Damping 21
3.2.5 Wind Damping 21
3.3 Mooring Line Damping: the Hypothesis of Huse 22
3.4 Problem Definition of Investigation 23
3.5 Objective of Investigation 23

4 Mathematical Description of the Model 24
4.1 Introduction 24
4.2 Basic Catenary Equations 24
4.2.1 General Catenary Equation 24
4.2.2 Slack Lines 25
4.3 Model for Energy Dissipation from Mooring Lines 27
4.3.1 Analytical Approach 27
4.3.2 Remarks 30
4.4 Analytical Expression for the Energy Dissipation in Experiment 31
4.4.1 Introduction 31
4.4.2. Calculation of the Transverse Motion Amplitude 31
4.5. Numerical Calculation of Energy Dissipation 32

4.5.1. Introduction 32
4.5.2. Graphical Method by Huse 32
4.5.3. Numerical calculations of Current Investigation 35
4.5.4. Comparison Numerical Results of Both Methods 37
4.6. Theoretical Calculation of the Linear Damping Coefficient 38

5. Experiment Design and Scaling Analysis **39**
5.1. Introduction 39
5.2. Energy Dissipation in Experiments 40
5.3. Experiment Design 41
5.3.1. Introduction 41
5.3.2. Test Facility 41
5.3.3. Choice of the Mooring Line in Experiment 42
5.3.4. Experiment description 42
5.3.5. Model Set Up 44
5.4. Scaling analysis 45
5.4.1. General equations of motion of the mooring line 45
5.4.3. Dimensionless numbers 46
5.4.4. The scale formula in the model 47
5.4.5. Characteristic Prototype Parameter Values 47
5.4.6. Parameter scale-range and values proposed for the model 48
5.4.7. Summary 48
5.5. Influence of inertia forces in the model 49
5.6. Actual Experiment set up 50
5.6.1. Dimensions of chain legs in set up 50
5.6.3. Installed equipment 51
5.6.4. Calibration of dynamometers 51
5.6.5. Determination of top end positions 52
5.6.6. Necessary Daily Routines 53
5.7. Testing programme 53
5.7.1. Introduction 53
5.7.2. Choice of Oscillation Frequencies and Amplitudes 54
5.7.3. Influence of Waves 54

6. Experimental Results **55**
6.1. Introduction 55
6.2. Static Load-Displacement Test 56
6.3. Results of Oscillation Experiments in Still Water 58
6.3.1. Recorded Data Signals 58
6.3.2. Hysteresis of Dynamic Load-Displacement Diagram 60
6.3.3. Calculation of Dissipated Energy 61
6.3.4. Measured Energy Dissipation 62
6.4. Influence of waves 64
6.5. Calculation of Energy Dissipation in 'Dry-Tests' 65
6.6. General Observations during Experiment 66
6.6.1. Vortex induced vibrations 66
6.6.2. Chain damage 66
6.6.3. Damage of attachment hook 67
6.6.4. Galloping 67

Chapter 7. Verification of the Model **68**
7.1. Introduction 68
7.2. Test for the Verification of the Model 68
7.2.1. Estimation of (DC_D)-value for Chain 68
7.2.2. Verification Test 69
7.3. Results According to the Calculations by Huse 71
7.4. Results of Calculations in Current Investigation 73
7.5. Conclusion 74

8. Conclusions and Recommendations **75**
8.1. Conclusions 75
8.2. Recommendations for Future Investigations 76

Appendix A. The Logbook of Executed Experiments **77**

Appendix B. Experiment Results **84**
B.1. Results for all configurations at amplitude 0.06 m 84
B.2. Results for all configurations at amplitude 0.10 m 85
B.3. Results for all configurations at amplitude 0.14 m 86
B.4. Results for Position 5 at all tested amplitudes 87

Appendix C. Computer Program **88**
C.1. Turbo-Pascal Source Code 88
C.2. Input File 92
C.3. Output File 94

Literature **95**

List of Symbols Used

Symbol	*Description*
a	Added mass
B	Damping coefficient
c	Ratio of horizontal pretension and submerged weight
C	Linear spring constant in mean offset position
C_A	Added mass coefficient
C_D	Drag coefficient
D	Diameter which C_D refers to
EA	Axial stiffness of line
E_{diss}	Energy Dissipation
F, F(t)	Force as function of time
F_0	Force magnitude
F_D	Drag force
F_{in},F_{it}	Inertia force (normal and tangential)
g	Acceleration of gravity (9.81 m/s^2)
h	Top end (fairlead) elevation in reference position
H_w	Waterdepth
I	Integral
K	Linear spring constant
m	Mass of the line per unit length
M	Total mass of the structure
n	Scale
n	Number of periods (integer)
p	Submerged weight per unit length
s	Length co-ordinate along the line
S	Total line length
S	Surface below load-displacement diagram
t	Time
T	Period of oscillation
T,T_t	In-line tension
T_0	Horizontal top end pretension
T_x	Horizontal in-line tension component
T_z	Vertical in-line tension component
TE	Period of top end oscillation
v,v_x	Measured, instantaneous, top end velocity
X,Z	Global co-ordinate
x',z'	Local co-ordinate
x_0	Lift off point
xlo	Lift off point in lowest position during oscillation
xuo	Lift off point in ultimate position during oscillation
Xmax	X-co-ordinate of top end in reference position
Zmax	Z-co-ordinate of top end in reference position

Symbol	*Description*
β	Ratio between magnitudes of drag force and inertia force
ΔL	Portion of the line laying on the seabed
Δs	Line element
Δt	Sample time interval
$\Delta z(x)$	Difference in peak to peak elevations of the line during oscillation
ϕ	Tangent angle along the line
η	Transverse displacement of the line
η_0	Transverse displacement amplitude
λ	Factor for equivalent diameter
μ	Ratio between magnitude of drag force and submerged weight
μ	Friction coefficient of line to seabed
π_1, π_2, π_3	Non-dimensional numbers in graphical method of Huse
ρ_s	Density of steel
ρ_w	Density of water
ω	Angular frequency
ω_n	Natural frequency
ξ, $\xi(t)$	(LF)-surge excursion
ξ_0	Surge amplitude

1. Introduction

Moored offshore structures show pronounced low frequency oscillatory motions around a mean offset. The large mass of the floating structure and the relatively small effective stiffness of the mooring system provide low natural frequencies, while the effective relative damping is typically well below critical damping. Therefore, environmental, low frequency excitation forces can give rise to resonant oscillations with considerable amplitudes. Motions at resonance are highly determined by the system damping.

A good prediction of the low frequency (LF)-resonant motions of a floating offshore structure, and therefore of the systems damping, is of great importance for structural engineers. Peak offsets and velocities of the structure determine maximum loading conditions for the risers, the mooring system and other important engineering aspects of the structure. In the preliminary design stages, a simple LF-dynamic model is used to analyse the LF-motions of the structure, based on a damped spring-mass system with one degree of freedom.

The current investigation focuses on the influence of the mooring system on the damping of the LF-motions of such a structure. Due to the motion of the structure, the mooring lines are forced through the water. The hydrodynamic forces induced by the motion of the structure cause energy dissipation and, thus, a damping of the LF-motion of the structure.

In 1986, Huse (Marintek, Trondheim,N) introduced a model on *mooring line damping* to calculate the energy dissipation due to the motion of the mooring lines through the water. The objective of the current study is the verification of this model. Laboratory experiments are executed for this purpose. In the following, a description is given of the contents of this report. This also reflects the approach to the problem.

A complete overview of all parameters involved in LF-dynamic models for a description of low frequency motions of moored floating structures is given. The purpose is to provide the necessary background for the understanding and positioning of the problem of mooring line damping. This is the main topic of chapter 2.

A typical feature of moored structures is their LF-oscillatory resonant motions around a mean offset. Thus, knowledge of the damping parameters is crucial in the understanding and the description of the LF-motions. The total system damping consists of several contributing mechanisms. The influence of mooring lines to the total system damping is the subject of the current investigation. Chapter 3 gives the overview of damping mechanisms involved and treats the hypothesis of Huse on mooring line damping.

Chapter 4 presents an analytical formulation of the hydrodynamic model by Huse (1986). This model provides a tool for the determination of the total energy dissipation of a full period of oscillation. Two calculation methods are introduced for the numerical evaluation of this model. A general linearisation method for the determination of a linear damping coefficient is given.

The experiment design is treated in chapter 5, in which the scaling analysis is a very important issue. A program has been made for tests for a wide range of prototype mooring line configurations. Therefore ranges are obtained of possible values for each parameter. These parameters-range are all scaled down to experiment parameter ranges. Finally, the test programme is given.

The results of the executed tests are the subject of chapter 6. Of all executed tests, the amount of dissipated energy is determined. The results are used for the verification of the model. Tests have been carried out in still water and in waves. The latter tests were merely performed in order to obtain a qualitative impression of the influence of waves.

In chapter 7, the actual verification of the model takes place. The experimental results are compared with the numerical calculation results from the model. The calculations of Huse (1988) are compared with the calculations of the author. Finally, all conclusions are presented in chapter 8.

2 Dynamic Behaviour of Moored Floating Structures

2.1 Introduction

This chapter provides an overview of the dynamic processes which are involved in the Low-Frequency (LF) motions of moored floating offshore structures. A simple model will be presented which is frequently used to perform preliminary design calculations and to gain insight in the characteristics of the structure considered.

Problems concerning the dynamic behaviour of structures are difficult. The large number of parameters involved and the complex nature of the problems (non-linear material behaviour, wave-loading, etc.) usually demand a thorough computer analysis. In some cases, however, it is possible to use a fairly simple model to describe the global behaviour of a moored floating structure.

Dynamics of Structures may be divided into two classes. The first class is referred to as structural dynamics, which concerns the dynamics of deformable bodies. In this case, the body hardly moves from its reference position. The second class is the dynamics of rigid bodies, to which the so called classical mechanics apply. The latter is typically of use for floating structures and vessels. The deformations of the structure are negligible compared to the motions of the body as a whole. Combinations of the two classes are, of course, also possible.

In principle, there are two different approaches to dynamic problems: the frequency-domain analysis and the time-domain analysis. The frequency-domain analysis is often used to predict the long term responses of floating structures. Random wave input can be used through spectral formulations. The main limitation of this method is that it is only feasible for linearised problems. The advantage of this analysis, however, is the availability of simpler computational techniques than for time-domain calculations and its results are easier to interpret. For these reasons, the frequency domain analysis is often preferred in preliminary design stages.

Time-domain analysis allows the incorporation of non-linearities. The main disadvantage is the considerable computer-processing time needed and increased complexity of the produced results, which make this method less interesting for preliminary design. Since all problems concerning hydrodynamics are practically 'loaded' with empirical coefficients, the time-domain analysis does not automatically guarantee better results than the frequency-domain analysis

In the following, the emphasis is on the dynamics of floating structures for LF-motions. In paragraph 2.2, the types of mooring systems considered in this report and a low frequency dynamic model are described. The parameters involved in this LF-model will be explained in the following paragraphs. The forces responsible for the low frequency excitation are the topic of paragraph 2.3. The characteristics of the mooring structure considered will be discussed in paragraph 2.4. The damping mechanisms are presented in paragraph 2.5. Finally, an explanation will be given of the so called 'added mass' in paragraph 2.6.

2.2 Dynamics of Moored Floating Structures

The following overview applies to various types of structures or vessels. The emphasis is on the mooring system used and its effects on the global, low frequency, dynamic behaviour of the whole system.

2.2.1 Types of Mooring Systems Considered

Over the years, there has been a tendency to operate under conditions of increasing waterdepths. In many cases, the use of fixed structures was no longer feasible. Thus, a logical step was to shift the attention to compliant and floating units for drilling, production, storage and off-loading. This again led to several new forms of moored structures, like for instance : the tension leg platforms (TLP), articulated towers, semi-submersibles and the (re-) use of tankers. These structures have in common that they are connected to the seafloor ('moored') by some flexible construction.

In the literature, one can find a variety of mooring systems, which can be broadly divided into three categories: dynamic positioning, multi point mooring systems (MPMs) and single point mooring systems (SPMs) [Ghosh, 1992]. Dynamic positioning and rigid anchor leg mooring systems, which form a part of MPMs and SPMs, are not considered in this report.

The MPM systems are made up of several mooring lines, connected at several points to floating structure. Examples are the TLPs and spread mooring systems. The figure below gives an impression of two types of MPMs.

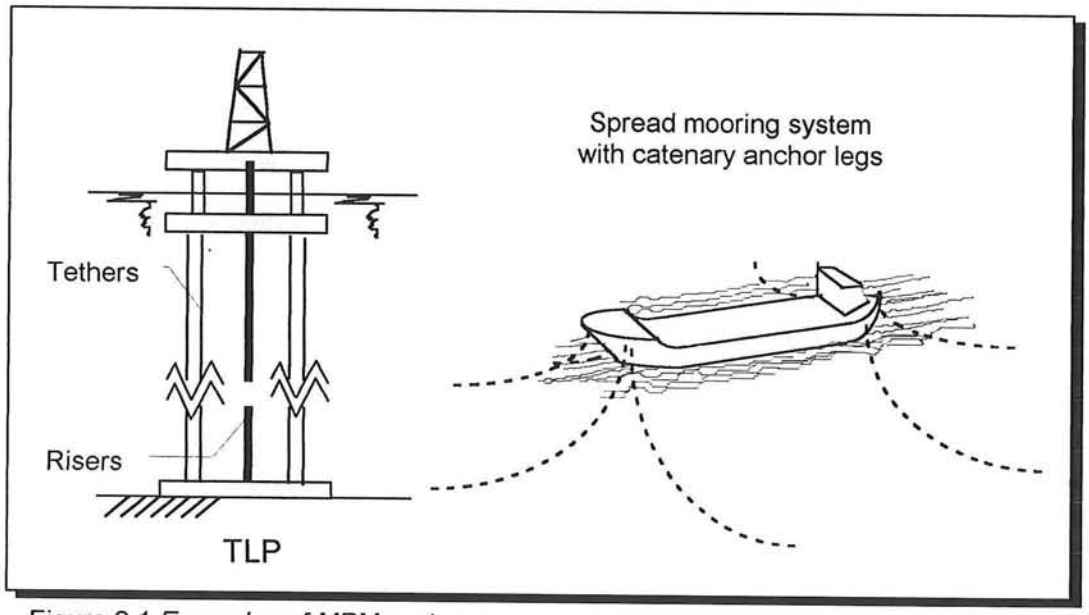

Figure 2.1 *Examples of MPM systems.*

A trend of the last ten years is clearly the use of Single Point Mooring (SPM) systems. The concept is a wheatervaning floating structure connected by some means to the seafloor. It is called a single point mooring system, since all the mooring attachments converge to a single area. The most commonly known SPMs are: catenary anchor leg mooring (CALM), single anchor leg mooring (SALM) and turret mooring. Many more

combinations and systems are developed and have been patented. It is beyond the scope of this introductory chapter to describe them all.

The SALM type of structure involves a rigid, articulated tower, and will not be discussed here. In the CALM type of structure, the vessel is moored to a buoy by means of a flexible or rigid connection and is allowed to *weathervane*. The buoy itself is anchored to the seafloor by a number of catenary mooring lines.

The turret type of mooring is also a weathervaning type of mooring system. The turnability of the system is provided by the placing of a swivel structure in the turret- or buoy-system. The location of the turret can be either internal (near the bow of the ship) or external (fixed in front of the bow). The mooring legs are attached to a chain table, which does not rotate with the ship. In the figure below examples are given.

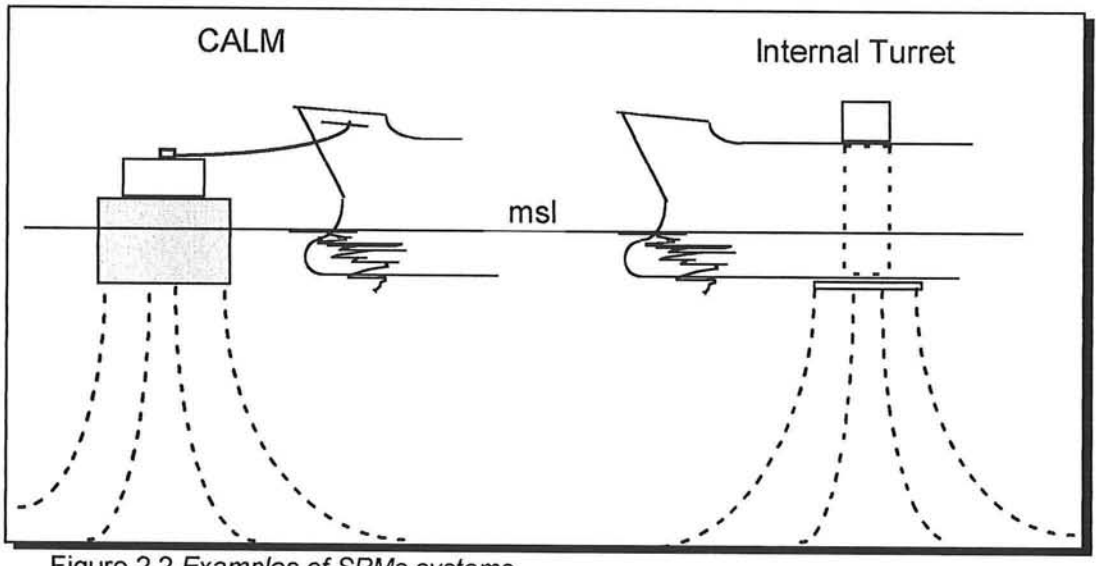

Figure 2.2 *Examples of SPMs systems*

In conclusion, we can say that we are looking at MPM and SPM systems containing anchor legs with catenary configurations. The vertical tethers of the TLPs can be considered as an ultimate limit-case of catenary configurations. In practical applications, the anchor legs are often made up of different sections of chain or steel wire, with clump weights or buoys along the lines. It will be clear that many combinations can be designed, all having their specific characteristics.

Our main interest goes to the determination of the LF-motions of the moored structure or vessel. The next paragraph gives a description of a dynamic model to analyse the LF-behaviour of the moored structure.

2.2.2 Dynamic LF-Model for Moored Floating Structures

Moored floating offshore structures are connected to the seafloor by some mechanical means. When describing the dynamics of these structures, the main interest goes out to the displacement of the structure as a whole. The floating structure is described as a *rigid body*, where the reactions of the seafloor connection (rigid arm, anchor lines, mooring buoy, etc.) are introduced as external forces acting on the body. The flexibility of the seafloor-connection should be accounted for.

In general, a floating structure has six independent degrees of freedom, as drawn in figure 2.3.

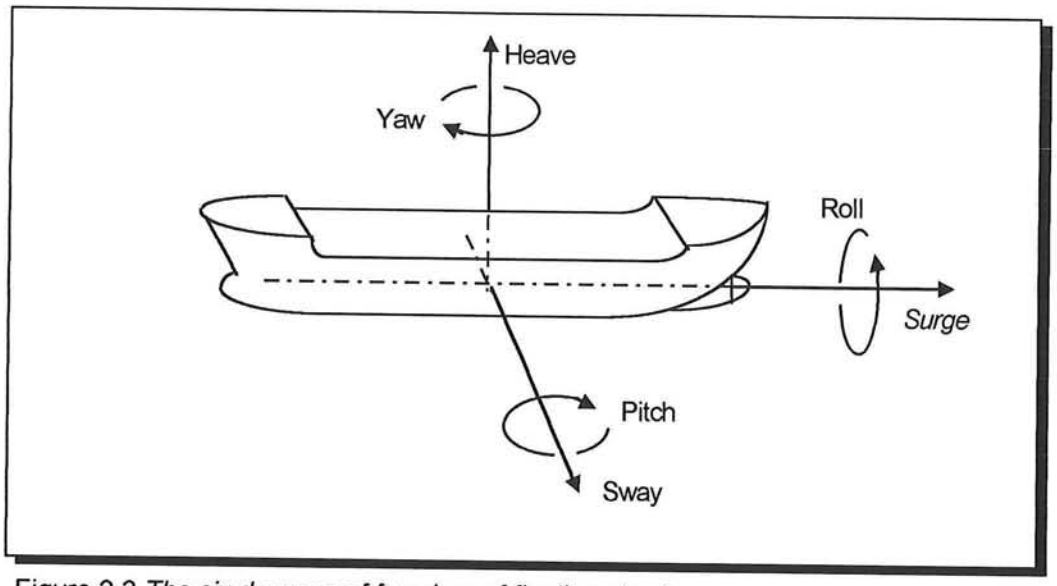

Figure 2.3 *The six degrees of freedom of floating structures*

The moored structure, exposed to irregular seas performs small amplitude Wave Frequency (WF) motions, combined with relatively large amplitude LF motions, around a mean displacement. The MPMs and SPMs are exposed to LF-excitation forces, which act in the horizontal plane, resulting in LF surge, sway and yaw motions. This is a typical feature for these constructions.

These large amplitude motions are characterised by low damping and a frequency which corresponds to the mooring system's natural frequency. Motions at resonance are dominated by the effective damping of the system. The LF-yaw motions are not as important for the dynamic analysis as the LF-surge and sway motions. These have a major effect on the design-requirements for the complete mooring system and the sub-sea structure (consisting of risers, spider structure, etc.).

In order to predict the dynamic behaviour of the moored structure, a simulation technique is presented for the co-linear case in which current, wind and waves all come from the same direction.

The equation of Low Frequent surge motion reads:

$$\boxed{(M+a)\ddot{\xi}+B\dot{\xi}=F_{wind}+F_{current}+F_{waves}-F_{mooring}} \qquad (2.1)$$

in which:

M = Total mass of the structure
a = Added mass of the structure
B = Total linear damping coefficient
ξ = Low frequency surge excursion of the structure
F_i = Forces due to wind, current, waves and mooring system

The mooring force, which is often represented as a spring force, in equation (2.1) is non-linear and is determined from the static load displacement diagram. The mass, added mass and damping values are estimated, either from approximate calculation methods or by actual model decay tests. In general, the moored systems are lightly damped [Wichers & van Sluijs, 1979]. The forces are calculated and substituted into the equation of LF-motion. In the following paragraphs the terms of equation (2.1) will be discussed further.

2.3 Environmental Loads

This paragraph gives a description of the mean and the low-frequency forces on the moored structure. These forces were introduced in equation 2.1.

2.3.1 Wind

The forces on the structure-part above sealevel are mainly determined by the wind velocity. Since the influence of the wind force is usually small compared to wave and current forces, a simple model is often used to describe the velocity profile above the sea-level.

The wind velocity is modelled as a constant time-independent velocity, varying with elevation above MSL (mean sea level) according to a power law, plus a randomly fluctuating component in the horizontal plane. The constant part of the wind velocity leads to a steady force, partly determining the mean surge-offset of the structure.

The fluctuating part of the wind velocity is described by means of a so called wind gust spectrum. The periods of this fluctuating part of the wind velocity range from a few seconds up to several minutes, with most energy concentrated around a minute. For moored floating structures, with a natural frequencies of around 100s, these wind gust forces may be an important source of excitation, resulting in resonant low frequency motions.

2.3.2 Current

Currents are created by astronomical forces, Coriolis force, density gradients and heat patterns in the oceans and wind stresses on the watersurface. The ocean currents show a fixed pattern which are dominated by geostrophic and astronomical effects. The currents in seas and nearshores are much more determined by local boundary conditions like water depth, local wind fields, density and temperature differences.

The resulting current force can be described by a model like the wind force. The main difference is that the current fluctuations are of much longer periods than the natural period of the moored structure. Therefore, the system responds quasi-statically only in a mean offset of the structure.

The flow field is considered to be uniform in the horizontal plane surrounding an offshore structure, while the vertical velocity distribution is determined like the wind velocity.

2.3.3 *Waves*

The influence of waves is by far the dominant source of excitation of the moored structure, and offshore structures in general. Surface waves on water can be classified by means of a (spectral) function of the wave frequency. For offshore structures, the gravity waves are considered to be dominant, having periods between 1 s and 30 s. Intragravity waves (seiches and groundswell) also have an influence, but only on catenary moored structures having very low natural frequencies.

The low frequency oscillations are generated by the so called second-order wave forces, resulting from the gravity waves (periods 1s to 30s) [Chakrabarti, 1987]. The low frequency forces appear due to the difference in the neighbouring frequencies in the irregular waves, and are called second order wave forces or wave drift forces. Several calculation methods have been developed to calculate these forces for a variety of floating structures and are considered beyond the scope of this report.

2.4 Restoring Force Characteristics of the Mooring System

The restoring force in the dynamic LF-model is provided by the mooring system. A typical feature of a catenary mooring system is its non-linear load-displacement relation.

The restoring force characteristics are determined by the chosen mooring pattern, the pretensions of the lines, the line parameters and the loading direction. The figure 2.4 below gives an example of a load-displacement curve of a SPMs. A model for the approximation of a *linearised spring constant* in the dynamic LF-model and the determination of the natural frequency will be presented in the following.

The dynamic LF-model is a damped spring-mass system with one degree of freedom. The displacement of the structure is denoted as ξ. The ξ-axis will be chosen such that it coincides with the loading-direction. For ξ=0, the whole system is in the neutral position.

In order to determine the natural frequency of the SPMs, we look at the undamped spring-mass system, in which the spring force is a non-linear function $f(\xi)=\xi.k(\xi)$. Since the damping is assumed to be absent, there is no phase-difference.

Assuming harmonic excitation the equation of motion reads:

$$M\ddot{\xi} + f(\xi) = F_0 \cos(\omega t) \qquad (2.2)$$

Equation 2.2 is also referred to as the *Duffin*-equation.

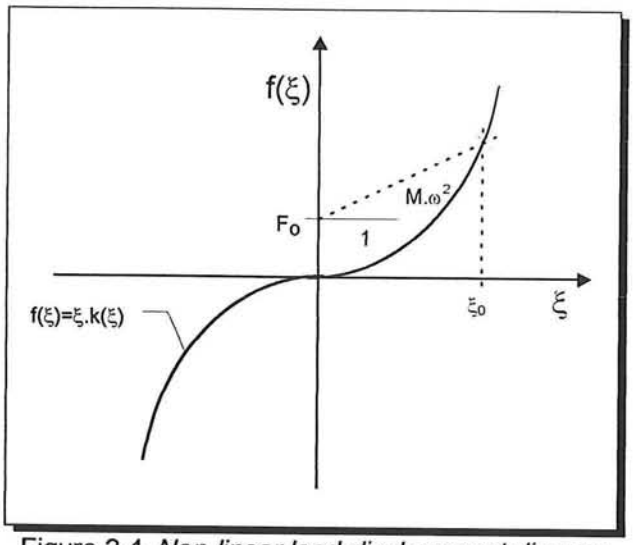

Figure 2.4. *Non-linear load-displacement diagram*

In order to find a linearised spring-constant 'K', two basic assumptions are made, which are, in fact, incorrect (except for linear springs!).

1. Response is sinusoidal
2. Response frequency = Force frequency

Thus,

$$\xi(t) = \xi_o \cos(\omega t) \Rightarrow \ddot{\xi}(t) = -\omega^2 \xi_o \cos(\omega t) \qquad (2.3)$$

And, for :

$$\begin{aligned} &\xi = 0 \Rightarrow F_0 \cos(\omega t) = 0 \Rightarrow f(\xi) = 0 \\ &\xi = \xi_o \Rightarrow F_0 \cos(\omega t) = F_0 \Rightarrow f(\xi) = f(\xi_0) \end{aligned} \qquad (2.4)$$

The following relationship can be found from (2.4) and (2.2):

$$f(\xi_0) = F_0 + M\omega^2 \xi_0 \qquad (2.5)$$

Equation (2.5) gives the opportunity to find a graphical solution with the aid of the load-displacement diagram. In figure 2.4, the solution has been drawn in.

Assume the surface below the load-displacement diagram between the zero and ξ_0 to be known, equalling S [Nm]. This surface represents the amount potential energy. The linearised spring constant is now found by putting:

$$\frac{1}{2} K {\xi_0}^2 = S \Rightarrow K = \frac{2S}{{\xi_0}^2} \qquad (2.6)$$

By repeating the described procedure for different excitation frequencies, a response function can be found. The figure below gives an impression of possible results.

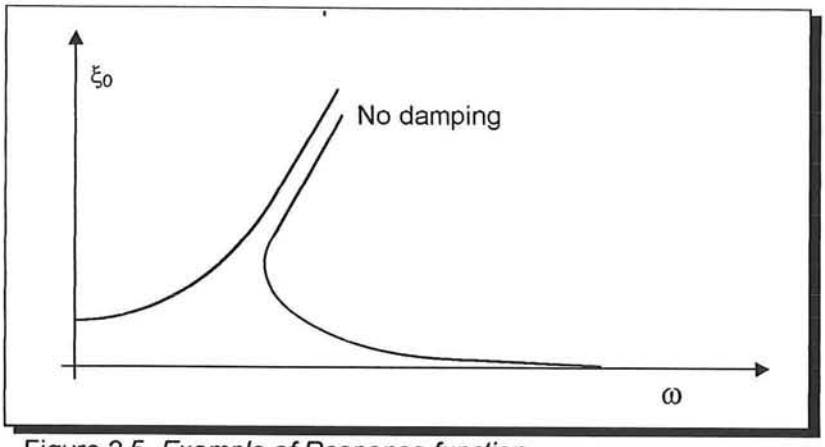

Figure 2.5. *Example of Response function*

As can been seen in figure 2.5, the natural frequency is not a fixed solution. In some cases, the graphical solution gives three results for equation (2.5). This range of frequencies is the range of natural frequencies.

When damping plays a role, the asymptotic part of the ξ_0-ω function is truncated.

2.5. Damping Mechanisms

All mechanisms which involve energy dissipation of the motion energy of the floating structure, contribute to the damping of that motion. In the dynamic LF-model, this damping manifests itself in the form of a linear damping coefficient *B*.

Several mechanisms are contributing to the total system damping: viscous forces on the hull of the structure, wave drift forces, forces on the mooring system, wave radiation forces and wind forces. In the following chapter, these mechanisms are treated more specifically, except for the radiation of waves, which is treated in the next paragraph.

The total system damping for moored floating structures is much lower than the critical damping of the system. The total, linearised, relative damping is approximately in the range of 5 to 20 %. The wave drift damping contributes significantly to the total system damping. In some cases, estimated values of about 15% were confirmed in full scale tests. [Triantafyllou, 1994].

2.6 Added Mass

The LF-behaviour of the floating structure is influenced by the so called added mass effect in the water. This quantity, related to the floating structure, can be obtained in an analytical manner.

Making use of the linear potential flow theory, the Froude-Krylov force, the diffraction force on the structure in its equilibrium position, and the radiation force due to the structure's motion about its equilibrium position can be calculated [Chakrabarti, 1987]. It is considered beyond the scope of this report to give a full explanation on this matter.

The radiation force may be decomposed into two parts: an in-phase part, proportional to the acceleration of the body, and an out-of-phase part, proportional to the body's velocity. The in-phase force component is treated as an added inertia term, which leads to the definition of an *added mass*. The out-of-phase force component leads to a damping force, the so called wave radiation.

Thus, in the damped spring-mass system with a single degree of freedom, the structure's mass is increased by the added mass (a).

2.7 Dynamic LF-Model : Equation of Motion

The equation of motion of the proposed dynamic LF-model in paragraph 2.2 can now be written as follows:

$$(M+a)\ddot{\xi}+B\dot{\xi}+K\xi = F_{Static} + F_0 \sin(\omega t) \qquad (2.7)$$

The static and harmonic forces in the right hand side of (2.7) are the combined effects of the environmental loadings. The static part of the loading is responsible for the mean offset of the floating structure. The next chapter will focus on the linear damping coefficient.

3 Mooring Line Damping in the Dynamic LF-model

3.1 Introduction

In the previous chapter, a simple model has been presented for the analysis of the Low Frequency (LF) behaviour of moored structures. This model represents the LF-behaviour of the moored structure as a damped spring-mass system with one degree of freedom in the direction of the imposed harmonic external force.

The proposed dynamic LF-model is of interest for the engineer in the preliminary stages of the structure design. A clear description and a good prediction of the LF-motions involved are important for the design of the complete mooring system and its influence on the floating structure and riser system. Large offsets will result in high mooring line tensions and severe loading of the structure. For practical use, it is quite common that in early design stages the methods for determining the WF- and the LF-behaviour of the floating structure are decoupled.

The LF resonant motions are a characteristic feature of moored structures. Since we are dealing with low-damped systems at resonance, the large amplitude motions are very dependent on the total system damping. The prediction of the total system damping is therefore crucial in the accurate prediction of the LF-motions.

All coefficients in the equation of motion (like equation 2.1) have to be determined. The discussion of the excitation forces, the mass and added mass of the structure and the (non-linear) spring force due to the mooring system has been given in the previous chapter. The systems damping is the topic of this chapter. The emphasis will be put on the influence of the mooring system on the total system damping.

In the LF-model we are interested in a linear damping coefficient. There are several mechanisms contributing to this linearised damping. These mechanisms are : wave-drift damping, wind damping, current and viscous flow damping and mooring line damping.

The main interest of the present investigation goes to the determination of the contribution of the mooring system to the total linear model damping. Unless otherwise specified, only LF-surge motions are discussed in the following. The presented theories can easily be transformed to the LF-sway motions of the moored structure.

After a brief description of all the components in the damping coefficient in paragraph 3.2, the hypothesis of Huse (1986) for the calculation of the mooring line damping will be presented in paragraph 3.3. Finally, the problem description and the objective of this investigation are given in paragraph 3.4 and 3.5.

3.2 Damping Coefficient in Dynamic LF-model

3.2.1 Introduction

The linear damping coefficient in the equation of motion (eq. 2.1) comprises the contributions of several damping mechanisms. Since we are dealing with a linear problem, this damping coefficient can be written as follows:

$$B_{total} = B_{Wave-drift} + B_{Current} + B_{Mooring} + B_{Wind} \qquad (2.2)$$

This paragraph will give a brief discussion of the four components of the total linear damping. The remaining part of this report will focus on the encircled component of the total linear damping coefficient : the damping due to forces on the mooring lines, or the *'Mooring Line Damping'*.

Each mechanism will give rise to an energy dissipation per cycle of the LF-surge motion, which has to be translated into a linear damping coefficient. In chapter 4, paragraph 4.5, a linearisation of mooring line damping will be made. The same method is applicable to the other damping mechanisms.

3.2.2 Wave Drift Damping

The wave drift forces, also known as second order wave forces, consisting of a constant and an oscillating part, are proportional to the square of the wave group envelope and the corresponding frequency [Wichers & van Sluijs, 1979]. The oscillating part of this wave drift force is an important source of low frequency excitation of the moored vessel. The constant part of the wave drifting forces contributes to the total mean offset of the structure, with respect to the unperturbed state of the moored structure.

Because of the low frequency surge motion, the wave drift forces are changed. One can distinguish the influences of the wave encounter frequency, the incident and the relative wave height and the floating structure's motions. Thus, the wave force excitation is also a function of the LF-surge motion amplitude.

The effect of the changes in the constant wave drift force can be considered as a wave damping force. Several studies have shown that these damping forces are proportional to the square of the wave height and that they are dependent of the ambient wave frequency. [Triantafyllou, 1994 ; Wichers & van Sluijs, 1979] .

3.2.3 Current and Viscous Flow Damping

The moored floating structure experiences viscous drag and lift forces, caused by the presence of a current. These forces are altered by the LF-motions of the structure. [Triantafyllou, 1994]. Eventually, this results in an energy dissipation, transformable to an effective damping coefficient in the Dynamic LF-model.

Thus, this damping contribution is strongly dependent on the current velocity and its direction. In some cases, this damping mechanism can give a substantial contribution to the total system damping.

3.2.4 *Mooring Line Damping*

The LF-motion of the floating structure is influenced by the restoring forces of the mooring system and the damping mechanisms. The contribution of the mooring lines to the total system damping is the sum of the contributions to the energy dissipation due to the hydrodynamic forces on the lines, friction between the lines and the seabed and material damping of the lines.

Due to the motion of the floating structure, the mooring lines are forced to move through the water, resulting in drag- and lift forces on the line. These forces are taken up primarily by the fairlead and to a smaller degree by the anchor. The hydrodynamic drag forces result in an energy dissipation, and thus in a damping of the LF-motion of the structure.

In some cases, vortex formation behind the line can cause a resonant response of the line transverse to the primary motion of the line. The primary motion is in the plane of the line due to the LF-top end motion. This situation of resonant response is called a 'lock-in' situation. The frequency of this response is determined by the Strouhal number, with a nominal value in the range of 0.17 to 0.20. These so called *Vortex Induced Vibrations* (VIV) can lead to a substantial in-line tension fluctuation, which result in a higher energy dissipation.

When the line has a strong curvature or when the flow velocity vary over the waterdepth, the effective normal velocity varies along the line. In these cases the Strouhal frequency of vortex shedding also varies along the line and the 'lock-in' situation is not likely to occur.

The imposed motion at the top end of the line (the fairlead) also leads to movement of the mooring line on the seabed. This friction also contributes to the energy dissipation, caused by the mooring lines. There is still some disagreement about the influence of bottom friction on the LF-motion of moored structures. A Joint Industry Project concluded that the influence of bottom friction is negligible for the LF-motions of moored structures. [Triantafyllou, 1994].

3.2.5 *Wind Damping*

The energy dissipation caused by the wind forces can be explained in the same manner as in the case of viscous flow. The fluctuating part of the wind force is responsible for (a part of) the LF-excitation of the moored structure. The steady part of the wind force contributes to the mean offset of the structure.

The steady force component is again altered by the LF-motion of the structure. As for currents, this leads to an energy dissipation, which can be translated into a linear damping contribution.

3.3 Mooring Line Damping: the Hypothesis of Huse

In 1986, E.Huse of Marintek, Trondheim (N), presented a paper at the Offshore Technology Conference [Huse, 1986] in which he presented a theory on Mooring Line Damping. In the following, the hypothesis will be presented. In chapter 4, this theory will be treated mathematically.

The hypothesis is the following. When a moored floating structure is forced into a (large amplitude) LF-surge motion, the displacement of the top end of a mooring line will cause the line to be tensioned or released, depending on the direction of the LF-surge motion. This in-line tension fluctuation will result in a change of the mooring line configuration. Thus, the mooring line will have to move through the water. The viscous, hydrodynamic forces induced in this manner will give rise to an energy dissipation and cause a damping of the LF-surge motion of the structure. Adding the contributions of all the individual mooring lines gives the total mooring-system damping.

For simplicity, assume a single line, of which the top end is subjected to a horizontal, sinusoidal displacement in the plane of that line. The line is now forced to move normal to its axis, in the plane of the line. The amplitude of this motion can be several times larger that the amplitude of the surge motion, depending on the initial configuration of the line. (See figure 3.1).

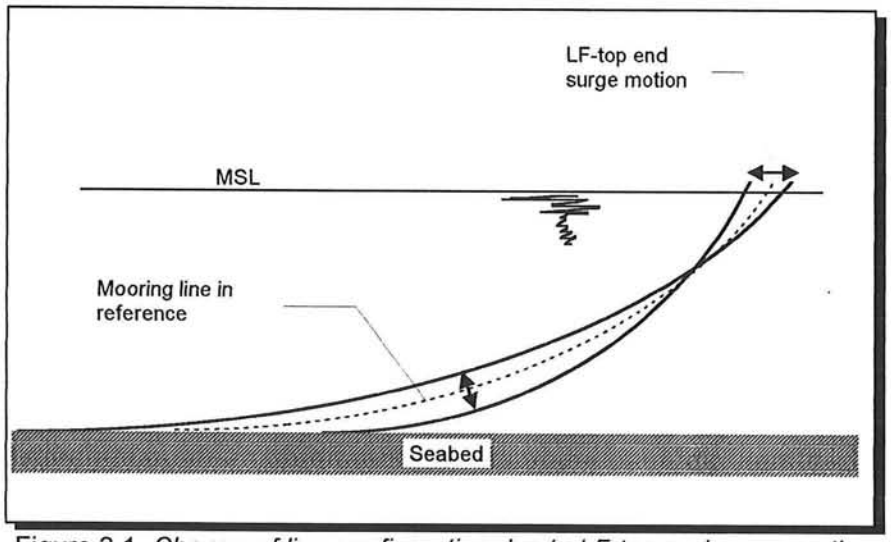

Figure 3.1. *Change of line-configuration due to LF-top end surge motion*

Huse's theory assumes the drag forces normal to the line to be the only source of energy dissipation. Thus, drag forces tangential to the line and internal material damping of the line are neglected. Also, the friction between the line and seafloor is excluded.

3.4 Problem Definition of Investigation

The hypothesis of Huse (1986) says that drag forces normal to the line are the main source of energy dissipation of the LF-surge motion due to the mooring lines. Our primary interest goes to a good description and approximation of the dissipated energy per cycle of LF-surge motion in the plane of the line. The conversion of this dissipated energy into a contribution to the total linear damping coefficient is straightforward, as will be shown in chapter 4.

Thus, the problem definition for the present investigation reads:

> 'A verified (analytical) calculation method for the determination of the contribution to the total linear system damping for LF-surge motions due to the mooring lines is still unknown.'

3.5 Objective of Investigation

As becomes clear in the problem definition, the verification of Huse's model should be carried out.

The objective of the investigation is :

> 'A Verification of the model, as proposed by Huse, for the calculation of the dissipated energy due to drag forces normal to the line, in the case that the mooring line is given LF-sinusoidal top end motion.'

The verification of Huse's model has been performed by means of laboratory experiments. It is necessary to have a good mathematical formulation of the energy dissipation per cycle of LF-surge motion. An experiment will have to be designed in which mooring lines similar to relevant prototype configurations are subjected to top end oscillation tests. This will be described in chapter 5. The actual verification will be the comparison between the results of Huse's model and the experimental results.

4 Mathematical Description of the Model

4.1 Introduction

This chapter presents the analytical model for the estimation of the total energy dissipation during one full cycle of a Low-Frequency (LF) surge motion due to drag forces on the mooring lines. The basic theory was derived by Huse (Marintek - Trondheim, Norway) and presented at the Offshore Technology Conference in Houston,1986.

The model shows an analytical expression for the energy dissipation per cycle due to drag forces on a mooring line when the top end of the line is given a horizontal, (LF) sinusoidal motion. A number of assumptions and simplifications are introduced, which should be carefully accounted for when using this model.

In paragraph 4.2, the basic catenary equations are presented. For the case of slack lines, some useful derivations will be presented. These equations will be used extensively in further analysis. Paragraph 4.3 gives a detailed derivation of Huse's analytical expression for the energy dissipation per cycle of low-frequent-surge motion.

The derived analytical formula for the energy dissipation per cycle contains an undetermined variable. Making some assumptions, relevant for the proposed experiments for verification, an analytical formula can be derived. This is the topic of paragraph 4.4.

Two methods for the numerical evaluation of the formula of energy dissipation are explained and compared in paragraph 4.5. Finally, the calculated or measured energy dissipation per cycle has to be 'converted' to a linear damping coefficient. Paragraph 4.6 shows how this is done.

4.2 Basic Catenary Equations

The following paragraph presents the catenary equations in different forms. It is stressed that no explanation is given about the theory and derivation of the differential equation for suspended cables, which can be found in many textbooks on applied mechanics.

4.2.1 General Catenary Equation

When a uniform line is suspended between two different points and loaded by its own weight, the line configuration is described by the so called catenary equation. In the static case, the main line parameters are the line-length, the (submerged) weight of the line and the horizontal pretension, which is constant along the entire suspended line. The definitions of the used symbols can be found in Figure 4.1 below.

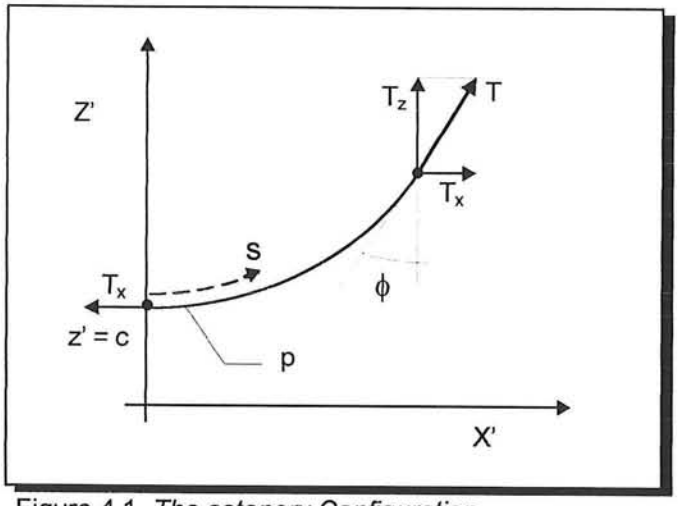

Figure 4.1 *The catenary Configuration*

When the system of co-ordinates (x',z') is defined as in figure 4.1, the catenary equation reads:

$$z' = c.cosh(\frac{x'}{c})$$
$$c = \frac{T_x}{p} \qquad (4.1)$$

In which: T_x = horizontal component of the pretension
p = submerged weight of mooring line per unit length
x',z' = *local* co-ordinates

The *'hanging line- length (s)'* is defined as the distance measured along the line, starting at the lift-off point all the way to the top end. The *'lift-off point'* of a mooring line is defined as the point where the line is just tangential to the seabed.

The equation for '*s*' as a function of *x'* for a given pretension and (submerged) weight of the cable reads:

$$s = c.sinh(\frac{x'}{c}) \qquad (4.2)$$

A difference is made between 'slack' lines and 'taut' lines. For a slack line, the vertical component of the line tension will be zero at the lift-off point, unlike the taut line. The case of slack lines will be highlighted in the following paragraph.

4.2.2 Slack Lines

In most practical cases, the mooring line configuration will be 'slack'. Taut lines are still undesired because of the high pretensions which are involved and the vertical loading of the anchors.

The general catenary equation is defined in a *local* system of co-ordinates, as was shown in figure 4.1. For the slack line, the vertical component of the line tension is

zero at the lift-off point. This means that, for a total line length (S) which is longer than the hanging line length (s), a portion of the line ($\Delta L = S-s$) rests on the seabed.

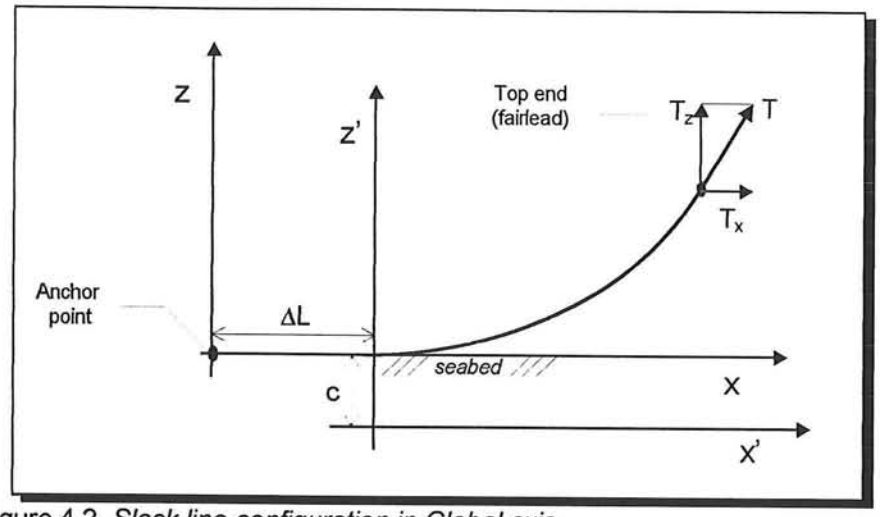

Figure 4.2 *Slack line configuration in Global axis*

For practical calculations the structure will be described in a global co-ordinate-system (x,z), with its origin at the anchor point. The co-ordinates (x,z) are chosen such that z is vertical and x is horizontal along the seabed (Figure 4.2). The figure gives a good insight in how the transition of variables should take place. The x' and z' co-ordinates shift to x and z :

$$\begin{aligned} x &= x' + x_o \\ z &= z' - c \\ x_o &= \Delta L = S - s \end{aligned} \qquad (4.3)$$

The position of the lift-off point along the x-axis, denoted as x_o , is equal to ΔL, which is the part of the line resting on the seabed. Making use of the basic catenary equations, it is now straightforward to determine all desired information. Two examples will be given : the elevation and the vertical component of the line tension. All other properties can be found in the same manner.

- The elevation of the mooring line, as a function of x, is now given by :

$$\begin{aligned} x \le x_o &\Rightarrow z(x) = 0 \\ x \ge x_o &\Rightarrow z(x) = c.\left[\cosh\left(\frac{x - x_o}{c}\right) - 1\right] \end{aligned} \qquad (4.4)$$

- The vertical component of the line tension is determined by the length of the suspended line and its (submerged) weight, and can be calculated as follows:

$$\begin{aligned} x \le x_o &\Rightarrow T_z = 0 \\ x \ge x_o &\Rightarrow T_z = p.s = p.c.\sinh\left(\frac{x - x_o}{c}\right) = T_x.\sinh\left(\frac{x - x_o}{c}\right) \end{aligned} \qquad (4.5)$$

4.3 Model for Energy Dissipation from Mooring Lines

4.3.1 Analytical Approach

Consider a uniform mooring line, like in Figure 4.2, suspended from a point on a floating object , the fairlead, to an anchorpoint on the seafloor and loaded by its own (submerged) weight.

The line tension T is the vector sum of a horizontal component $T_x=T_o$ (which is, in the static case, a constant along the line; 'the horizontal pretension') and a vertical component T_z. In figure 4.2, these forces are drawn.

The LF-surge-motions are now considered to be sinusoidal. Assume further that the top end of the line (fairlead) moves horizontally in the plane of the line. The displacement of the fairlead will be described by:

$$\xi = \xi_o \sin \omega.t \qquad (4.6)$$

A line element Δs along the mooring line will now experience a motion normal to the line tangent, in the plane of the line. Assuming a sinusoidal response, the transverse line displacement will be:

$$\eta = \eta_o \sin \omega.t \qquad (4.7)$$

where η_o is the transverse motion amplitude, which is a function of *s* or *x*.

Due to the top end motion, the line element will experience hydrodynamic drag forces, parallel and normal to the line, as well as hydrodynamic lift forces. This model considers the *drag forces* normal to the line element to be the dominant and *only source of energy dissipation* due to external forces as a results of the line motion. The energy dissipated due to drag on this line element during one full period T of the motion is thus considered to be determined by:

$$\Delta E_{diss} = 2 \int_{-\eta_o}^{\eta_o} \Delta F_D d\eta \qquad (4.8)$$

where the drag forces ΔF_D can be written as:

$$\Delta F_D = \tfrac{1}{2} \rho_w D C_D \left| \frac{d\eta}{dt} \right| \frac{d\eta}{dt} \Delta s \qquad (4.9)$$

Substitution (4.9) into (4.8) gives:

$$\Delta E_{diss} = \rho_w D C_D \Delta s \left(\int_{-\eta_o}^{\eta_o} \left| \frac{d\eta}{dt} \right| \frac{d\eta}{dt} d\eta \right) \qquad (4.10)$$

The remaining integral in expression (4.10) can now be solved by substituting equation (4.7). The transition of the integration variable η into t requires new expressions for the limits of integration.

With equation (4.7) one can find for the integration limits:

$$\eta = -\eta_o \Leftrightarrow -\eta_o = \eta_o \sin\omega t \Rightarrow \omega t = -\frac{\pi}{2}$$
$$\eta = +\eta_o \Leftrightarrow +\eta_o = \eta_o \sin\omega t \Rightarrow \omega t = +\frac{\pi}{2} \qquad (4.11)$$

This yields:

$$\Delta E_{diss} = \rho_w D C_D \Delta s \omega^2 \eta_o^3 \int_{-\frac{\pi}{2}}^{\frac{\pi}{2}} |\cos\omega t| \cos^2 \omega t d(\omega t) \qquad (4.12)$$

The remaining integral in the equation has been solved and equals 4/3, leading to the following expression for ΔE :

$$\Delta E_{diss} = \frac{4}{3} \rho_w D C_D \omega^2 \eta_o^3 \Delta s \qquad (4.13)$$

In order to get the result for the total energy dissipated by the entire line, equation (4.13) has to be integrated along the whole line, from the anchor point up to the top end of the mooring line, the fairlead. Therefore, it is necessary to obtain an expression for η_o as a function of x or s.

Assume that the top end motion is sufficiently slow so that a catenary shape of the line is retained at all times. The value of η_o will be approximated by the half of the difference in elevation Δz of the mooring line in maximum and minimum tension with respect to the global x-axis, multiplied by the co-sinus of the (local) tangent angle (ϕ) of the static mooring line. Figure (4.3) illustrates the used notations.

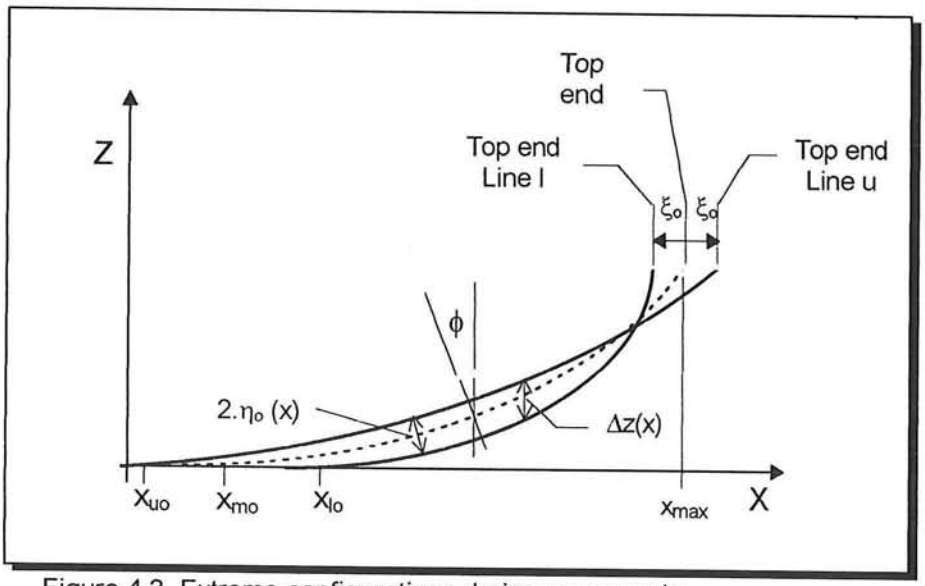

Figure 4.3 Extreme configurations during surge cycle

In figure 4.3:

x_{max} : x-co-ordinate of top end in reference position
x_{uo} : lift-off point when line is tensioned
x_{mo} : lift-off point when line is in reference position
x_{lo} : lift-off point when line is released

The values $z_U(x)$ and $z_L(x)$ are the highest and lowest values of elevation during the entire surge period.

$$\Delta z = z_U(x) - z_L(x) \tag{4.14}$$

And thus,

$$\eta_o = \frac{1}{2}\Delta z \cos\phi \tag{4.15}$$

- For the time being it is sufficient to realise that Δz is a function of the global x-co-ordinate. It is stressed that $\Delta z(x)$ only represents the difference of the elevations along the line between the two extreme positions, during one surge cycle with a given amplitude. Whether this function is calculated by means of simple catenary equations, neglecting the mechanical properties like bending stiffness and axial strain during loading, or making use of a sophisticated F.E.M. software package, will have an influence on the outcome of $\Delta z(x)$, but is does not influence the equations presented in the following.

The tangent angle of the mooring line is determined by the line tension and the horizontal component of the line tension, as follows:

$$\cos\phi = \frac{T_o}{T_t} \tag{4.16}$$

Making use of the catenary equation, we can derive an expression for the angle of the tangent as a function of the position (x), the lift-off point of the *static line* (x_o), the submerged weight per unit length of the mooring line (p) and the horizontal pretension, assumed to be constant along the line (T_x=T_o).

Thus,

$$\cos\phi = \frac{T_o}{\{T_o^2 + [T_o \sinh(p/T_o (x - x_o))]^2\}^{1/2}} \tag{4.17}$$

Substituting (4.14) into (4.15) and then (4.15) into (4.13) leads to :

$$\Delta E_{diss} = \frac{1}{6}\rho_w D C_D \omega^2 \Delta z^3 \cos^3\phi . \Delta s \tag{4.18}$$

Integrating equation (4.18) along the entire mooring line gives the total energy dissipated by the whole line during one surge cycle. Performing the integration gives:

$$E_{diss} = \frac{1}{6}\rho_w D C_D \omega^2 \int_0^S \Delta z^3 \cos^3 \phi . ds \qquad (4.19)$$

Since Δz and $cos\ \phi$ are expressed as a function of x, a transition of variables has to take place. Changing the integration variable to x implies that the limits and the differential of the integral have to change. Making use of the catenary equation gives:

$$s = \frac{T_o}{p}\sinh(\frac{p}{T_o}(x - x_o)) \Rightarrow ds = \cosh(\frac{p}{T_o}(x - x_o))dx \qquad (4.20)$$

Which can be transformed to:

$$ds = \sqrt{1 + \sinh(\frac{p}{T_o}(x - x_o))}.dx \qquad (4.21)$$

Substituting (4.21) and (4.17) into (4.19) gives:

$$\boxed{E_{diss} = \frac{1}{6}\rho_w D C_D \omega^2 \int_0^{X_{max}} \frac{(\Delta z(x))^3}{1 + \sinh^2(\frac{p}{T_o}(x - x_o))}.dx} \qquad (4.22)$$

Equation (4.22) was first presented by Huse. It gives an semi-analytical expression to calculate the total dissipated energy, due to the mooring line, during one full surge period. The factor Δz has yet to be determined. The form in which Δz is presented determines whether the expression is fully analytical or not.

4.3.2 Remarks

A model has been presented to calculate the energy dissipation of a mooring line, when its top end undergoes a slow sinusoidal motion, in 'the plane of the line'. A fairly simple expression was derived, in the form of equation (4.22).

The following fundamental assumptions were made during the analytical derivation :

- The mooring line is uniform.
- LF-surge motions are sinusoidal, in the plane of the line.
- Line configuration is catenary at all times during surge motion.
- Energy dissipation is due to drag forces normal to the line only.
- The *'$D.C_d$'* - value is a constant along the entire line.

In the mathematical calculation, it was necessary to make a reasonable choice for the transverse motion amplitude of the line. This amplitude was approximated with the aid of Δz, which is the difference in elevation along the line in the two extremes of the surge motion, each assumed to be of equilibrium (catenary) shape.
It is stressed that different solutions for the energy dissipation are most likely to be found for different calculations methods for Δz. The use of sophisticated F.E.M.-

software packages, incorporating all mechanical properties of the line will show different results than a calculation of a model based on a change in the catenary equation only. The choice of the applied method should therefore carefully be considered.

4.4 Analytical Expression for the Energy Dissipation in Experiment

4.4.1 Introduction

The theoretical approach of paragraph 4.3 resulted in a semi-analytical formula for the energy dissipation per cycle, presented in equation (4.22), in which the integral contains a variable, $\Delta z(x)$, which is still undetermined. As said in the concluding remarks of the last paragraph, the outcome of (4.22) is highly dependent on this factor.

In order to calculate the variable $\Delta z(x)$, we neglect the axial of the line. This assumptions leads to the use of catenary equations, where the line parameters stay the same at all phases of the surge motion, except for the horizontal position of and the horizontal pretension at the top end. In the following, an analytical expression is derived for the variable $\Delta z(x)$ and substituted in equation (4.22).

4.4.2. Calculation of the Transverse Motion Amplitude

The transverse motion amplitude, given in equation (4.15), is dependent on the elevation difference of the line in the two extreme positions during a full period of the (Quasi-static) top end oscillation and the tangent angle of the line in reference position. The tangent angle of the line had already been accounted for in the expression of the energy dissipation.

Since the line elasticity is neglected the expression of Δz is straightforward. The equations for catenary lines in a slack configuration, as given in paragraph 4.2.2, are defined in a local axis system. During the oscillation of the top end, the line will be tensioned and released. The parameters, described in the global axis system, of the line in highest tension will be given the subscript 'u', while those of the line in lowest tension will have the subscript 'l'. (See figure 4.3).

The expression for Δz in the global axis system has to be split in three parts, since the expressions for the elevation of the lines 'u' and 'l' are defined starting from the lift-off points, as follows:

For i = u or l :

$$x \le x_{io} \Rightarrow z_i(x) = 0$$

$$x \ge x_{io} \Rightarrow z_i(x) = c_i\left[\cosh\left(\frac{x - x_{io}}{c_i}\right) - 1\right] \qquad (4.23)$$

Thus, the positions of the lift-off points (x_{io}) and the pretensions of the line in extreme positions ($c_i = T_{xi}/p$) have to be known.

Substituting (4.23) into (4.22) gives the full (analytical) expression for the energy dissipation in the experiment, which reads:

$$E_{diss} = \frac{1}{6}\rho_w D C_D \omega^2 \int_{x_{uo}}^{x_{lo}} \frac{\left\{ c_u \cdot \left[\cosh(\frac{x - x_{uo}}{c_u}) - 1 \right] \right\}^3}{1 + \sinh^2(\frac{p}{T_o}.(x - x_o))} dx \qquad (4.24)$$

$$+\frac{1}{6}\rho_w D C_D \omega^2 \left\{ \int_{x_{lo}}^{X_{max}} \frac{\left\{ c_u \left[\cosh(\frac{x - x_{uo}}{c_u}) - 1 \right] - c_l \left[\cosh(\frac{x - x_{lo}}{c_l}) - 1 \right] \right\}^3}{1 + \sinh^2(\frac{p}{T_o}(x - x_o))} .dx \right\}$$

In which X_{max} is the x-co-ordinate of the top end of the line in reference position.

4.5. Numerical Calculation of Energy Dissipation

4.5.1. Introduction

In the determination of the dissipated energy per cycle, the integral (I) in equation 4.22 or 4.24 has to be calculated. Huse (1988) presented a graphical method to perform this numerical evaluation. For the current experiment, a simple computer program was developed in order to calculate the sum of the integrals in equation 4.24.

Since the line elongation is assumed negligible, the results of both methods have to be the same. In order to verify this, the methods are compared for the configurations which will be used during the experiments. The description of these configurations can be found in chapter 5.

4.5.2. Graphical Method by Huse

In his paper "Practical Estimation of Mooring Line Damping" [1988], Huse provided a graphical approach for the calculation of the integral I in (4.22). This paragraph gives the procedure and the results for the verification test following from this paper.

The integral to be calculated reads:

$$I = \int_0^{X_{max}} \frac{(\Delta z(x))^3}{1 + \sinh^2(\frac{p}{T_o}(x - x_o))} .dx \qquad (4.25)$$

The idea is to calculate the integral above with a systematic variation of all the parameters involved. The influence of the parameter $\Delta z(x)$ is significant, as said earlier. At Marintek, Trondheim (N), a computer program was developed in which all

parameters were varied systematically. The program takes into account the line elongation due to mechanical elasticity and the friction of the line against the seabed.

The parameters, by Huse considered in the evaluation of the integral (eq. 4.25) are:

H : Depth from top end (fairlead) to seabottom
L : Line length
ξ_0 : Amplitude of horizontal top end motion
p : Submerged weight of line
T_o : Horizontal component of pretension at top end
EA : Mechanical Tensile Stiffness
μ : friction coefficient of line to seabed

The line-length (L) is thought sufficiently long, so that the tension fluctuation is completely absorbed by bottom friction. Huse considered the parameters L and μ eliminated.

Making use of the Buckingham PI Theorem [Chakrabarti, 1994], the remaining 5 parameters are reduced to 3 non-dimensional groups. Thus, the integral can be expressed as :

$$\frac{I}{H^4} = f(\pi_1, \pi_2, \pi_3) \qquad (4.26)$$

in which π_1, π_2, π_3 are the following non-dimensional expressions:

$$\begin{cases} \pi_1 = \dfrac{\xi_0}{H} \\ \pi_2 = \dfrac{p.H}{T_0} \\ \pi_3 = \dfrac{EA}{T_0} \end{cases} \qquad (4.27)$$

Huse's presented values for I/H^4 in a few simple diagrams (see figure 4.4). With the relevant values of the parameters the non-dimensional numbers can be determined. By means of interpolation in the diagrams below, the value for I/H^4 can be calculated.

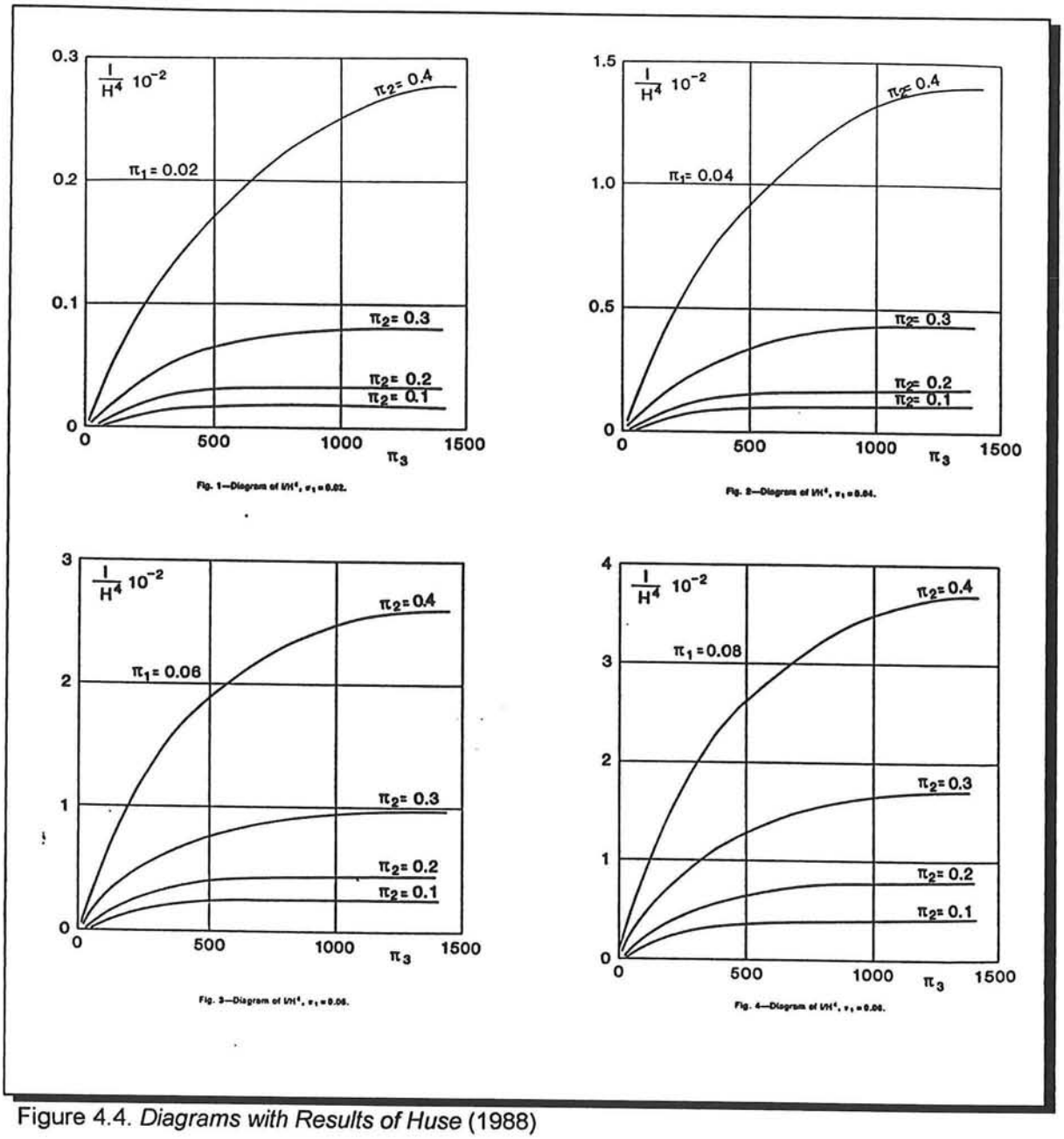

Figure 4.4. *Diagrams with Results of Huse* (1988)

Twelve test configurations have been evaluated in the following. In chapter 5, a full explanation of these configurations will be given. For now, it is sufficient to realise that the configurations considered are exactly the same as in the next paragraph.

The diagrams for the results of Huse (figure 4.4) provided for the twelve test configurations a solution for I/H^4. These results are presented in table 4.1 on the next page.

The results found were:

Line Configuration *[Pos & Amp]*	π_1 *[-]*	π_2 *[-]*	I/H^4 *[-]*	I *[m^4]*
2-A ; 0.06 m	0.043	0.396	0.01592	0.08841
2-A ; 0.08 m	0.057	0.396	0.02429	0.13489
2-A ; 0.10 m	0.071	0.396	0.03199	0.17765
3-A ; 0.06 m	0.043	0.338	0.00826	0.04587
3-A ; 0.08 m	0.057	0.338	0.01608	0.08930
3-A ; 0.10 m	0.071	0.338	0.02094	0.11629
4-A ; 0.06 m	0.043	0.286	0.00413	0.02294
4-A ; 0.08 m	0.057	0.286	0.00806	0.04476
4-A ; 0.10 m	0.071	0.286	0.01297	0.07203
5-A ; 0.06 m	0.043	0.239	0.00334	0.01855
5-A ; 0.08 m	0.057	0.239	0.00690	0.03832
5-A ; 0.10 m	0.071	0.239	0.00939	0.05215

Table 4.1. *Results of the Integral in eq.(4.25) according to Huse*

An explanation of the notation for the line configurations in table 4.1 is given in chapter 5. These results will be compared with the results of the following paragraph.

4.5.3. Numerical calculations of Current Investigation

Like in the previous paragraph, the twelve test configurations are evaluated. The full description of these configurations is given in chapter 5. For now, it is suffiecient to realise that the same configurations are evaluated as in the previous paragraph.

In paragraph 4.4, the analytical expression for the calculation of the energy dissipation has been derived. The result was given as follows:

$$E_{diss} = \frac{1}{6}\rho_w D C_D \omega^2 \int_{x_{uo}}^{x_{lo}} \frac{\left\{ c_u \left[\cosh\left(\frac{x - x_{uo}}{c_u}\right) - 1 \right] \right\}^3}{1 + \sinh^2\left(\frac{p}{T_o}(x - x_o)\right)} . dx \qquad (4.24)$$

$$+ \frac{1}{6}\rho_w D C_D \omega^2 \left\{ \int_{x_{lo}}^{x_{max}} \frac{\left\{ c_u \left[\cosh\left(\frac{x - x_{uo}}{c_u}\right) - 1 \right] - c_l \left[\cosh\left(\frac{x - x_{lo}}{c_l}\right) - 1 \right] \right\}^3}{1 + \sinh^2\left(\frac{p}{T_o}.(x - x_o)\right)} . dx \right\}$$

When we follow the same route as we did for the approach of Huse, the integral I has to be determined for each tested line configuration. In this case, the integral I will be the sum of the two integrals in the equation (4.24). Therefore, a small computer program was developed to perform this calculation. In Appendix C, the source code, the full input- and outputfiles are listed.

Necessary input are the line parameters for each test case. The program will ask for:

pos	:Position number	(1..5)
line	:Line	(A,B)
amp	:Amplitude of oscillation	[m]
xuo	:Lift-off point of line in maximum top end position	[m]
cu	:Static horizontal component top end force in max. pos.	[m]
xlo	:Lift-off point of line in minimum top end position	[m]
cl	:Static horizontal component top end force in min. pos.	[m]
xmo	:Lift-off point of line in reference top end position	[m]
cmo	:Static horizontal component top end force in ref. pos.	[m]
xmax	:x-co-ordinate of top end in reference position	[m]
zmax	:z-co-ordinate of top end in reference position	[m]

These input parameters have been determined with the aid of MAPLE V- worksheets and are listed in the appendix C.2. The basic catenary equations for slack lines form the basis to calculate these input parameters. The top end positions of the lines '*u*' and '*l*' are found by respectively adding up and subtracting the oscillation amplitude with the top end reference position, xmax.

The computer program has calculated the value for the integral in all configurations of the experiment (see chaper 5). The results are given in non-dimensional form in the following graph. (Note that 'so' means the displacement amplitude (ξ_0).

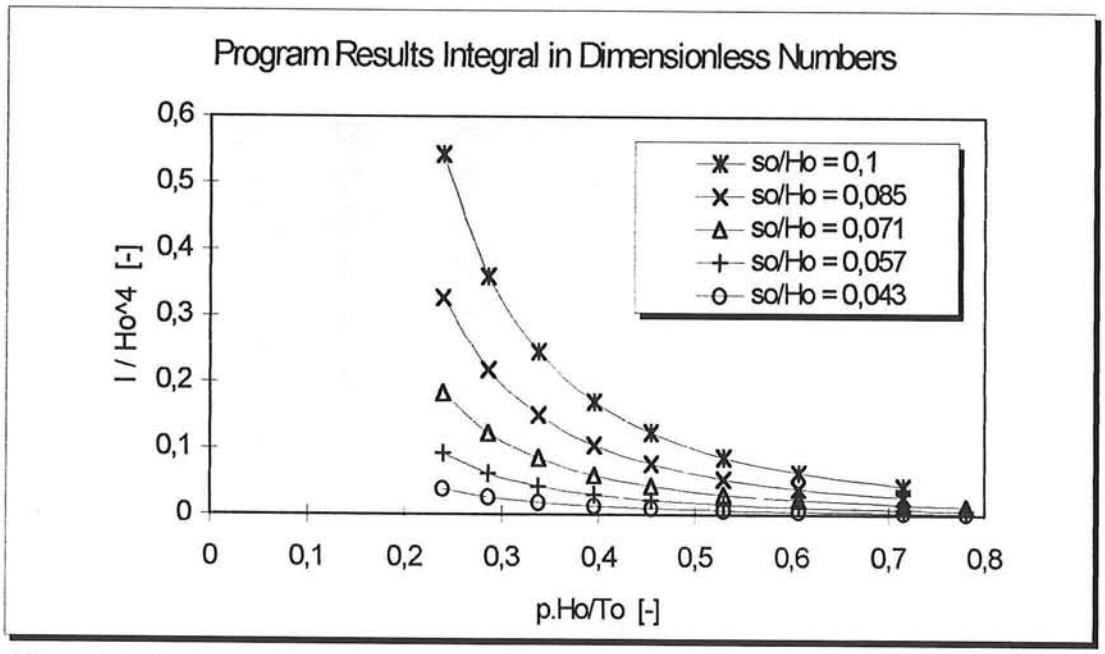

Figure 4.5. *Results of computer program*

For comparison with the results of Huse, the results of the computer program for the twelve test cases are listed below.

Line Configuration *[Pos & Amp]*	I/H^4 *[-]*	I *[m^4]*
2-A ; 0.06 m	0.00227	0.00894
2-A ; 0.08 m	0.00541	0.02131
2-A ; 0.10 m	0.01067	0.04205
3-A ; 0.06 m	0.00323	0.01274
3-A ; 0.08 m	0.00772	0.03042
3-A ; 0.10 m	0.01527	0.06018
4-A ; 0.06 m	0.00465	0.01833
4-A ; 0.08 m	0.01112	0.04383
4-A ; 0.10 m	0.02206	0.08694
5-A ; 0.06 m	0.00688	0.02713
5-A ; 0.08 m	0.01650	0.06502
5-A ; 0.10 m	0.03285	0.12948

Table 4.2. *Results of program for Integral-values*

4.5.4. Comparison Numerical Results of Both Methods

The table below gives the results for the graphical method by Huse and the program results of the current investigation.

Line Configuration *[Pos & Amp]*	A = HUSE I/H^4 *[-]*	B=Program I/H^4 *[-]*	Factor Difference *A/B*
2-A ; 0.06 m	0.01592	0.00227	7.013
2-A ; 0.08 m	0.02429	0.00541	4.490
2-A ; 0.10 m	0.03199	0.01067	2.998
3-A ; 0.06 m	0.00826	0.00323	2.557
3-A ; 0.08 m	0.01608	0.00772	2.083
3-A ; 0.10 m	0.02094	0.01527	1.371
4-A ; 0.06 m	0.00413	0.00465	0.888
4-A ; 0.08 m	0.00806	0.01112	0.725
4-A ; 0.10 m	0.01297	0.02206	0.587
5-A ; 0.06 m	0.00334	0.00688	0.485
5-A ; 0.08 m	0.00690	0.01650	0.418
5-A ; 0.10 m	0.00939	0.03285	0.286

Table 4.3. *Factor difference between results by Huse and Program*

The method of calculating the integral I is causing problems, as can be seen from the factor A/B in table 4.3. The computer calculations performed by Huse (1988) incorporated mechanical line elongation and bottom friction. It is not quite clear how these results of Huse were obtained. The results of the computer program are based on the neglection of the axial strain of the line.

4.6. Theoretical Calculation of the Linear Damping Coefficient

The final step in the analysis is the translation of the calculated energy dissipation into a linearised damping coefficient. To that end the result presented in equation (4.22) or (4.24) will be used.

The general equation of motion in the Dynamic LF-model, with respect to the mean offset reference position, is :

$$(M+a)\ddot{\xi}(t)+B\dot{\xi}(t)+C\xi(t)=F_o\sin(\omega.t) \qquad (4.25)$$

The damping coefficient in equation 4.25 represents to the sum of all linearised damping mechanism contributions.

The determination of the linearised damping coefficient, $B_{Mooring}$, due to drag forces on the mooring lines, can now be found by the requirement that the energy dissipation calculated according to equation (4.24) equals the value from the damping term in equation 4.25, which yields:

$$E_{diss}=\int_0^T B_{Mooring}\dot{\xi}(t)d\xi(t) \qquad (4.26)$$

With for the top end the slow oscillatory motion, described by:

$$\xi(t)=\xi_0\sin(\omega t) \qquad (4.27)$$

Substituting (4.27) into (4.26) leads to:

$$E_{diss}=\int_0^T B_{Mooring}\xi_0^2\omega^2\cos^2(\omega t)dt \qquad (4.28)$$

Transforming to the variable $x = \omega.t$, this can be transformed to:

$$E_{diss}=B_{Mooring}\xi_0^2\omega\int_0^{2\pi}\left(\frac{1+\cos(2x)}{2}\right)dx \qquad (4.29)$$

Solving the integral gives:

$$E_{diss}=B_{Mooring}\xi_0^2\omega\pi \qquad (4.30)$$

This leads to the following simple formula to derive the lineairised damping coefficient due to the mooring lines:

$$\boxed{B_{Mooring}=\frac{E_{diss}}{\xi_0^2.\omega.\pi}} \qquad (4.31)$$

in which E_{diss} is given by equation (4.24)

5. Experiment Design and Scaling Analysis

5.1. Introduction

A conducted literature survey has shown that mooring line damping can be an important contributor to the total system damping of the Low Frequency (LF) surge or sway motions of moored offshore structures and vessels. A number of tests even showed that mooring line damping can be the major part of the total system damping.

A model has been presented for the determination of Mooring Line Damping. Drag forces normal to the mooring line are assumed to be the main source of energy dissipation due to the motion of the mooring lines through the water. A small offset of the top end (fairlead) can result in large transverse displacements along the mooring line. This is the reason why in some cases considerable drag forces, and thus energy dissipation, can be expected.

Given the catenary configuration of the mooring line, it is assumed possible to calculate the energy dissipation by the line in the case of a LF-sinusoidal surge motion of the top end of the line. A necessary condition for such a calculation is that the configuration of the mooring line stays catenary at all times. Chapter 4 has given the mathematical derivation of the expression for the energy dissipation.

The main purpose of the current experiment is to provide test data to verify the model which was presented in the previous chapter. This will be the reason why there will be no prototype involved. A large number of catenary configurations of a single mooring line will be tested for forced LF-sinusoidal top end motions.

It should be noted that the mooring lines considered in this entire investigation are of one type of line only. More specifically, it has been decided to investigate the behaviour of a chain. No combinations, for instance steel wire rope and chain, are considered.

Paragraph 2 gives the basic strategy of the experiment for the verification of Huse's model. The experiment design is described in paragraph 5.3. In order to examine relevant catenary configurations, a scaling analysis is performed in paragraph 5.4. Making use of the drawn up scaling law, parameter values for the experiment are calculated. A method to investigate the influence of inertia forces in the model is given in paragraph 5.5. The actual set up of the experiment is described in paragraph 5.6. Finally, the testing programme is presented in paragraph 5.7.

5.2. Energy Dissipation in Experiments

The objective of the current investigation is to verify Huse's model, presented in chapter 4. The model resulted in an analytical expression to calculate the energy dissipation of the LF-surge motion of a floating structure due to the motion of the mooring lines through the water. In the following, the approach of the present experiments is made clear by comparison with the usually performed tests.

Usually, tests on mooring line damping are performed by means of a surge decay test on the structure model with a complete mooring system incorporated. The procedure is as follows. The complete model, mooring system included, is given an initial offset in surge direction. After releasing the structure-model, the surge decay of the free oscillation is measured, from which the total energy dissipation of the moored structure is estimated.

Next, the modelled mooring system is detached from the floating structure and coupled to a set of horizontal lines and springs, above waterlevel, which has the same restoring force characteristics as the modelled mooring system. The surge decay test is then repeated. By subtracting the results of both surge decay tests, one finds a contribution to the system damping from the mooring system.

It will be clear that these tests are inaccurate, if one only remembers that the modelling of mooring lines for small scales is extremely difficult, if not impossible. This method is therefore not suitable for the present investigation. Therefore, a different approach is needed.

Consider a submerged mooring line, suspended from a fixed anchor to a certain point at the waterlevel, representing the fairlead of a floating structure. Instead of assuming a free motion of the floating structure, the top end is now forced into an oscillation in the plane of the line. The forced oscillation represents the LF-resonant motion of the floating structure.

During the forced oscillation, the horizontal and vertical components of the in-line tension are measured and recorded as a function of time. The product of the horizontal force component and the instantaneous oscillation velocity of the top end and is integrated over one oscillation cycle. The result obtained is the energy dissipation per cycle, representing the surge damping.

The method using a forced oscillation of the top end of the mooring line is followed in the current experimental investigation. In the following paragraphs, the design of the experiment set up is determined.

5.3. Experiment Design

5.3.1. Introduction

As said earlier, the purpose of the experiment is to provide general data on mooring line damping. The results obtained will be used for the verification of the presented model. The test set-up should therefore be adjusted to various mooring line configurations.

It has been decided to do tests with a chain; this choice will be argumented in paragraph 5.3.3. The top end of the line will be subjected to an oscillation with various amplitudes and frequencies. The oscillation parameters, amplitude and frequency, will be determined in a scaling analysis in paragraph 5.4.

Several parameters are involved in the configuration of the mooring line. Because of the restriction to a single type of line, the line-parameters (weight, diameter, etc.) are fixed. In order to obtain a large spectrum of geometrical configurations to be tested, the pretension at the top end should therefore be varied from nearly zero until a certain maximum, depending on the limitations of the testing facility.

There are two ways of changing the pretension of the mooring line. The first is to bring in the top end of the line. This means that the line will be lengthened or shortened when changing the pretension. This was not considered to be very practical, because it requires additional mounting operations during testing.

The second way to change the pretension is by changing the zero position of the top end of the mooring line. Since the tests will be performed from a rail-mounted-carriage, it will be easy to change the top end position, just by moving the carriage. The test set-up with several top end positions to determine the pretensions will be the basis for the experiment set-up design.

5.3.2. Test Facility

Tests are executed in the towing tank of the Ships Hydromechanics Laboratory at the TU Delft. The small tank (L=75 m x B=2.75 m x d=1.40 m) of the laboratory has been used for the experiments.

A fully equipped, rail mounted, towing carriage was installed. The facility provides the opportunity to use an oscillator for the excitation of the top end of the mooring line. This makes the facility very attractive for experiments on mooring line damping. Some characteristic data of the facility are given below.

- The oscillators are able to produce a smooth sinusoidal motion with a maximum displacement in the range of 25 to 30 centimetres at a frequency between 0.0033 Hz and 1.66 Hz.
- Forces at the top end of the mooring line can be measured in both vertical and horizontal directions. Use will be made of dynamometers with a loading capacity of 400 N each.
- A wave generator is installed, able to produce regular as well as random waves. In the case of this experiment, regular waves will be used for qualitative tests only.

- The measured data will be digitally recorded in Asyst_4.0-format files. Software is available to convert these data files into ASCII-files or files of a spreadsheet format.

5.3.3. Choice of the Mooring Line in Experiment

In paragraph 4.4, two assumptions were made in order to find a fully analytical expression for the energy dissipation per cycle in the experiment. The first was the neglect of the axial strain, the second the neglect of bottom friction. The validity of both assumptions is dependent on the axial stiffness of the line. The higher the axial stiffness, the lesser the influence of bottom friction and dynamic elongation [Huse, 1986].

In order to find relevant results, the flow pattern around the line in the experiment should be comparable to prototype situations. The streamlines of the flow around the line (-element) should therefore be separating from the body. Since velocities are low, the choice of a fairly large diameter line will therefore produce better results. An other important issue is that the model to be verified assumes that the line is catenary at all times. It is therefore desired that the used chain is fairly heavy.

All has led to the choice of a steel chain (DIN-766) with a diameter of 6 mm, which is fairly heavy. In the Laboratory of Fluid Mechanics, Delft , a simple experiment was carried out to measure the submerged weight of the chosen chain per unit length.

Assuming that the specific mass of the water in the tank is ρ_w= 1000 kg/m^3, it was found that the submerged weight of the chain $\underline{p = 6.446\ N/m}$.

5.3.4. Experiment description

To investigate the relative influence of the geometry and pretension is on the mooring line damping, the following testing strategy has been designed. Figure 5.1, on the next page, is a visual guide for the following paragraph.

A chain will be used in this investigation. Thus, the geometry of the mooring is determined by the relative position of the top end of the line to its anchor point. As all line parameters are fixed, the pretension at the top end can be calculated by solving the catenary equation, as presented in chapter 4. And, vice versa, the position of the top end can be calculated by solving the same equation if the pretension at the top and the position of the anchor point are known.

At first, two extreme positions of the top end of the line are determined. The first one is determined by considering a very low pretension, so that the catenary shape of the line is in its "slackest" form (See figure 5.1 - position no. 1). The second position will be determined by the maximum loading-capacity of the dynamometers, using a safety factor of 2 to account for additional dynamic forces during the experiment. (See figure 5.1 - position 9).

The distance between the extreme top end positions is then divided into eight equal parts. The nine points obtained will be the top end positions of nine different geometrical configurations.

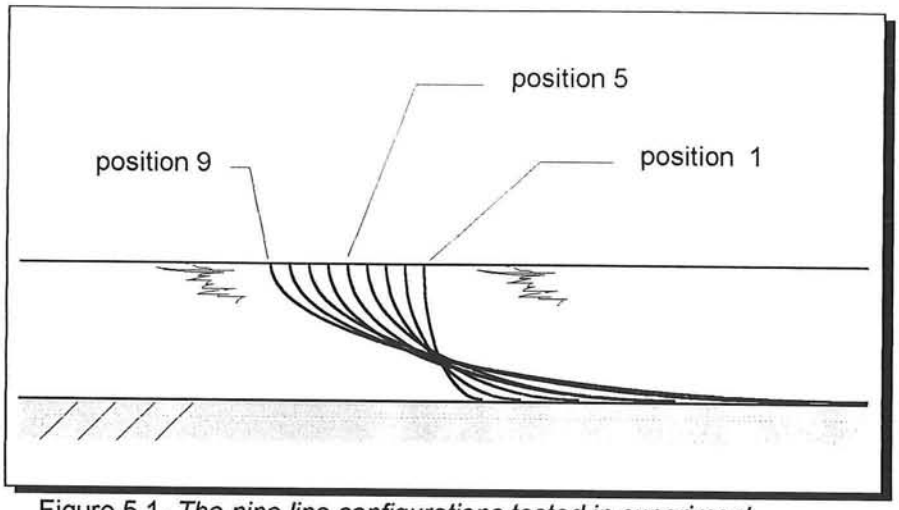

Figure 5.1- *The nine line configurations tested in experiment*

Next, for each top end position a series of tests will be executed in which the top end (fairlead) will be oscillated sinusoidally in the plane of the mooring line, with the amplitude and the frequencies systematically varied.

5.3.5. Model Set Up

The chosen 6 mm chain will be used in of the current investigation. The anchor point of the line is fixed on the tank-floor. This means that the catenary shape of the mooring line can only be varied by changing the horizontal pretension of the line at the top end. As said, this will be done by changing the top end position.

In order to save time in executing the tests, a second chain, equal to the first one, will be attached to the oscillator, in the opposite direction of the first line. (See figure. 5.2)
.

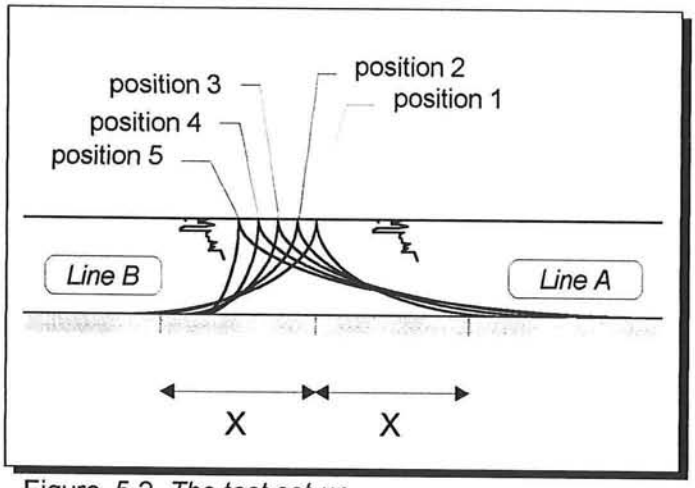

Figure. 5.2. *The test set-up*

The top end position number 1 in figure 5.2. coincides with position 5 in figure 5.1. This means that in position 1 both lines A en B, will have identical configurations. When the top end is moved to position 5, line A will be in the maximum loading position, determined by the maximum load capacity of the dynamometers, while line B will be in the slackest position, determined by a very low pretension.

The result of this set-up is that two configurations are tested simultaneously, which allows US to do twice as many tests within the same time.

5.4. Scaling analysis

5.4.1. General equations of motion of the mooring line

The mooring line is modelled as a uniform line of zero flexural rigidity. This assumption is relevant, since we will be using a chain. The line particulars like (submerged) weight and diameter are considered to be constant. The line element can be schematised as in the figure below. The line element is drawn with a circular cross-section. This is purely hypothetical, in order to account for a certain surface area, blocking the flow. The diameter used is the one the drag coefficient will refer to.

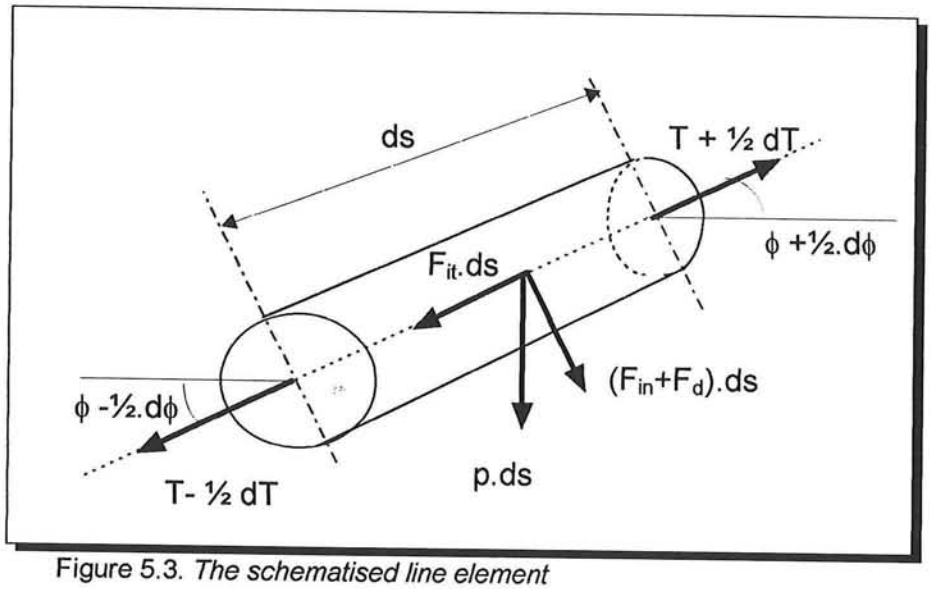

Figure 5.3. *The schematised line element*

The equations of motion in both the tangential and normal direction to the line element as shown in figure 5.3. read:

$$\frac{\partial l'}{\partial s} = p\sin\phi + F_{it}$$
$$T\frac{\partial \phi}{\partial s} = p\cos\phi + F_{in} + F_d \qquad (5.1)$$

In which :

T	=	tension in the line
p	=	submerged weight of mooring line per unit length
F_{it}	=	total tangential inertia force
F_{in}	=	total normal inertia force
F_d	=	drag force normal to the line

The experiment focuses on the hydrodynamic interaction between the line and the surrounding water due to transverse motions of the line. Therefore the equation of motion normal to the line (second equation of 5.1) will be used to find the necessary scaling rules.

The complete equation of motion normal to the line, when the full expressions of the inertia and drag force are used, reads :

$$T\frac{d\phi}{ds} = p\cos\phi + D^*\eta_0{}^2(s)\omega^2\cos^2(\omega t)$$
$$-m(1+\frac{\rho_w}{\rho_s}C_A)\eta_0(s)\omega^2\sin(\omega t) \qquad (5.2)$$

The following expressions are substituted in this equation:

$$F_d = \frac{1}{2}\rho_w dC_D(\frac{\partial\eta}{\partial t})^2$$
$$F_{in} = m(1+\frac{\rho_w}{\rho_s}C_A)\frac{\partial^2\eta}{\partial t^2} \qquad (5.3)$$
$$D^* = \frac{1}{2}\rho_w dC_D$$
$$\eta = \eta_0\sin(\omega t)$$

In which:

C_D	=	drag coefficient
C_A	=	added mass coefficient
m	=	mass of line per unit length
$\eta(t)$	=	displacement of the line normal to its axis
η_0	=	amplitude of $\eta(t)$
d	=	nominal diameter

Remark : The diameter of a cylinder equals its nominal diameter. The nominal diameter is the one the drag coefficient refers to. In the case of different types of mooring lines, d represents a measure of a surface area 'blocking' the flow. The drag coefficient is then related to d. There are several procedures available for the approximation of dC_D for a chain. This will be treated further in chapter 6.

5.4.3. Dimensionless numbers

Making use of the equation of motion normal to the axis of the line element, it is possible to state two dimensionless numbers.

The first one is the ratio between the magnitude of the drag force and the magnitude of inertia forces of the line with both the mass of the line and the added mass of the surrounding fluid. The drag-inertia ratio reads:

$$\beta = \frac{\hat{F}_d}{\hat{F}_{in}} = \frac{D^*\eta_0{}^2(s)\omega^2}{m(1+\frac{\rho_w}{\rho_s}C_A)\eta_0(s)\omega^2} = \frac{D^*\eta_0(s)}{m(1+\frac{\rho_w}{\rho_s}C_A)} \qquad (5.4)$$

For practical situations this ratio is much larger than unity [Polderdijk, 1985]. This implies that the inertia forces in prototype situations can be neglected with respect to

the damping forces due to drag. In the model situation however, we will have to investigate the influence of inertia on the measured line tension.

The second number to consider is the ratio between the magnitude of the drag force and the (submerged) weight of the line. The drag - weight ratio reads:

$$\mu = \frac{\hat{F}_d}{p} = \frac{D^* \eta_0^{\,2}(s)\omega^2}{p} \qquad (5.5)$$

The two components (drag force and submerged weight) in this ratio are considered to be the dominating contributors to the line tension in prototypes, since inertia does not play an important role in practical situations. Therefore, it will be clear that the time scale has to be derived from this ratio.

5.4.4. The scale formula in the model

The scale of the 'drag-weight ratio' (μ) in the model should be equal to unity. Therefore it will be possible to derive an expression for the time scale.

n_t = time scale
n_L = length scale
$n_{\eta\rho(s)}$ = n_L
n_p = scale of submerged weight
n_ω = n_t^{-1}
n_d = scale of chain diameter
n_{D^*} = n_d

If we substitute the scales of all parameters into equation (5.5), we find:

$$\boxed{n_\mu = 1 \Leftrightarrow \frac{n_d n_L^2 n_t^{-2}}{n_p} = 1 \Leftrightarrow n_t = \sqrt{\frac{n_L^2 n_d}{n_p}}} \qquad (5.6)$$

5.4.5. Characteristic Prototype Parameter Values

The nature of the proposed experiment requires concessions to be made with regard to the scales used. It is not possible to present a clear geometrical scale, since applications can be considered to relate to water-depths ranging from 50 m to 500 m.

The characteristic submerged weight in prototype ranges from 500N/m to 6000N/m. The corresponding diameters of chains are between 26 mm and 200 mm. In order to guarantee the catenary shape of the model-line, it has been necessary to use a line which is "fairly" heavy. An important aspect which determined the choice of model-chain is the flow-regime in the model versus prototype situations. In order to obtain comparable results, the characteristic diameter of the model must be fairly large, so that the streamlines of the flow around the model line separate, like they do in the prototype situations.

Especially the time scale is of interest in this experiment. In practice, the LF-surge-motions have periods in the range of 100 s - 300 s. It is very dependent on the location and structure-type which resonant period occurs. Therefore it will be necessary to investigate a large range of frequencies.

Finally, the representative resonant surge-amplitudes in prototype situations are in the range of 1% - 10% of the local waterdepth.

5.4.6. Parameter scale-range and values proposed for the model

It will be clear that it is impossible to give exact scales and parameters. In the following the choices will be made with regard to the parameters mentioned in the previous paragraph. The waterdepth in the towing tank will be fixed at 1400 mm. Therefore the length scale n_L will be between 1/360 and 1/36.

Next, the choice has been made to use the DIN-766 chain, which has a diameter of 6 mm, and a submerged weight of 6.446 N/m. This chain is slightly heavier than scale-rules would imply. This is done deliberately in order to be sure that the chain stays in a catenary shape at most times. The submerged weight scale, n_p , will be in between 1/1000 and 1/100. Also, the chain diameter scale will range from 1/33 to 1/4.

The amplitude in prototype situations varies between 1% and 10% of the local waterdepth. This means that the tested surge amplitude should vary between 14 mm and 140 mm.

Except for the time scale, all parameter scales (ranges) are fixed in the model. Making use of the derived scale formula in the previous paragraph, we are able to find a scale range for the time as well, using firstly the maximum of the scales and then the minima of the same parameter scales we than get:

$$n_{t,\max} = \sqrt{\frac{(1/36)^2 \cdot 1/4}{1/1000}} = 0.439 \approx 0.44$$

$$n_{t,\min} = \sqrt{\frac{(1/360)^2 \cdot 1/33}{1/100}} = 0.0048 \approx 0.005 \qquad (5.7)$$

Making use of these derived time scale maximum and minimum values, we see that the range of the periods in the model should vary between 0.5 s and 132 s.

5.4.7. Summary

Parameter	*Scale range*	*Model-value*
waterdepth [m]	1/360 < n(L) < 1/36	1.40 m
subm. weight line [N/m]	1/1000 < n(w) < 1/100	6.446 N/m
chain diameter [mm]	1/33 < n(d) < 1/4	6 mm
LF-motion period [s]	1/200 < n(t) < 1/2	0.5 s < T < 132 s
horiz. amplitude top [m]	1/100 < n(x) < 1/10	0.014 m < x < 0.14 m

Table 5.1. *Parameter scale and value-ranges in model*

It must be noted that the chosen model will not be representative of all prototype situations, particularly for the cases in which the scale formula results in low periods (i.e. high frequencies) of oscillation. In these circumstances, quasi-static behaviour of the model-line will not occur.

5.5. Influence of inertia forces in the model

As said earlier, the magnitude of the inertia forces in the model has to be examined. A simple way to investigate the influence of these forces is to make an estimation of the value of the dimensionless number β, as stated in paragraph 5.4.3., which is, in prototype situations, much bigger than unity.

The ratio between the drag force and the inertia forces, fully written out, reads:

$$\beta = \frac{\frac{1}{2}\rho_w d C_D \eta_0(s)}{m(1+\frac{\rho_w}{\rho_s}C_A)} \qquad (5.8)$$

The numerical values of all parameters, except for $\eta_0(s)$, are fixed in the model. The following (estimated) values are taken into account :

ρ_w = 1000 kg/m^3
ρ_s = 7900 kg/m^3
p = 6.446 N/m
d = D = 0.006 m
g = 9.81 m/s^2
C_D = 3.5 [-]
C_A = 2.6 [-]

It is noted that the mass m (per unit length) can be expressed in terms of the submerged weight p, namely by :

$$m = p.\left(\frac{\rho_s}{\rho_s - \rho_w}\right).\frac{1}{g} \qquad (5.9)$$

Substituting all the known values for the different parameters in equation (5.8), we find the following expression for β:

$$\beta = 2.625 m^{-1} \eta_0(s) \qquad (5.10)$$

The following conclusions can be drawn from expression (5.10), if one notes that $\eta_0(s)$ in the model will be (roughly) in the range of 0.01 m to 0.5 m :

1. In all cases in the current experiment, the inertia forces play an important role in the instantaneous values of in-line tension. In quasi-static situations, however, the inertia forces are out of phase with the damping forces on the line. Thus, the influence of inertia will not be noticeable in the calculation of the energy dissipation.

2. The influence of inertia decreases with increasing amplitude of transverse motion of the line and, thus, also with increasing horizontal amplitude of the LF-motion of the top end of the line.
3. The drag-inertia ratio is independent of the frequency of the forced top end oscillation.

The relative influence of inertia on the calculation of energy dissipation will be demonstrated by performing dry oscillation tests at all top end positions.

5.6. Actual Experiment set up

5.6.1. Dimensions of chain legs in set up

As stated above, two lines are installed. This set-up has the advantage that in every test run actually two experiments are carried out simultaneously. In order to obtain comparable results for both lines, it will be useful if the dimensions of the chain legs are, as much as possible, the same.

Two problems made it difficult to pre-determine the exact top end positions. The first is that the exact size of the different attributes, like for instance the extension- and angular connection-pieces, were difficult to account for. The second is the possible error in measuring the height of a top end above floor level, due to inaccurate measuring devices (use has been made of a plummet).

After taking into account the restrictions and difficulties, as mentioned earlier, the following configurations of the chain legs were found (See figure-5.4 as a guidance).The position of the carriage was about 25 m from the wave-generator and 50 m from the beach, at the spot where windows are installed in the walls of the towing tank. Two lines are installed, line A from the carriage towards the wave-generator and line B towards the beach.

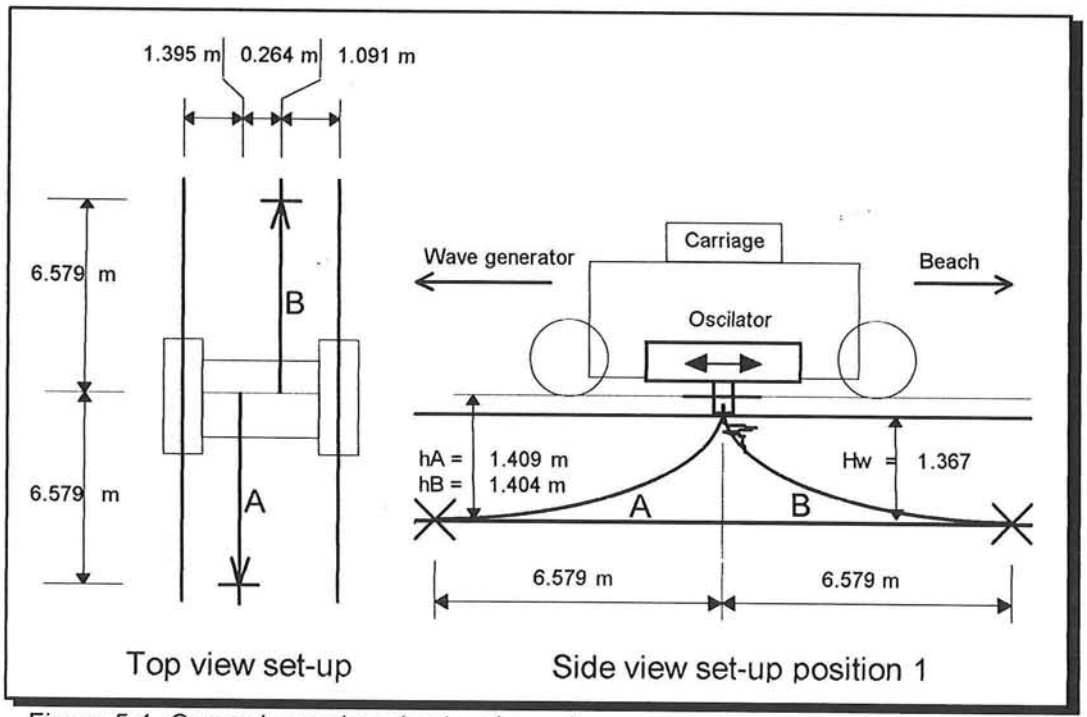

Figure 5.4. *General experiment set up lay-out.*

The two top end positions are determined by the positions of the dynamometers and hook on the oscillator. After installation it was determined that the heights of the two top ends are 1.409 m and 1.404 m for line A and line B respectively. The distance between the top ends is 0.264 m. Making use of a plummet, the top end positions were marked on the tank-floor. The anchor points were determined, by calculation of the catenary equation, with the measured horizontal pretension in positions 1, at a distance of 6.579m from the plummet marks.The total line length is 7m.

5.6.3. Installed equipment

An oscillator is used to obtain the desired sinusoidal motion of the top end. The oscillator is powered by direct current. The frequency of the oscillation is controlled by the setting of the potentiometer. By changing the eccentric arm setting of the oscillator, the amplitude of motion is set.

In order to record both the horizontal and the vertical forces at the top end, use has been made of dynamometers with a loading-capacity of 400 N each. These measure a difference in the electrical current, while being loaded. To measure and record these (very small) differences by computer, it is necessary to amplify this signal. Thus, when four dynamometer are used (Line A -F_x & F_z and Line B- F_x & F_z), also four amplifiers are needed. The signal then goes through a data filter, which is set at 20 Mhz to eliminate noise caused by the systems circuits, to an A/D-converter. Finally, the signal goes into the computer, where the calibration factor 'transforms' the signal into the desired quantity.

The connection of the top end of the chain to the dynamometer is ensured by the specially made hook-connector. The illustration below presents the construction of the top end-dynamometer-oscillator connection.

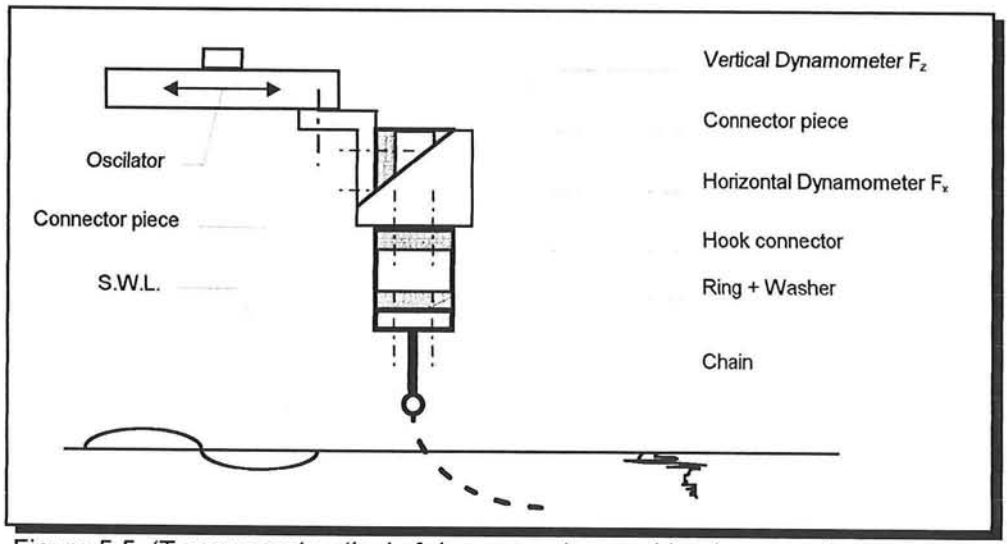

Figure 5.5. *'Tower construction' of dynamometers and hook-connector*

5.6.4. Calibration of dynamometers

A dynamometer is in fact a large form of a Wheatstone bridge (electrical connector - see figure-5.6 below). Due to loading, the beams will bend and cause four electrical

resistances (R_i) to change. To be able to measure loads in the set-up, it is necessary to find a relationship between the measured voltage change by the dynamometer (i) and the applied load.

The calibration now goes as follows. The change of current is measured when the dynamometer is loaded by a mass of 1 kg. This will be repeated for several masses and in both opposite directions. There are two conclusions to be drawn form these tests with respect to the dynamometer set-up: the loading direction (sign) and the linearity of the calibration factor. If all is well, the system is linear and the calibration factor (with sign) may be entered into the computer.

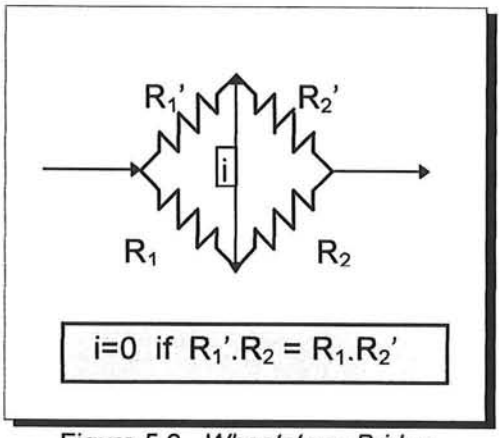

Figure 5.6. *Wheatstone Bridge*

One should take care that the chosen combination of amplifier, cables and dynamometer remains fixed during the entire experiment (labelling !). This means that the failure of one item of a dynamometer-system leads to the re-calibration of a completely new system. Fortunately, this has not happened during the execution of these experiments.

5.6.5. Determination of top end positions

As said earlier, the whole set-up was 'built' around position 1, since the anchor points were determined from this position. The four remaining points (2..5) are to be located on the 'beach-side' of position 1, so that line A will be tensioned when moving from point 1 to 5.

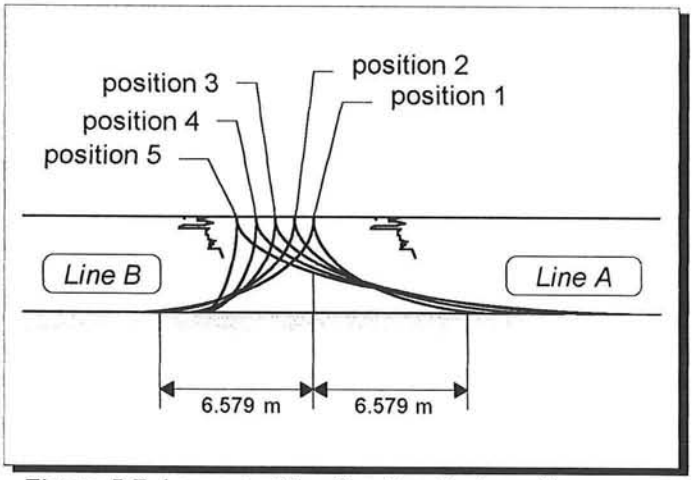

Figure 5.7. Lay-out of the five Top End positions

After reviewing the calculations from the preliminary design, it was found that the five top end positions should be at a mutual distance of 0.0265 m. The top end position is changed by moving the carriage back- and forwards.

A pin was firmly mounted on the carriage pointing at a measuring-line, fixed on the rails of the towing tank. The accuracy that can be obtained in this manner is about 0.0005 m, which is in agreement with the required mutual distances.

5.6.6. Necessary Daily Routines

Every day of testing, the four amplifiers of the dynamometer-signals have to be re-calibrated. This is needed because the zero of the amplifier can drift in time. Also, the capacitive settings of the amplifiers have to be re-checked every day. Due to some change in tension or bending of the electrical cables in the system (from amplifiers to dynamometers) the total electrical resistance can vary as well. In the same manner as the zero settings are changed, this problem can be accounted for by changing the capacitive setting of the amplifier.

5.7. Testing programme

5.7.1. Introduction

The intent is to propose an experimental programme which covers a wide range of practical mooring situations. As said earlier, the line parameters like weight and diameter are fixed during the entire experiment. Therefore, a test set-up has been designed in which the pretension (position of the top end), the surge amplitude and the surge frequency can be varied (See paragraph 5.5).

Covering all combinations of amplitudes, frequencies and pretensions (top end positions), resulting from the scaling analysis, is impracticable. Therefore, a limitation of the number of the top end positions had already been accounted for. This was done by restricting the number of top end positions to 5 equidistant points (see paragraph 5.6.5).

A restriction on the number of amplitudes and frequencies still has be made. As can be expected, the larger the top end oscillation amplitude will be, the larger the amount of energy which will be dissipated. The same can be said for the oscillation frequency, and vice versa. Therefore, the larger amplitudes and higher frequencies resulting from the scaling analysis will be used in the experiment. Paragraph 5.7.2. focuses on this subject.

Most tests will be performed in quiescent water. For qualitative insight only, a number of tests will be performed in regular waves, as will be described in paragraph 5.7.3.

The main test programme consists of series of test-runs. In each series the 'surge'-amplitude will be fixed, while in every run the frequency and the top end position are varied one by one. In Appendix A, the full logbook of the executed tests is given, with specific data on the settings of the different parameters. Also listed are the dry tests, to investigate the influence of inertia, and a static test, in order to obtain the static load displacement curve.

5.7.2. Choice of Oscillation Frequencies and Amplitudes

The results for the relevant model values of the oscillation parameters are calculated by means of a scaling analysis. These results were presented in the summary of paragraph 5.3.7.

The dissipation of energy is calculated by integrating the product of the instantaneous velocity and horizontal component of the in-line tension over one oscillation period. Thus, the measured velocities and force changes are extremely important. In order to obtain accurate results, these changes may not be too small (in comparison with the accuracy of the dynamometers). Therefore, large amplitudes and high frequencies will probably give the best result.

The amplitudes, resulting from the scaling analysis, vary between 0.014 m and 0.14 m. An arbitrary choice has been made to examine the following five amplitudes: 0.06 m , 0.08 m , 0.10 m , 0.12 m and 0.14 m.
The choice of the frequencies is based on the following. The range of possible oscillation periods is 0.5 s to 100 s. We are again interested in the lower periods (= higher frequencies) because of the desired accuracy of the measurement.

Since the energy dissipation is proportional to the oscillation frequency squared, a logarithmic spreading of the investigated frequencies is assumed to give a good picture of the phenomenon. Starting at the lowest period possible (=0.62 s), determined by the limitations of the oscillator (see paragraph 5.3.2), we chose the following ten periods: 0.62s , 0.8s , 1.0s, 1.6s, 2.0s , 4.0s, 8.0s, 16.0s and 32s.

In some cases we have departed from the initially planned oscillation periods (frequencies). This was done because for high frequencies and large amplitudes, the measured peak-loads exceeded the maximum loading capacity of the dynamometers.

5.7.3. Influence of Waves

A number of experiments were performed in waves. These experiments were merely done for qualitative purposes, in order to investigate the relative importance of gravity waves on the energy dissipation.

Gravity waves with periods of 1s to 30 s are responsible for the WF-motions of the floating structure. The influence of gravity waves on LF-mooring line behaviour including mooring line damping should in fact be considered including the effect of WF-motions of the top end of the line. This was not done.

The LF-periods in prototype situation vary between 100 s and 300 s. Therefore, the ratio between LF- and WF- periods lies between 3 and 300. The wave period in the tank was set at 1s, with heights of 0.05m and 0.10m.

The oscillation periods were: 0s , 2s , 4s, 8s and 16s. These tests are listed in the logbook with the remark 'WAVE'.

6. Experimental Results

6.1. Introduction

This chapter presents the results of the executed experiments. The testing programme has been highlighted in paragraph 5.7, while the full logbook of the executed experiments can be found in the appendix. In total, 269 test runs have been carried out, each testing lines A & B simultaneously. Thus, some 538 individual tests have been executed.

The results will be presented for two test cases, both with top end position 5, having oscillation amplitudes of 0.06 m and 0.10 m. These cases were tested for more than 10 oscillation frequencies, which provides a better picture of the results. All other results for unperturbed water conditions are listed in Appendix B.

In order to determine the static in-line forces in all top end positions, a static load-displacement diagram was obtained form a simple test. This will be treated in paragraph 6.2. The results of the actual experiment programme, for the verification of the model of Huse (1986), are the topic of paragraph 6.3. As said, a qualitative investigation is performed of the influence of waves on the energy dissipation. The results of these tests are described in paragraph 6.4. In paragraph 6.5, the results of the so called dry-tests are presented for the determination of the relative influence of the inertia forces on the energy dissipation in the model. Finally, some general observations during the experiments are presented in paragraph 6.6.

6.2. Static Load-Displacement Test

In view of time-management during the execution of the experiment, it was considered inconvenient to measure the pretension before each test run. In order to determine the pretension at the top end, the static load-displacement curve provides the solution.

To cover all cases that will be investigated during the experiment, a 'quasi-static' oscillation has been performed in RUN no.16, with the top end in position 1. The oscillation has an amplitude of 250 mm and a period of 305 s. The measured time was 320 s with a sample time interval of 0.612 s. The figure below gives the results for the static load-displacement characteristic of line A.

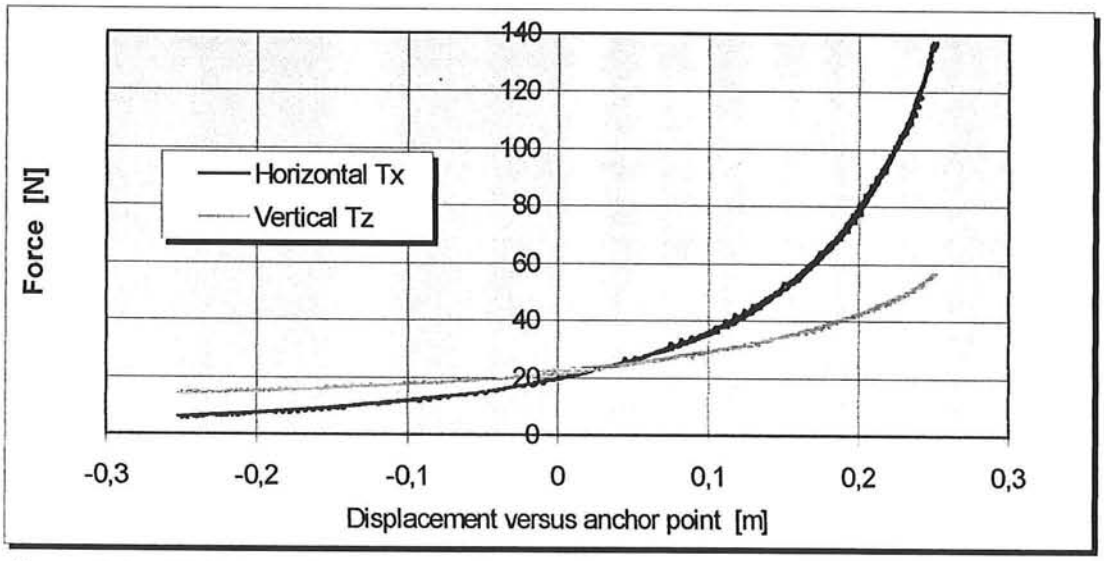

Figure 6.1. : *Static load-displacement diagram -line A*

As can be seen from the static load-displacement diagram, the top end displacement is measured relative to the reference point of position 1 (this is the zero of the oscillation). If one remembers that position 1 is the top end position halfway between the anchor points of the lines A and B, it is straightforward to calculate the horizontal distance of each top end position to the anchor points of lines A and B.

It is considered inaccurate to determine the pretensions at all top end positions by reading the static load displacement diagram directly. Therefore, use has been made of the numerical output of the quasi-static test. By means of interpolation between two sample-values of both the horizontal and the vertical forces versus the reference signal (which represents the top end displacement from position 1), accurate results for the pretensions can be obtained.

The table below gives the outcome of such a calculation for both lines at all top end positions. The horizontal distances (x) of the top end of each line to its anchor point have been included. For completeness, the elevations (h) of the top end have also been recorded, since they are not the same for line A and line B.

Top-end	Line A Tx [N]	Tz [N]	x [m]	h [m]	Line B Tx [N]	Tz [N]	x [m]	h [m]
1	19.988	22.334	6.5790	1.409	19.699	21.357	6.5790	1.404
2	22.940	24.015	6.6055	1.409	17.069	20.576	6.5525	1.404
3	26.905	25.786	6.6320	1.409	14.892	19.469	6.526	1.404
4	31.721	27.831	6.6585	1.409	12.642	18.097	6.4995	1.404
5	37.951	29.895	6.6850	1.409	11.587	17.329	6.4730	1.404

Table-1. *Static line data of lines A&B for different top end reference positions*

In a later stage of the investigation, use will be made of dimensionless numbers to describe the different line-configurations. The results presented in table-1 will serve as the basis for these descriptions.

6.3. Results of Oscillation Experiments in Still Water

These tests form the major part of the current investigation. The emphasis is on the determination of the dissipated energy per period of oscillation.

6.3.1. Recorded Data Signals

As planned, five signals were recorded during each test run. Of both lines, the horizontal and vertical components of the in-line tension were measured at discrete times. The fifth signal is the reference, this is the phase of the sinusiodal oscillation at the discrete times. The sample time interval (Δt) was 1/500 of the measured time. It was decided to record 10 full periods of oscillation, except for the longer periods. For an oscillation period of 16s, 5 full periods were measured, while for a period of 32 s, 2.5 full periods were recorded.

As an example, the recorded signals of RUN 84 are presented below. The figures present the results of the measured horizontal (T_x) and vertical (T_z) components of the in-line tension ($T = \{T_x^2 + T_z^2\}^{1/2}$) for respectively line A and line B. In both figures, the reference signal is plotted as well.

Run 84 Data :		
	Top end position	: 5 (lines A & B)
	Amplitude	: 0.10 m
	Measured frequency	: 3.927 rad/s
	Measured period	: 1.600 s
	Recorded time	: 16 s
	Sample time	: 32 ms

The measured results for line A are:

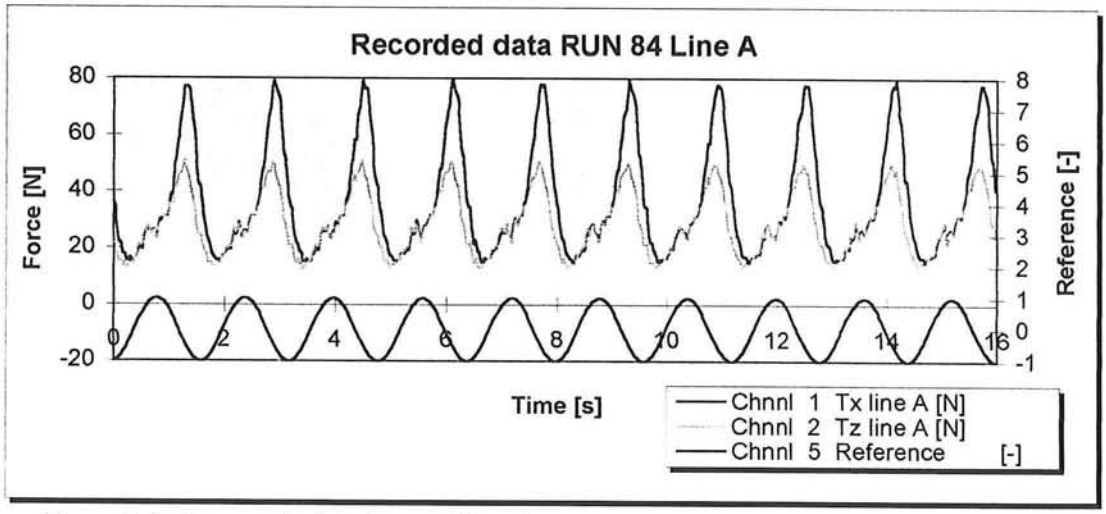

Figure 6.2. *Recorded data Run 84 Line A*

It is interesting to see that the highest and lowest extremes occur near the zeros of the reference signal. At these stages of the oscillation, the top end velocity is the highest. Since damping forces are in phase with the velocity, thus in counter-phase

with the reference, one can make the provisional conclusion that damping forces are dominant in these force signals.

When looking at the results of line B, one finds the following:

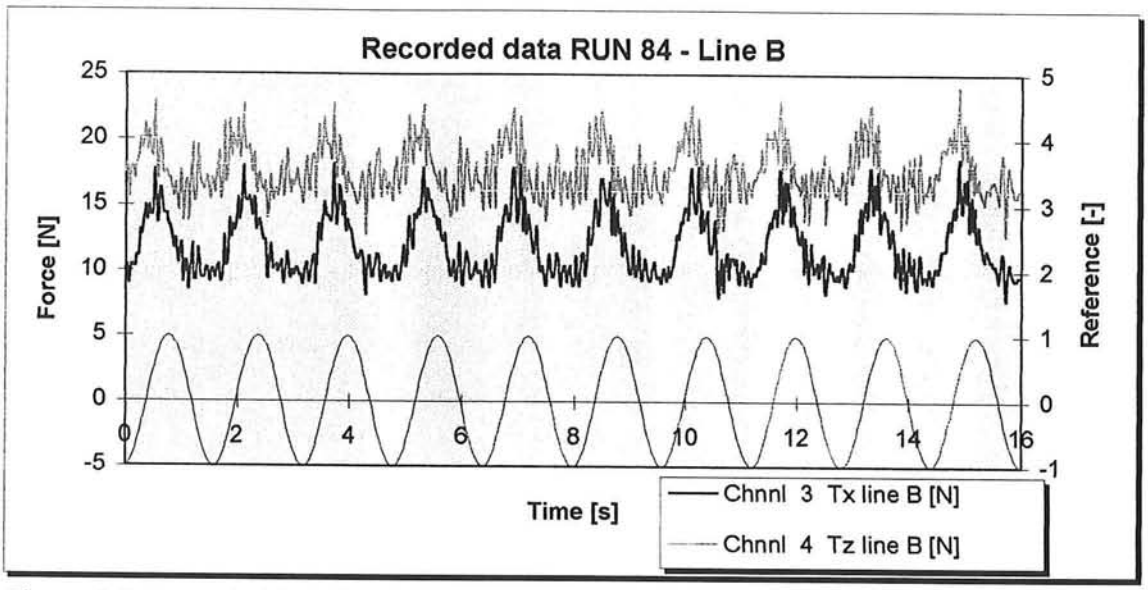

Figure 6.3. *Recorded data Run 84 Line B*

The graph of figure 6.3. shows a much more capricious pattern. Also, the extremes in the measured force signal-pattern seems to fall together with the extremes of the reference signal, which is the phase of the top end displacement. This means that the influence of inertia and restoring forces, due to the effective stiffness of the line are dominant in the measured magnitude of the forces, compared to the damping forces. Thus, the relative influence of inertia is dependent on the (horizontal) pretension. An increasing pretension leads to a decreasing relative influence of inertia. This is in good agreement with the statement of paragraph 5.5 , where the influence of the inertia forces was investigated by means of a 'drag-inertia' ratio.

6.3.2. *Hysteresis of Dynamic Load-Displacement Diagram*

The calculation of the energy dissipation was described in paragraph 5.2. It is emphasised that only the measured horizontal component of the in-line force (T) is participating in the calculation of the dissipated energy per period. The figures below present the dynamic load displacement diagrams for RUN 84.

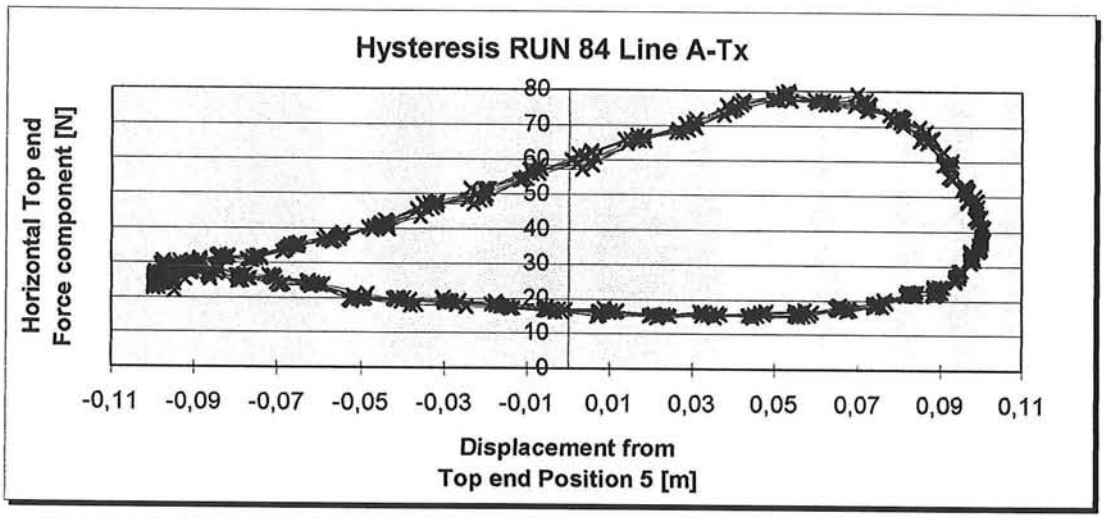

Figure 6.4. *Hysteresis in Dynamic load displacement diagram for RUN 84 line A*

The dissipation of energy can be visualised by the Hysteresis of the dynamic load displacement diagram. In fact, the dissipated energy is proportional to the enclosed area in the dynamic load-displacement diagram. In the ideal case, where inertia forces are negligible, the dissipated energy equals the surface of this area.

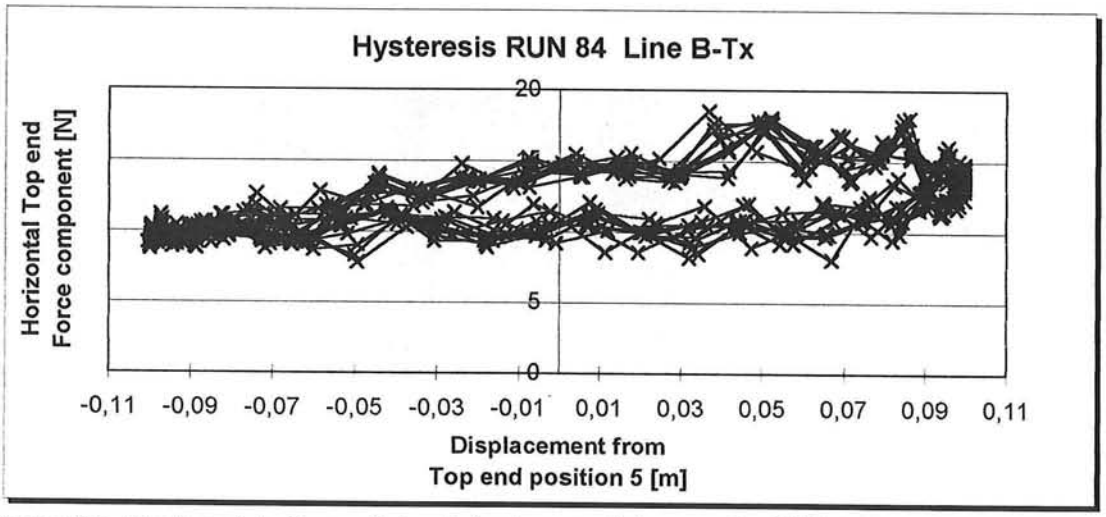

Figure 6.5. *Hysteresis in Dynamic load displacement diagram for RUN 84 line B*

The difference between the dynamic load displacement diagrams for lines A and B is clear. For line A, the results show a smooth curve, while for line B, the hysteresis is not accurately determined. This is a result of the capricious nature of the measured signals for line B.

6.3.3. Calculation of Dissipated Energy

In paragraph 5.2, the method of determining the Energy Dissipation per period (E_{diss}) in the experiments was explained. We will derive the expression for the calculation of E_{diss} in the following:

Work can be expressed by :

$$A = \int \vec{T} \bullet \vec{v} dt \qquad (6.1)$$

The force (T) and velocity (v) are vectors, as a function of time, and the integration variable is time.

In the executed experiments, the top end oscillation (surge) velocity is directed along the (horizontal) x-axis only, in the plane of the line at rest. Thus, for the calculation of the scalar product in equation (6.1), only the measured horizontal force (T_x) is needed.

The work done by the oscillator per period, E_{diss} , can now be calculated as follows :

$$E_{diss} = \frac{1}{n} \int_0^{n.TE} T_x . v_x dt \qquad (6.2)$$

In which:

TE	: period of top end oscillation
n	: number of periods measured (= integer!)
T_x	: horizontal force component as function of time
v_x	: top end velocity in x-direction
t	: time

Since we have the measured forces and velocities only at (k) discrete times, a numerical integration will be performed for the calculation of E_{diss}. The expression for the numerical calculation of E_{diss} is in the following form:

$$E_{diss} = \frac{1}{n} \sum_{i=1}^{i=k} (F_{xi} . v_{xi}) \Delta t \qquad (6.3)$$

In which:

Δt	: sample-time
k	: number of samples $k = nTE\ \Delta t$
F_{xi}	: Measured horizontal force component at $t = i\ \Delta t$
V_{xi}	: instantaneous velocity (proportional to differential of reference signal)

As can be seen from the expressions above, the measuring time always has to be an integer number of oscillation periods. In those cases where the recorded time differs from this demand, a correction to the recorded data has been made, such that only an integer number of oscillation periods is considered.

6.3.4. Measured Energy Dissipation

As said in the introduction, the results of all (50) tests concerning position 5, with amplitudes 0.06 m and 0.10 m will be presented here. The procedure of paragraph 6.3.3. is carried out with the aid of a spreadsheet program (MS-Excel).

The results for all other executed experiments are given in Appendix B. All results show the same, smooth pattern.

The results for position 5, amplitude 0.06 m are obtained from RUNS no. 60-79. Figure 6.6. presents these results for both lines A & B. The results for position 5, amplitude 0.10 m are obtained from RUN no. 80-89 and 140-159. Figure 6.7. presents these results for both lines A&B.

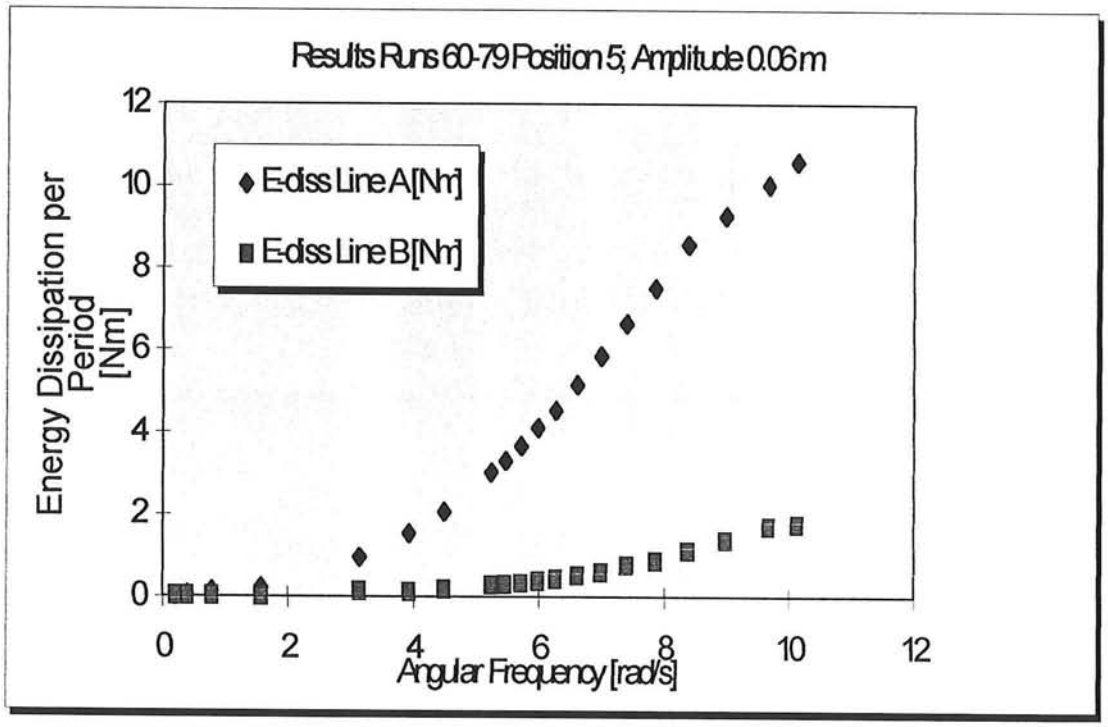

Figure 6.6. *Energy Dissipation per period , position 5 and amplitude 0.06 m*

In all test runs, the reliability of the numerical results for the (very) low frequencies (ω <1 rad/s) may be doubted. The dynamic tension fluctuations in these cases are in the order of 0.1 to 0.01 % of the application range of the dynamometers. The accuracy of the measured signals is therefore most likely to be poor. One can imagine that the hysteresis in these cases is so small that an accurate determination of the dissipated energy is nearly impossible under these circumstances.

Also, for the low frequencies, the relative influence of inertia becomes noticeable and the calculated energy dissipation will be somewhat higher than would have been expected, as will be shown in paragraph 6.5.

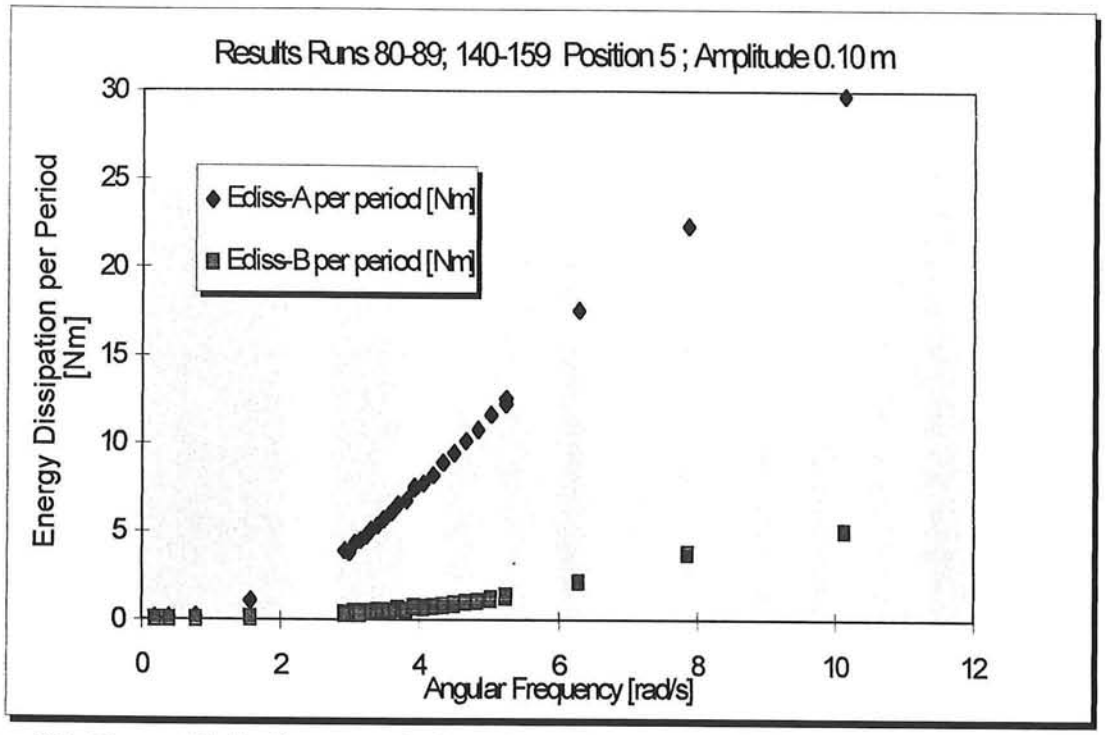

Figure 6.7. *Energy Dissipation per period , position 5 & amplitude 0.10 m*

The figures 6.6 and 6.7 make it clear that energy dissipation per cycle increases with increasing amplitude, frequency and/or horizontal pretension. This result is straightforward, if one investigates the derived formula for the calculation of energy dissipation (eq. 4.22).

6.4. Influence of waves

Some series of tests were performed under wave conditions (Runs 300 to 339). As said, the purpose of these tests is qualitative only. The simulated periods of the LF-surge motions have prototype values between 50-300 s, while the considered gravity waves have periods ranging from 1 to 30 s. So, the ratio between the LF-top end motion periods and the wave periods varies from 1.67 to 300.

For practical use, the wave-generator was set to make waves with a period of 1s. Test were performed for two wave heights : 0.05 m and 0.10 m. The investigated ratios of the oscillation period versus the wave period were 2,4,8 and 16. The results for position 1 and 5 are presented in the following figures. (Runs 300-305 and 320-329).

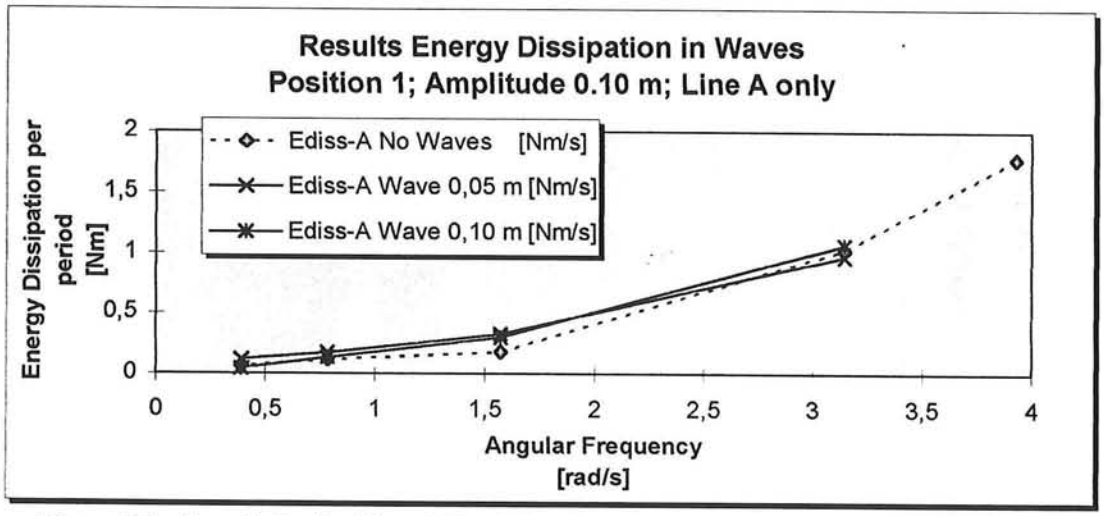

Figure 6.9. *Results for Position 1 (line A) in Waves*

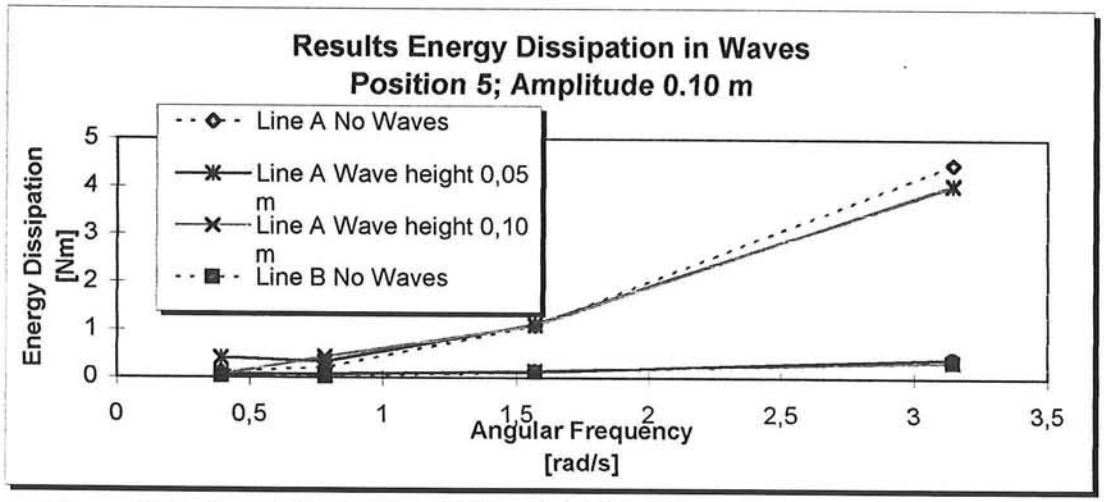

Figure 6.10. *Results for Position 5 (lines A & B) in Waves*

As can be seen from the two graphs, the influence of gravity waves in the cases shown is negligible on the energy dissipation for LF-top end oscillations. One must note that the wave frequency (WF) motions of the top end are not included. The influence of these top end motions will have to be evaluated.

6.5. Calculation of Energy Dissipation in 'Dry-Tests'

In chapter 5, paragraph 5.5, a simple parametric study has been performed in order to quantify the relative influence of the inertia forces in the model, compared to the viscous damping forces. It was stated that inertia forces could play an important role in the measured in-line tensions of the model. In prototype situations, however, the influence of inertia forces for LF-top end motions can be neglected [Polderdijk, 1985].

Since the experiments have been carried out with a fairly heavy chain, the influence of inertia forces on the measured in-line tension fluctuations may be considerable. However, this experiment is concerned with the calculation of energy dissipation due to a top end motion of the line. The calculation procedure for energy dissipation per cycle, described in paragraph 6.3.3, uses the measured horizontal component of the in-line tension (T_x). Since T_x contains a contribution due to inertia effects, it is essential that the influence of this 'inertia-contribution' on the energy dissipation is investigated. This has been investigated qualitatively by performing so called 'dry-tests'.

During the dry-tests, the top ends of the lines were subjected to an oscillation test, while the tank was empty. The presented calculation procedure, described in paragraph 6.3.3, for the determination of the dissipated energy has been applied to these measured force signals. For top end position 5, amplitude 0.10 m, the following results were obtained:

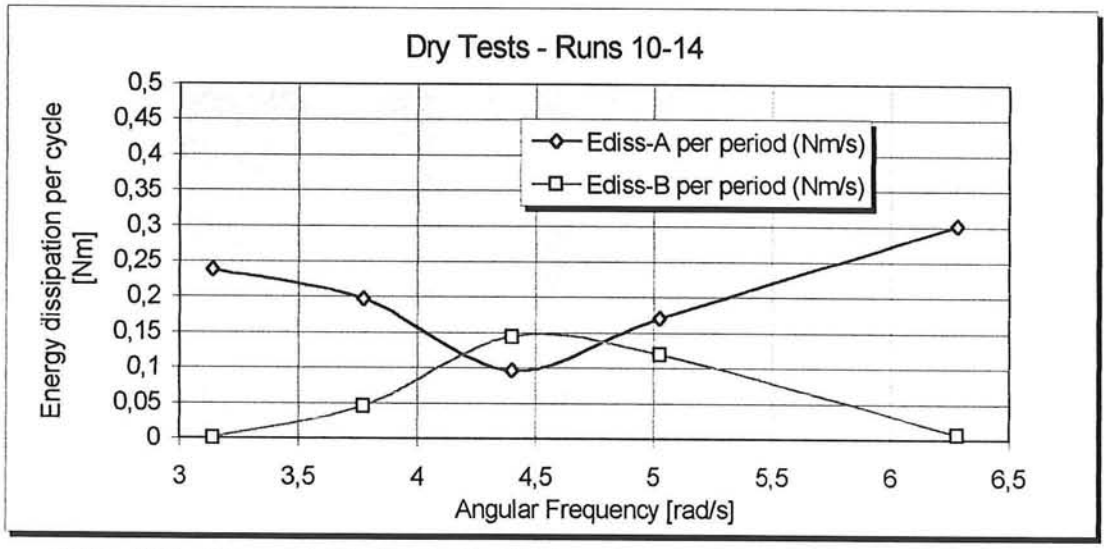

Figure 6.11. *Energy dissipation in Dry Tests*

The results for tests in water at position 5 and with amplitude 0.10 m were presented in paragraph 6.3.4. If we examine the obtained results in figure 6.11, we see that the energy dissipation does not exceed 0.3 Nm.

1. The relative influence of inertia on the amount of measured dissipated energy increases, with *decreasing* horizontal top end pretension.
2. The relative influence of inertia on the amount of measured dissipated energy increases, with *decreasing* frequency of the top end oscillation.

The relative influence of inertia on the energy dissipation will be noticeable in the results for Low Frequencies, especially for the cases with lower horizontal pretension.

6.6. General Observations during Experiment

6.6.1. Vortex induced vibrations

In paragraph 3.2.4, it was mentioned that due to vortex-shedding along the line a lock-in situation could appear, causing a vibration of the entire line. Especially with (steel) wire ropes this would be the case. There was not a clear conclusion about chains. These 'vortex induced vibrations' (V.I.V), perpendicular to the general line motion, would increase the drag-resistance considerably. Therefore, these motions would lead to a higher energy dissipation per period.

As one can imagine, the streamlines separate quite randomly along the chain mooring line (due to edges and corners of the links), while for a smooth line the pattern is more predictable. This will give the first indication that V.I.V.-motions are not expected in the case of a mooring chain.

There has been special attention to this phenomenon. Since a Fourrier analysis of the measured force signal gave a large number of components, it was impossible to make a clear statement. But, since the V.I.V.-motions would have an influence on the dissipated energy per period, the graphs of the calculated results for the dissipated energy should show some kind of discontinuity or a change in pattern in the frequency range at which the V.I.V. motions start. This does not occur in our tests; the dissipated energy versus period curve shows a very smooth pattern.

Also, during each test run, the possible occurrence of V.I.V.-motions has been checked visually. In none of the executed tests a motion or vibration has been noticed. Therefore, considering all mentioned arguments, one has to make a provisional conclusion that no lock-in situations, thus no V.I.V.-motions, occur in the case of a mooring chain.

The phenomenon of drag amplification, due to VIV-motions of the line, could be of major importance to the total energy dissipation. Especially for smooth cables, the influence of vortex induced vibrations is assumed to be important , since in these cases lock-in situations are more likely to develop [Triantafyllou, 1994]. Additional investigation on this matter would be very interesting.

6.6.2. Chain damage

After five weeks of testing, the difference between the two used lines was significant. Chain-line A was far more corroded than line B. Also, the damage on the chain of line A was higher than of line B. The galvanised protection layer on the chain was completely gone.

6.6.3. Damage of attachment hook

The attachment hook provided the connection between the top end of the chain and the dynamometers. The pin with length of 65 mm was twisted slightly. The top end of the pin for line A was deflected for almost 3 mm, while the pin for line B was only deflected for 1 mm.

These plastic deformations for the pin of line A are most likely to have occurred during the tests at position 5, with an amplitude of 0,14 m at high frequencies. Unexpectedly high peak-line tensions in the order of 800 N occurred in line A. This was most likely to have happened in RUN no. 200. This would imply that the earlier tests where done with almost undeformed pins.

The errors resulting from these deformations are in the order of a few percent. It is most likely that the errors in the cases with low pretension (line B) is less than the cases with high pretension (positions 4 and 5 for line A).

6.6.4. Galloping

The quasi-static oscillation tests dealt with lines which are, at all times, described by the catenary equation. When the top end oscillation frequency becomes too high, galloping motions occur. These motions are dominated by inertia-effects and the limitation of the free-fall velocity of the line in water. These motions cause high peak-loads in the line, when the line is tensioned. When the line is released quickly, the fall-velocity of the line in water is low. The transversale line motion lags behind the top end motion.

The observations during the tests have shown that the transition of quasi-static behaviour to 'galloping' motions, takes place in the range of high frequencies, in the order of 1-2 Hz. It is not yet clear which parameters are also involved in this phenomenon, besides the frequency. It has been noticed that the transition of quasi-static to galloping motions shifts to lower frequencies with increasing pretension (in reference position) or with increasing amplitude of the oscillation.

The theory for the calculation of energy dissipation per period has not been derived for these 'galloping' cases. However, in the next chapter it will be shown that the derived theory nevertheless predicts the energy dissipation in these galloping-situations very well.

Chapter 7. Verification of the Model

7.1. Introduction

The evaluation of the (semi-) analytical model, based on the theory of Huse and presented in Chapter 4, is the topic of this chapter. Therefore, the results of the experiments will be compared with the calculation method presented by Huse (1988) and the method of the current investigation, for which a fully analytical model exists.

The graphical calculation method by Huse and the numerical calculation method of the current investigation are explained in paragraph 4.5. In was observed that the numerical results for the integral in equation (4.22) of both methods differed significantly. Special attention should be paid to this difference.

An important parameter to be estimated from the observations is the product of the dragcoefficient and the nominal diameter. The determination of this product is a typically empirical problem. In order to have a rough estimation of the DC_D-value in the current investigation, two simplified models are presented.

The verification will be based on the assumption that the product of the dragcoefficient and the nominal diameter is a constant in all executed experiments.

Before analysing the theoretical results for the energy dissipation per period, a verification test has to be proposed for the evaluation of the theoretical models.
This will be the topic of paragraph 7.2. The results, obtained by Huse, are treated in paragraph 7.3, while the of the current investigation are presented in paragraph 7.4. Paragraph 7.5 provides a conclusion.

7.2. Test for the Verification of the Model

The derivation of the analytical model for the calculation of energy dissipation per cycle was partly based on the fact that the product (DC_D) of the drag-coefficient (C_D) and the diameter to which it refers to (D) is a constant in each considered situation.

7.2.1. Estimation of (DC_D)-value for Chain

The determination of the DC_D-value for any object is in principle an empirical matter. By means of experiments, the actual DC_D-values should be established for every individual case. However, practical experience has led to a number of approximations (rules of thumb) of this DC_D-value, which will be presented.

- ***Equivalent diameter-method :***

This method calculates the nominal diameter (d_n) for a (steel) cylinder, having the same weight per unit length as the chain-line. This diameter, combined with the flow information in terms of a good approximation of the Reynolds-number, determines a drag-coefficient C_{dn}.

The DC_D-value is now approximated by the following expression:

$$DC_D = \lambda . d_n C_{dn} \qquad (7.1)$$

In which:
- λ : Factor dependent on type of chain ($\approx$ 1.5)
- C_D : Drag coefficient referring to D
- D : Chain diameter
- d_n : Nominal, equivalent diameter of cylinder
- C_{dn} : Drag coefficient referring to d_n

In order to make a good estimation of the DC_D-value, the nominal diameter and the Reynolds number (range) have to be determined. The nominal, equivalent diameter can be calculated from the following formula:

$$\rho_s g \frac{\pi}{4} d_n^2 = p \qquad (7.2)$$

In which :
- ρ_s : 7 900 kg/m^3
- g : 9.812 m/s^2
- p : 6.446 N/m (paragraph 5.3.3)

Thus,

$$d_n = \sqrt{\frac{4 * 6.446\ ^N/_m}{7900\ ^{kg}/_{m^3} * 9.812\ ^N/_{kg} * \pi}} = 0.0103m \qquad (7.3)$$

For the investigated situations, the Reynolds number varies between 200 and 4900. Thus, $C_D \approx 1.3$.

Substituting of (7.1) gives the following a priori estimate for DC_D:

$$\boxed{DC_D = 1.5 * 1.3 * 0.0103m = 0.0201m} \qquad (7.4a)$$

- ***Approximated C_D-value for Chain lines:***

Model tests investigations and experience has led to a quick estimation for the C_D value for all chains: C_D = 2.2 , related to the chain-diameter D. This result is valid for all practical situations. (*Source*: Marin, the Netherlands).

In the our experiments this would lead to:

$$DC_D = 0.006\ m * 2.2 = 0.0132\ m \qquad (7.4b)$$

7.2.2. Verification Test

The theory gave the following expression for the energy dissipation per period:

$$E_{diss} = \frac{1}{6} \rho_w DC_D \omega^2 \int_0^{X_{max}} \frac{(\Delta z(x))^3}{1 + \sinh^2\left(\frac{p}{T_o}(x - x_o)\right)} . dx \qquad (4.22)$$

It was assumed that DC_D is a constant for the practical range of applications. Further more, DC_D has to be a constant in each test run.

The investigated situations had Reynolds numbers between 200 and 4900 and the drag coefficient for nominal cylinders can be assumed constant in all investigated situations ($C_D \approx 1.3$). Thus, the product DC_D for a cylinder has to be a constant in all experiments as well.

Since E_{diss} is calculated in all experiments, as was explained in the previous chapter, the model can be verified by requiring that DC_D is a constant in every experiment. The verification requirement will be derived in the following.

Denote the integral in equation (4.22) as I:

$$I = \int_0^{X_{max}} \frac{(\Delta z(x))^3}{1+\sinh^2(\frac{p}{T_o}(x-x_o))}.dx \qquad (7.5)$$

The value of DC_D can be calculated for every test run by:

$$\boxed{DC_D = \frac{6E_{diss}}{\rho_w I \omega^2}.} \qquad (7.6)$$

The latter expression provides the verification test, which states that for each executed test, the calculated DC_D-value has to be one and the same constant. Preferably, the obtained DC_D-value should be in the range of the calculated values in paragraph 7.2.1 ($DC_D \approx$ *in range of 0.0132 m and 0.0201 m*).

As became clear in the derivation of the expression for the calculation of energy dissipation per period (eq.4.22), the influence of the variable $\Delta z(x)$ (peak to peak motion of the line during surge cycle [m]) is very important. The method of determining this variable will have an important effect on the outcome of DC_D and , thus, also on the result of E_{diss}, as was discussed earlier.

7.3. Results According to the Calculations by Huse

We are interested in the results for the verification test (equation 7.6). Therefore, the measured energy dissipation per period will be compared with the model. The obtained values for DC_D should result in the same constant value for all performed tests.

The graphical method of Huse requires the calculation of the non-dimensional numbers of equation. Of all executed tests, the parameters are known. They have been mentioned in earlier paragraphs and in the logbook in Appendix A.

Only the mechanical tensile stiffness of the line EA still has to be determined. Therefore, a stress-strain test has been performed in the Laboratory of Steel Structures of the faculty Civil Engineering on the chain-line. The resulting tensile stiffness was: $EA = 4 . 10^6 N$.

The horizontal pretension is in all experiments in the order of 10N to 40 N. Thus, the value of π_3 is always larger than 10^5. The diagrams of Huse in figure 4.3 reach the asymptotic values for lower π_3-numbers than this. Therefore, π_3 does not play a role anymore.

The diagrams for the results of Huse were presented in paragraph 4.5-figure 4.4. These provided only for twelve test configurations a solution for I/H^4. The results of the other executed tests were not in the range of the presented diagrams. The results found were:

Line Configuration *[Pos & Amp]*	π_1 *[-]*	π_2 *[-]*	I/H^4 *[-]*	I *[m^4]*
2-A ; 0.06 m	0.043	0.396	0.01592	0.08841
2-A ; 0.08 m	0.057	0.396	0.02429	0.13489
2-A ; 0.10 m	0.071	0.396	0.03199	0.17765
3-A ; 0.06 m	0.043	0.338	0.00826	0.04587
3-A ; 0.08 m	0.057	0.338	0.01608	0.08930
3-A ; 0.10 m	0.071	0.338	0.02094	0.11629
4-A ; 0.06 m	0.043	0.286	0.00413	0.02294
4-A ; 0.08 m	0.057	0.286	0.00806	0.04476
4-A ; 0.10 m	0.071	0.286	0.01297	0.07203
5-A ; 0.06 m	0.043	0.239	0.00334	0.01855
5-A ; 0.08 m	0.057	0.239	0.00690	0.03832
5-A ; 0.10 m	0.071	0.239	0.00939	0.05215

Table 7.1. *Results of the Integral in eq.(7.5) according to Huse*

The next step is to evaluate equation (7.6) for these cases. The dissipated energy for each line configuration was obtained from the experiments. The results of DC_D can now be plotted as a function of the frequency, per line configuration.

The results, for the verification test (eq.7.6), of Huse obtained using the I-values from table 7.1 are presented in the following graph:

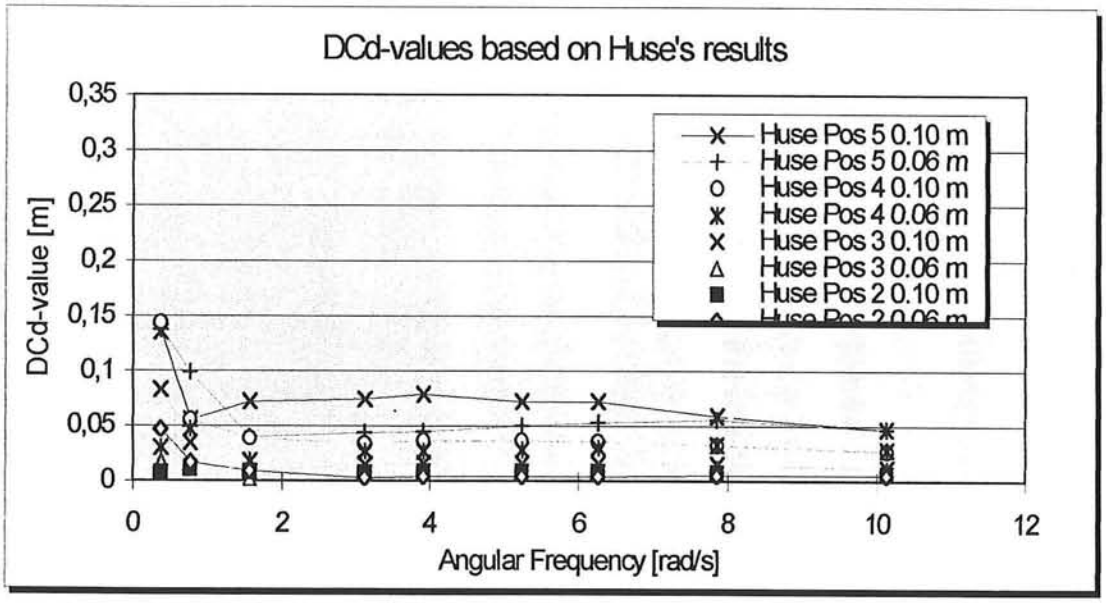

Figure 7.2. *DC_D -values according to Huse's Results.*

The results in the range of angular frequencies between 0 and 1 rad/s are not very reliable, as was stated and explained in chapter 6. This was due to inaccuracy of the dynamometers for very small tension fluctuations and due to the fact that the relative influence of inertia forces increases in the determination of the dissipated energy for the low frequencies ($\omega < 1$ rad/s) .

The remaining part of the frequency range ($\omega > 1$ rad/s) shows an approximately constant value for DC_D for each individual line configuration. This confirms the assumption that energy dissipation is proportional to the angular frequency squared. However the DC_D - values differ significantly between the different line configurations, although they should have been expected to be the same for all line configurations.

Thus, the results of Huse, as presented in this paragraph, are not confirmed in the present verification test. The calculation of the integral I is crucial. It may be that the results presented in the diagrams in figure 4.4 should be doubted.

7.4. Results of Calculations in Current Investigation

The method for the numerical evaluation of the integral I was described in paragraph 4.5. The computer program has calculated the value for the integral in all configurations of the experiment. The results were given in non-dimensional form in a graph (see figure 4.5). For comparison with the results of Huse, the results of the computer program for the twelve test cases are listed below.

Line Configuration *[Pos & Amp]*	I/H^4 *[-]*	I *[m^4]*
2-A ; 0.06 m	0.00227	0.00894
2-A ; 0.08 m	0.00541	0.02131
2-A ; 0.10 m	0.01067	0.04205
3-A ; 0.06 m	0.00323	0.01274
3-A ; 0.08 m	0.00772	0.03042
3-A ; 0.10 m	0.01527	0.06018
4-A ; 0.06 m	0.00465	0.01833
4-A ; 0.08 m	0.01112	0.04383
4-A ; 0.10 m	0.02206	0.08694
5-A ; 0.06 m	0.00688	0.02713
5-A ; 0.08 m	0.01650	0.06502
5-A ; 0.10 m	0.03285	0.12948

Table 7.2. *Results of program for Integral-values*

As for the results of Huse, these calculated values for the integral of equation (7.5) have to be evaluated by means of the verification test of equation (7.6). The results are presented for experiments with amplitude 0.06m and 0.10m, as a function of the angular frequency.

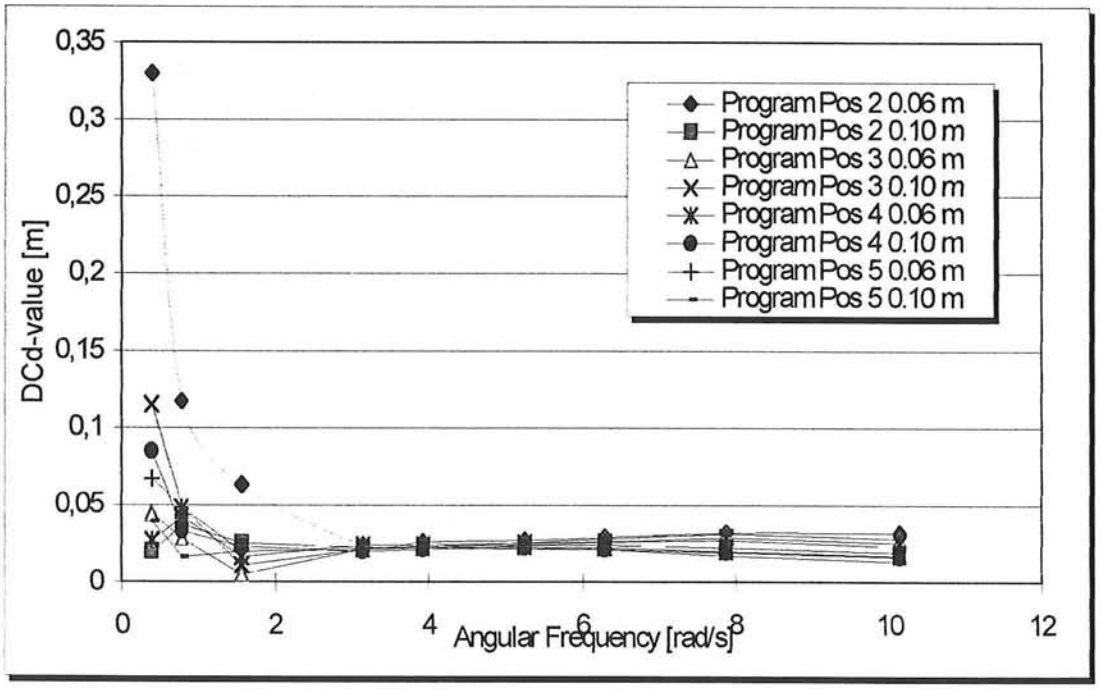

Figure 7.4. DC_D *-value results from computer program*

Since the results at the low frequencies (for $\omega < \approx 1$ rad/s) are subject to measuring errors, due to the limitations of the accuracy of the dynamometers, and the relative influence of inertia, especially for low pretensions, these are omitted from further discussion. Apart from these results, the calculated DC_D-values show a clear constant pattern for the remaining frequencies.

The calculated DC_D-values for the different line configurations, also give the same constant value for the DC_D-values. The frequency range between 2 rad/s and 6 rad/s describes the 'quasi-static' line behaviour.

At the higher frequencies, the 'galloping' motions of the lines are also governed by inertia influences. Even so, the results seem to hold in this region fairly well. Furthermore, the obtained *DCd* -values which were found are in excellent agreement with the *DCD* -values *(= 0.0201 m)* calculated in paragraph 7.2.1., even in the range were the line motion is <u>not</u> quasi-static anymore ($\omega > \approx 2\pi$).

7.5. Conclusion

The influence of the calculation method seems significant. As it was observed in paragraph 4.5., the results for the calculation of the integral in the equation for the calculation of energy dissipation per cycle appears important. The obtained results of the graphical method of Huse (1988) do not agree with the proposed verification test, while the computer-program delivers very good results.

The figure below gives the average DC_D-values as a function of the angular frequency, obtained by the developed computer program of the current investigation.

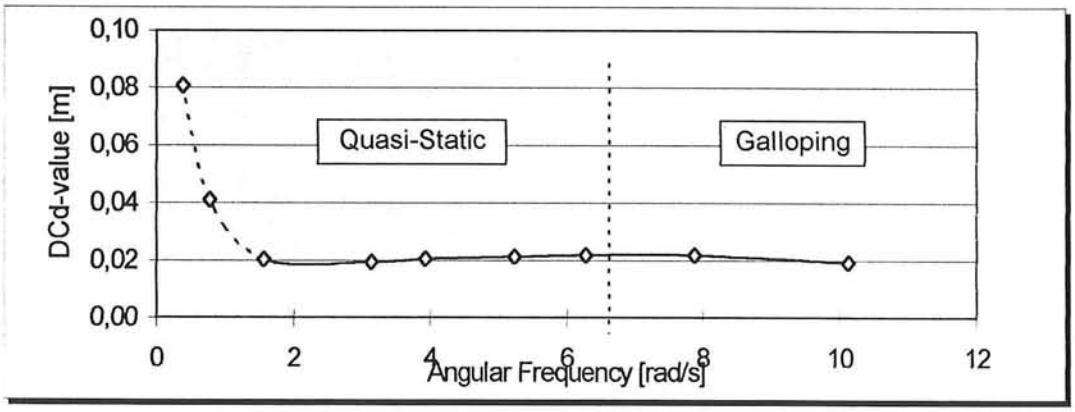

Figure 7.5. *Average DC_D -values from Developed Program Results*

The results in figure 7.5 show that Huse's model (1986), for the calculation energy dissipation per cycle, produces good results, even for the case of galloping motions of the line. The obtained average DC_D-values are in excellent agreement with the proposed equivalent diameter model (paragraph 7.2.1).

8. Conclusions and Recommendations

8.1. Conclusions

The conducted investigation has been focused on the verification of a model to calculate the energy dissipation, resulting from hydrodynamic forces on the mooring lines due to a forced low frequency (LF) sinusoidal surge-motion of the top end of a mooring line. This energy dissipation per cycle can be converted to a linear damping coefficient for the dynamic LF-model.

The following conclusions with respect to the investigated model can be drawn from this study :

- Huse's hydrodynamic model for the calculation of the energy dissipation (E_{diss}) during one surge cycle, due to drag forces normal to the mooring lines, describes the measured E_{diss} very well.

- An analytical expression for the calculation of the energy dissipation per cycle exists for those cases, in which bottom friction and line elongation due to material elasticity can be neglected. The presented model produces accurate results, provided the right value is taken for the product DC_D. The described equivalent diameter method (paragraph 7.1) seems to be well suited.

- The results of Huse's graphical calculation method for the calculation of the energy dissipation did not agree with the results obtained during this investigation.

- The influence of the determination of the peak to peak vertical motion of the line [Δ z(x)] is of great influence on the outcome of the model. This is considered the main reason why the results of Huse did not comply with the measured E_{diss} in the experiment.

- Drag amplification due to Vortex Induced Vibrations did not occur during the executed experiments with the chain line.

- The influence of waves on the energy dissipation, due to a LF-top end surge motion, was found to be negligible in all cases investigated.

- The relative influence of inertia on the calculated amount of dissipated energy increases with *decreasing* horizontal top end pretension and with *decreasing* frequency of the top end oscillation.

- The model assumes the configuration of the mooring line to be catenary at all times. However, the model also predicted the energy dissipation per cycle in the 'Galloping' zone very well.

- The presented hydrodynamic model is considered a useful element in the description of LF-dynamics of moored floating structures, when the WF-motions are very small compared to the LF-motions of the structure. Thus, the influence of

mooring line damping for moored structures in very low sea-states can be analysed with the model.

8.2. Recommendations for Future Investigations

The conducted literature survey and the insight gained during the performed investigation and have led to a number of unsolved items, which are assumed to lead to significant problems in actual prototype situations. It is considered interesting and relevant to investigate the following problems :

- *Investigation of V.I.V. for wire lines:* In cases of 'lock-in' situations, the V.I.V.-motions of the line are assumed to increase the drag resistance. Thus, with an increase of the apparent drag force on the lines, a higher energy dissipation may be expected. Therefore, the conducted experiments should be repeated for a smooth cable, in order to investigate the effects of VIV-motions on the energy dissipation.

- *Influence of LF-Heave motions in the Model:* Horizontal motions of the floating structure induce variations in the vertical mooring forces of the mooring system on the structure. In many cases, these vertical motions are negligible. In some cases, however, these fluctuations in the vertical mooring force, combined with vertical LF-excitation due to waves, can result in significant (resonant) heave motions. Thus, the top end motion of the mooring line can be significantly influenced by these heave motions. It is suggested to complete the current mathematical model for the energy dissipation per cycle by incorporating the LF-heave motions of the structure.

- *Effect of 'Out-Of-Plane' Surge Motions:* The total energy dissipation due to the mooring system is a result of the motions of all mooring lines. The proposed method is to decompose the top end motion of the fairlead in a 'in-plane' and 'out-of-plane' motion component for each line. The 'in-line' top end motion is included in the current model. The total energy dissipation of the mooring system is the sum of all separate contributions of the lines. The 'out-of-plane' top end motion, however, is excluded in the proposed model. In order to find a better description of the total contribution of the separate lines to the total energy dissipation, investigate the effect of motions out of plane of the mooring line.

- *Effect of WF-motions on the Mooring Line Damping*: Waves have little effect on the total energy dissipation per period, when the top end is subjected to a LF-sinusoidal top end surge motion. Waves have, however, a significant effect on the (WF) motions of the moored structure. Therefore, in waves, the top end of the mooring line will be subjected to both WF- as LF-motions. Investigate the effect of superimposed (small amplitude) WF-motions of the fairlead on the energy dissipation of the mooring line.

- *Effect of a Current on the Mooring Line Damping:* Incorporate the effect of a (constant) current in the hydrodynamic model. This is a purely mathematical problem.

Appendix A. The Logbook of Executed Experiments

Run no.	Date	Top end position	Remark	amplitude [mm]	Measured Period [s]	Recorded time [s]	Sample time [ms]	Measured frequency [rad/s]
1	3-08-95	none	No chain	0	0.000	10	20	
2	3-08-95	1	Air	0	0.000	20	20	
3	3-08-95	1	Air	60	1.000	10	20	
4	3-08-95	2	Air	60	1.000	10	20	
5	3-08-95	2	Air	60	2.000	20	40	
6	3-08-95	3	Air	60	1.000	10	20	
7	3-08-95	3	Air	60	2.000	20	40	
8	3-08-95	4	Air	60	1.000	10	20	
9	3-08-95	4	Air	60	2.000	20	40	
10	3-08-95	5	Air	60	1.000	10	20	6.283
11	3-08-95	5	Air	60	2.000	20	40	3.142
12	3-08-95	5	Air	60	1.250	16	32	5.027
13	3-08-95	5	Air	60	1.670	12	24	3.77
14	3-08-95	5	Air	60	1.430	14	28	4.398
15	3-08-95	1	Air	60	2.000	20	40	
16	4-08-95	1	Water	250	306.000	320	612	
17	4-08-95	1	Data -Filter errors					
18	4-08-95	1	Data -Filter errors					
19	4-08-95	1	Data -Filter errors					
20	7-08-95	1	Water	60	0.619	5	10	10.158
21	7-08-95	1	Water	60	0.998	10	20	6.297
22	7-08-95	1	Water	60	2.004	20	40	3.135
23	7-08-95	1	Water	60	3.991	40	80	1.574
24	7-08-95	1	Water	60	8.071	80	160	0.778
25	7-08-95	1	Water	60	16.400	80	160	0.383
26	7-08-95	1	Water	60	32.640	80	160	0.192
27	7-08-95	1	Water	60	0.798	8	16	7.871
28	7-08-95	1	Water	60	1.200	12	24	5.236
29	7-08-95	1	Water	60	1.607	16	32	3.91
30	7-08-95	2	Water	60	0.620	5	10	10.134
31	7-08-95	2	Water	60	0.800	8	16	7.854
32	7-08-95	2	Water	60	1.004	10	20	6.255
33	7-08-95	2	Water	60	1.200	12	24	5.236
34	7-08-95	2	Water	60	1.604	16	32	3.918
35	7-08-95	2	Water	60	2.013	20	40	3.121
36	7-08-95	2	Water	60	4.009	40	80	1.567
37	7-08-95	2	Water	60	8.142	80	160	0.772
38	7-08-95	2	Water	60	16.640	80	160	0.378
39	7-08-95	2	Water	60	33.920	80	160	0.185

Run no.	Date	Top end position	Remark	amplitude [mm]	Measured Period [s]	Recorded time [s]	Sample time [ms]	Measured frequency [rad/s]
40	7-08-95	3	Water	60	0.621	5	10	10.111
41	7-08-95	3	Water	60	0.802	8	16	7.837
42	7-08-95	3	Water	60	1.004	10	20	6.255
43	7-08-95	3	Water	60	1.203	12	24	5.224
44	7-08-95	3	Water	60	1.607	16	32	3.91
45	7-08-95	3	Water	60	2.013	20	40	3.121
46	7-08-95	3	Water	60	4.036	40	80	1.557
47	7-08-95	3	Water	60	7.892	80	160	0.787
48	7-08-95	3	Water	60	16.040	80	160	0.392
49	7-08-95	3	Water	60	32.080	80	160	0.196
50	8-08-95	4	Water	60	0.621	5	10	10.111
51	8-08-95	4	Water	60	0.800	8	16	7.854
52	8-08-95	4	Water	60	1.002	10	20	6.269
53	8-08-95	4	Water	60	1.200	12	24	5.236
54	8-08-95	4	Water	60	1.600	16	32	3.927
55	8-08-95	4	Water	60	2.000	20	40	3.142
56	8-08-95	4	Water	60	4.000	40	80	1.571
57	8-08-95	4	Water	60	8.000	80	160	0.785
58	8-08-95	4	Water	60	16.000	80	160	0.393
59	8-08-95	4	Water	60	32.080	80	160	0.196
60	8-08-95	5	Water	60	0.620	5	10	10.134
61	8-08-95	5	Water	60	0.800	8	16	7.854
62	8-08-95	5	Water	60	1.002	10	20	6.269
63	8-08-95	5	Water	60	1.200	12	24	5.236
64	8-08-95	5	Water	60	1.600	16	32	3.927
65	8-08-95	5	Water	60	2.000	20	40	3.142
66	8-08-95	5	Water	60	4.000	40	80	1.571
67	8-08-95	5	Water	60	8.000	80	160	0.785
68	8-08-95	5	Water	60	16.000	80	160	0.393
69	8-08-95	5	Water	60	31.920	80	160	0.197
70	10-08-95	5	Water	60	0.650	6,5	13	9.666
71	10-08-95	5	Water	60	0.700	7	14	8.976
72	10-08-95	5	Water	60	0.750	7,5	15	8.378
73	10-08-95	5	Water	60	0.850	8,5	17	7.392
74	10-08-95	5	Water	60	0.900	9	18	6.981
75	10-08-95	5	Water	60	0.950	9,5	19	6.614
76	10-08-95	5	Water	60	1.050	10,5	21	5.984
77	10-08-95	5	Water	60	1.100	11	22	5.712
78	10-08-95	5	Water	60	1.150	11,5	23	5.464
79	10-08-95	5	Water	60	1.400	14	28	4.488

Run no.	Date	Top end position	Remark	amplitude [mm]	Measured Period [s]	Recorded time [s]	Sample time [ms]	Measured frequency [rad/s]
80	10-08-95	5	Water	100	0.620	5	10	10.134
81	10-08-95	5	Water	100	0.800	8	16	7.854
82	10-08-95	5	Water	100	1.000	10	20	6.283
83	10-08-95	5	Water	100	1.200	12	24	5.236
84	10-08-95	5	Water	100	1.600	16	32	3.927
85	10-08-95	5	Water	100	2.000	20	40	3.142
86	10-08-95	5	Water	100	4.000	40	80	1.571
87	10-08-95	5	Water	100	8.000	80	160	0.785
88	10-08-95	5	Water	100	16.000	80	160	0.393
89	10-08-95	5	Water	100	32.080	80	160	0.196
90	10-08-95	4	Water	100	0.620	5	10	10.134
91	10-08-95	4	Water	100	0.800	8	16	7.854
92	10-08-95	4	Water	100	1.000	10	20	6.283
93	10-08-95	4	Water	100	1.200	12	24	5.236
94	10-08-95	4	Water	100	1.600	16	32	3.927
95	10-08-95	4	Water	100	2.000	20	40	3.142
96	10-08-95	4	Water	100	4.000	40	80	1.571
97	10-08-95	4	Water	100	8.000	80	160	0.785
98	10-08-95	4	Water	100	16.000	80	160	0.393
99	10-08-95	4	Water	100	31.920	80	160	0.197
100	10-08-95	3	Water	100	0.620	5	10	10.134
101	10-08-95	3	Water	100	0.800	8	16	7.854
102	10-08-95	3	Water	100	1.000	10	20	6.283
103	10-08-95	3	Water	100	1.200	12	24	5.236
104	10-08-95	3	Water	100	1.600	16	32	3.927
105	10-08-95	3	Water	100	2.000	20	40	3.142
106	10-08-95	3	Water	100	4.000	40	80	1.571
107	10-08-95	3	Water	100	8.000	80	160	0.785
108	10-08-95	3	Water	100	16.000	80	160	0.393
109	10-08-95	3	Water	100	31.920	80	160	0.197
110	11-08-95	2	Water	100	0.620	5	10	10.134
111	11-08-95	2	Water	100	0.800	8	16	7.854
112	11-08-95	2	Water	100	1.000	10	20	6.283
113	11-08-95	2	Water	100	1.200	12	24	5.236
114	11-08-95	2	Water	100	1.600	16	32	3.927
115	11-08-95	2	Water	100	2.000	20	40	3.142
116	11-08-95	2	Water	100	4.000	40	80	1.571
117	11-08-95	2	Water	100	8.000	80	160	0.785
118	11-08-95	2	Water	100	16.000	80	160	0.393
119	11-08-95	2	Water	100	32.000	80	160	0.196

Run no.	Date	Top end position	Remark	amplitude [mm]	Measured Period [s]	Recorded time [s]	Sample time [ms]	Measured frequency [rad/s]
120	11-08-95	1	Water	100	0.620	5	10	10.134
121	11-08-95	1	Water	100	0.800	8	16	7.854
122	11-08-95	1	Water	100	1.000	10	20	6.283
123	11-08-95	1	Water	100	1.200	12	24	5.236
124	11-08-95	1	Water	100	1.600	16	32	3.927
125	11-08-95	1	Water	100	2.000	20	40	3.142
126	11-08-95	1	Water	100	4.000	40	80	1.571
127	11-08-95	1	Water	100	8.000	80	160	0.785
128	11-08-95	1	Water	100	16.000	80	160	0.393
129	11-08-95	1	Water	100	32.000	80	160	0.196
130	14-08-95	5	Water	60	0.760	7.6	15.2	8.267
131	14-08-95	5	Water	60	0.770	7.7	15.4	8.160
132	14-08-95	5	Water	60	0.780	7.8	15.6	8.055
133	14-08-95	5	Water	60	0.790	7.9	15.8	7.953
134	14-08-95	5	Water	60	0.800	8.0	16.0	7.854
135	14-08-95	5	Water	60	0.810	8.1	16.2	7.757
136	14-08-95	5	Water	60	0.820	8.2	16.4	7.662
137	14-08-95	5	Water	60	0.830	8.3	16.6	7.570
138	14-08-95	5	Water	60	0.840	8.4	16.8	7.480
139	14-08-95	5	Water	60	0.850	8.5	17.0	7.392
140	14-08-95	5	Water	100	1.200	12.0	24	5.236
141	14-08-95	5	Water	100	1.250	12.5	25	5.027
142	14-08-95	5	Water	100	1.300	13.0	26	4.833
143	14-08-95	5	Water	100	1.350	13.5	27	4.654
144	14-08-95	5	Water	100	1.400	14.0	28	4.488
145	15-08-95	5	Water	100	1.450	14.5	29	4.333
146	15-08-95	5	Water	100	1.500	15.0	30	4.189
147	15-08-95	5	Water	100	1.550	15.5	31	4.054
148	15-08-95	5	Water	100	1.600	16.0	32	3.927
149	15-08-95	5	Water	100	1.650	16.5	33	3.808
150	15-08-95	5	Water	100	1.700	17.0	34	3.696
151	15-08-95	5	Water	100	1.750	17.5	35	3.590
152	15-08-95	5	Water	100	1.800	18.0	36	3.491
153	15-08-95	5	Water	100	1.850	18.5	37	3.396
154	15-08-95	5	Water	100	1.900	19.0	38	3.307
155	15-08-95	5	Water	100	1.950	19.5	39	3.222
156	15-08-95	5	Water	100	2.000	20.0	40	3.142
157	15-08-95	5	Water	100	2.050	20.5	41	3.065
158	15-08-95	5	Water	100	2.100	21.0	42	2.992
159	15-08-95	5	Water	100	2.150	21.5	43	2.922

Run no.	Date	Top end position	Remark	amplitude [mm]	Measured Period [s]	Recorded time [s]	Sample time [ms]	Measured frequency [rad/s]
160	17-08-95	1	Water	140	1.000	10	20	6.283
161	17-08-95	1	Water	140	1.100	11	22	5.712
162	17-08-95	1	Water	140	1.200	12	24	5.236
163	17-08-95	1	Water	140	1.400	14	28	4.488
164	17-08-95	1	Water	140	1.600	16	32	3.927
165	17-08-95	1	Water	140	1.800	18	36	3.491
166	17-08-95	1	Water	140	2.000	20	40	3.142
167	17-08-95	1	Water	140	4.000	40	80	1.571
168	17-08-95	1	Water	140	8.018	80	160	0.784
169	17-08-95	1	Water	140	16.040	80	160	0.392
170	17-08-95	2	Water	140	1.000	10	20	6.283
171	17-08-95	2	Water	140	1.100	11	22	5.712
172	17-08-95	2	Water	140	1.200	12	24	5.236
173	17-08-95	2	Water	140	1.400	14	28	4.488
174	17-08-95	2	Water	140	1.600	16	32	3.927
175	17-08-95	2	Water	140	1.800	18	36	3.491
176	17-08-95	2	Water	140	2.000	20	40	3.142
177	17-08-95	2	Water	140	4.000	40	80	1.571
178	17-08-95	2	Water	140	8.000	80	160	0.785
179	17-08-95	2	Water	140	16.000	80	160	0.393
180	18-08-95	3	Water	140	1.000	10	20	6.283
181	18-08-95	3	Water	140	1.100	11	22	5.712
182	18-08-95	3	Water	140	1.200	12	24	5.236
183	18-08-95	3	Water	140	1.400	14	28	4.488
184	18-08-95	3	Water	140	1.600	16	32	3.927
185	18-08-95	3	Water	140	1.800	18	36	3.491
186	18-08-95	3	Water	140	2.000	20	40	3.142
187	18-08-95	3	Water	140	4.000	40	80	1.571
188	18-08-95	3	Water	140	8.000	80	160	0.785
189	18-08-95	3	Water	140	16.000	80	160	0.393
190	18-08-95	4	Water	140	1.000	10	20	6.283
191	18-08-95	4	Water	140	1.100	11	22	5.712
192	18-08-95	4	Water	140	1.200	12	24	5.236
193	18-08-95	4	Water	140	1.400	14	28	4.488
194	18-08-95	4	Water	140	1.600	16	32	3.927
195	18-08-95	4	Water	140	1.800	18	36	3.491
196	18-08-95	4	Water	140	2.000	20	40	3.142
197	18-08-95	4	Water	140	4.000	40	80	1.571
198	18-08-95	4	Water	140	8.000	80	160	0.785
199	18-08-95	4	Water	140	16.000	80	160	0.393

Run no.	Date	Top end position	Remark	amplitude [mm]	Measured Period [s]	Recorded time [s]	Sample time [ms]	Measured frequency [rad/s]
200	18-08-95	5	Water	140	1.000	10	20	6.283
201	18-08-95	5	Water	140	1.100	11	22	5.712
202	18-08-95	5	Water	140	1.200	12	24	5.236
203	18-08-95	5	Water	140	1.400	14	28	4.488
204	18-08-95	5	Water	140	1.600	16	32	3.927
205	18-08-95	5	Water	140	1.800	18	36	3.491
206	18-08-95	5	Water	140	2.000	20	40	3.142
207	18-08-95	5	Water	140	4.000	40	80	1.571
208	18-08-95	5	Water	140	8.000	80	160	0.785
209	18-08-95	5	Water	140	16.000	80	160	0.393
210	21-08-95	5	Water	80	0.620	6	12	10.134
211	21-08-95	5	Water	80	0.800	8	16	7.854
212	21-08-95	5	Water	80	1.000	10	20	6.283
213	21-08-95	5	Water	80	1.200	12	24	5.236
214	21-08-95	5	Water	80	1.600	16	32	3.927
215	21-08-95	5	Water	80	2.000	20	40	3.142
216	21-08-95	5	Water	80	4.000	40	80	1.571
217	21-08-95	5	Water	80	8.000	80	160	0.785
218	21-08-95	5	Water	80	16.000	80	160	0.393
219	21-08-95	5	Water	80	32.000	80	160	0.196
220	21-08-95	5	Water	120	0.635	6	12	9.903
221	21-08-95	5	Water	120	0.800	8	16	7.854
222	21-08-95	5	Water	120	1.000	10	20	6.283
223	21-08-95	5	Water	120	1.200	12	24	5.236
224	21-08-95	5	Water	120	1.600	16	32	3.927
225	21-08-95	5	Water	120	2.000	20	40	3.142
226	21-08-95	5	Water	120	4.000	40	80	1.571
227	21-08-95	5	Water	120	8.000	80	160	0.785
228	21-08-95	5	Water	120	16.000	80	160	0.393
229	21-08-95	5	Water	120	32.000	64	128	0.196

Run no.	Date	Position	Remark	Amplitude [mm]	Measured Period-TE [s]	Measured frequency Te [rad/s]	WAVE period [s]	WAVE height [mm]
300	28-08-95	1	WAVE	100	0.000	0	1	50
301	28-08-95	1	WAVE	100	2.000	3.142	1	50
302	28-08-95	1	WAVE	100	4.000	1.571	1	50
303	28-08-95	1	WAVE	100	8.000	0.785	1	50
304	28-08-95	1	WAVE	100	16.000	0.393	1	50
305	28-08-95	2	WAVE	100	0.000	0	1	50
306	28-08-95	2	WAVE	100	2.000	3.142	1	50
307	28-08-95	2	WAVE	100	4.000	1.571	1	50
308	28-08-95	2	WAVE	100	8.000	0.785	1	50
309	28-08-95	2	WAVE	100	16.000	0.393	1	50
310	28-08-95	3	WAVE	100	0.000	0	1	50
311	28-08-95	3	WAVE	100	2.000	3.142	1	50
312	28-08-95	3	WAVE	100	4.000	1.571	1	50
313	28-08-95	3	WAVE	100	8.000	0.785	1	50
314	28-08-95	3	WAVE	100	16.000	0.393	1	50
315	28-08-95	4	WAVE	100	0.000	0	1	50
316	28-08-95	4	WAVE	100	2.000	3.142	1	50
317	28-08-95	4	WAVE	100	4.000	1.571	1	50
318	28-08-95	4	WAVE	100	8.000	0.785	1	50
319	28-08-95	4	WAVE	100	16.000	0.393	1	50
320	28-08-95	5	WAVE	100	0.000	0	1	50
321	28-08-95	5	WAVE	100	2.000	3.142	1	50
322	28-08-95	5	WAVE	100	4.000	1.571	1	50
323	28-08-95	5	WAVE	100	8.000	0.785	1	50
324	28-08-95	5	WAVE	100	16.000	0.393	1	50
325	29-08-95	5	WAVE	100	0.000	0	1	100
326	29-08-95	5	WAVE	100	2.000	3.142	1	100
327	29-08-95	5	WAVE	100	4.000	1.571	1	100
328	29-08-95	5	WAVE	100	8.000	0.785	1	100
329	29-08-95	5	WAVE	100	15.960	0.394	1	100
330	29-08-95	3	WAVE	100	0.000	0	1	100
331	29-08-95	3	WAVE	100	2.000	3.142	1	100
332	29-08-95	3	WAVE	100	4.000	1.571	1	100
333	29-08-95	3	WAVE	100	8.000	0.785	1	100
334	29-08-95	3	WAVE	100	15.960	0.394	1	100
335	29-08-95	1	WAVE	100	0.000	0	1	100
336	29-08-95	1	WAVE	100	2.000	3.142	1	100
337	29-08-95	1	WAVE	100	4.000	1.571	1	100
338	29-08-95	1	WAVE	100	8.000	0.785	1	100
339	29-08-95	1	WAVE	100	16.000	0.393	1	100

Appendix B. Experiment Results

B.1. Results for all configurations at amplitude 0.06 m

- Position 1: Runs 020-029;
- Position 2: Runs 030-039;
- Position 3: Runs 040-049;
- Position 4: Runs 050-059;
- Position 5: Runs 060-069; 070-079; 130-139;

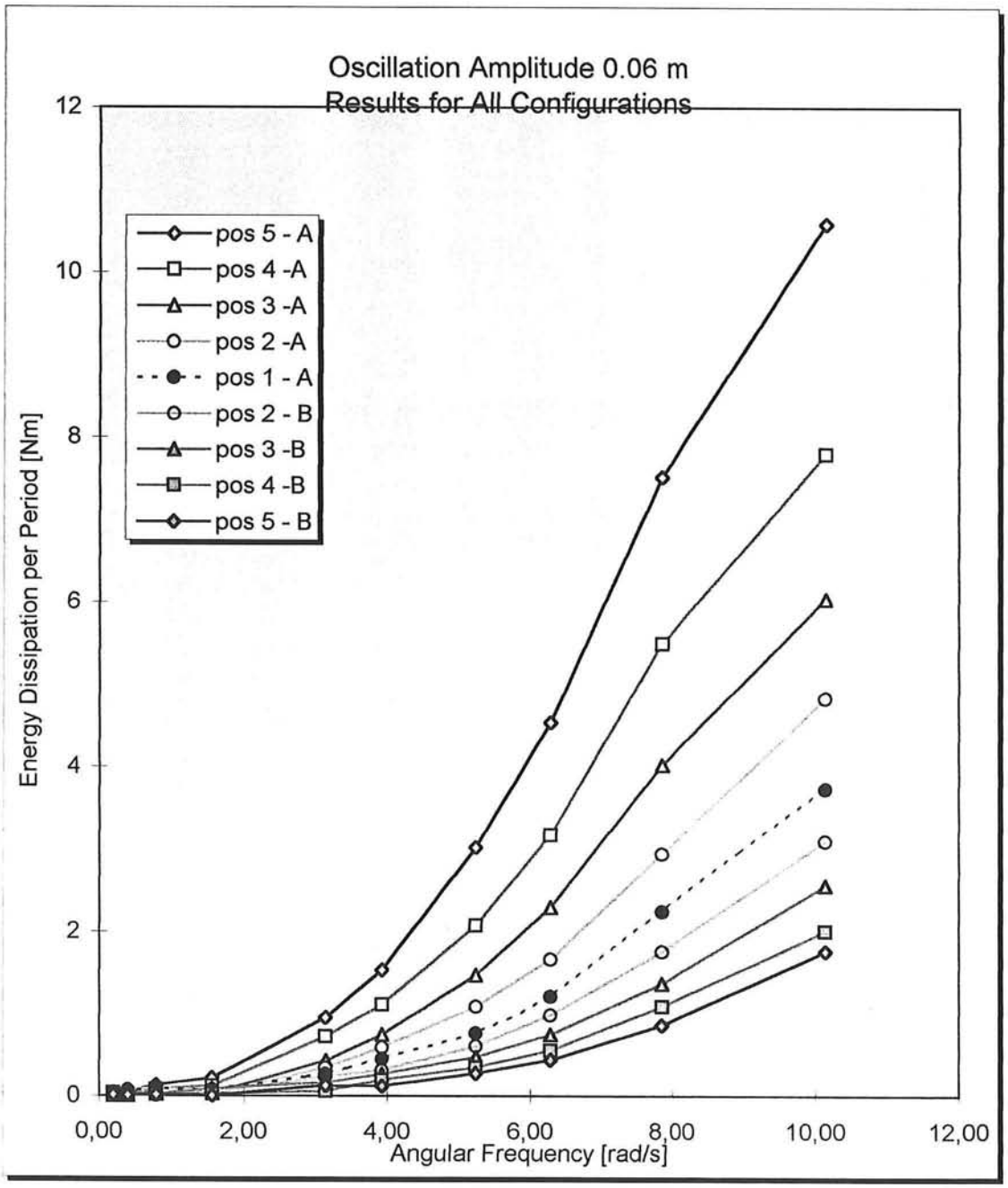

B.2. Results for all configurations at amplitude 0.10 m

- Position 1: Runs 120-129
- Position 2: Runs 110-119
- Position 3: Runs 100-109
- Position 4: Runs 090-099
- Position 5: Runs 080-089; 140-149; 150-159

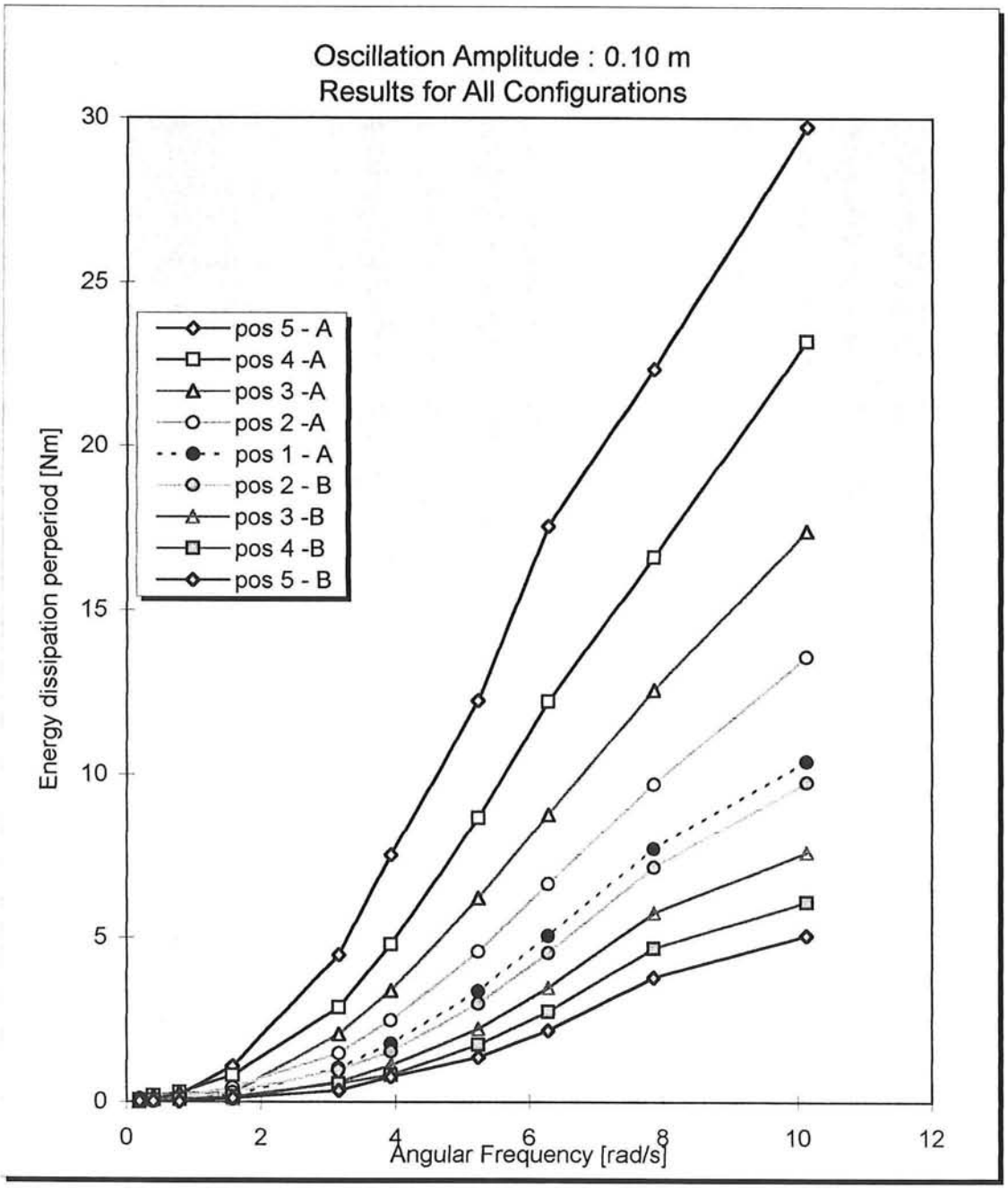

B.3. Results for all configurations at amplitude 0.14 m

- Position 1: Runs 160-169;
- Position 2: Runs 170-179;
- Position 3: Runs 180-189;
- Position 4: Runs 190-199; *{Possible errors occured due to deformed pin.}*
- Position 5: Runs 200-209; *{Possible errors occured due to deformed pin.}*

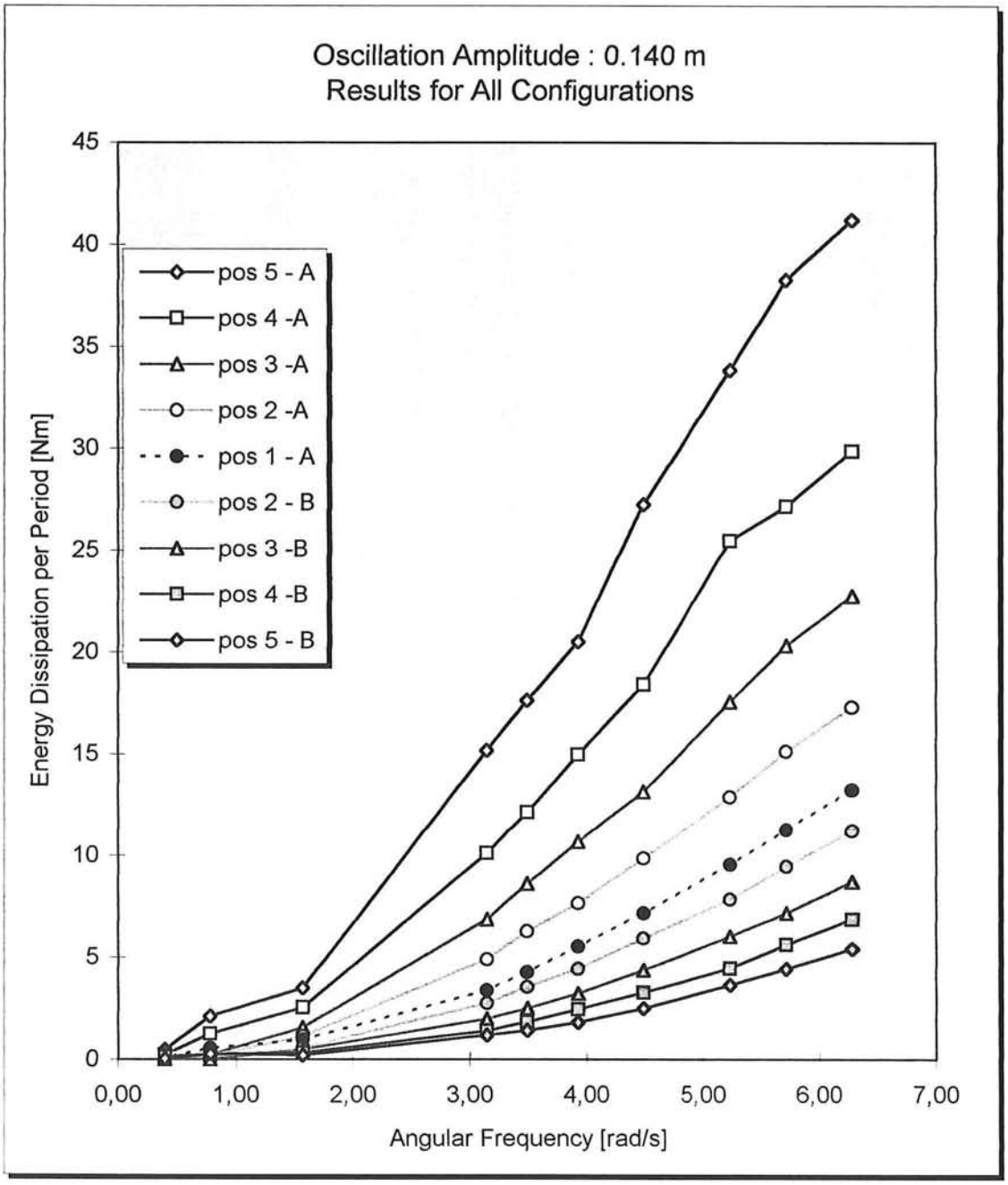

B.4. Results for Position 5 at all tested amplitudes

- Amplitude 0.06 m: Runs 060-069; 070-079;
- Amplitude 0.08 m: Runs 220-229;
- Amplitude 0.10 m: Runs 080-089; 140-149; 150-159;
- Amplitude 0.12 m: Runs 210-219;
- Amplitude 0.14 m: Runs 200-209; *{ Possible errors due to deformed pin.}*

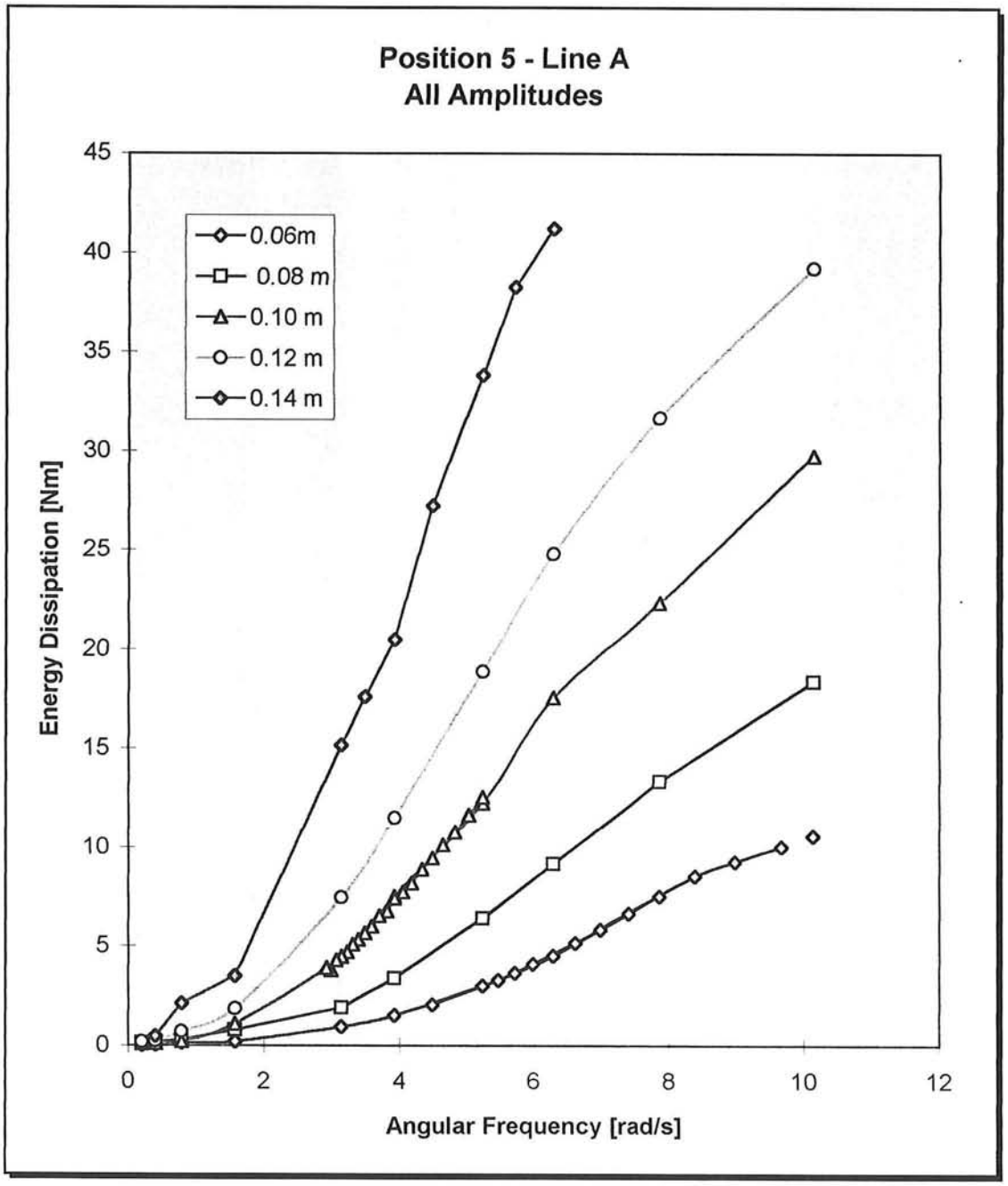

Appendix C. Computer Program

C.1. Turbo-Pascal Source Code

```
{This program calculates the integral in
the Energy dissipation calculation}

program integral(input,output);

uses WinCRT;

var  x,y,z,c,xo,h,i1,i2,i3,itot,idim                :real;
     a,b,ab,fa,fb,fab,dza,dzb,dzab                  :real;
     xuo,xlo,xmo,cu,cm,cl,amp,xmax,zmax             :real;
     i,pos,l,teller                                 :integer;
     d,k                                            :char;
     datafile,results                               :text;

function coshyp(e:real):real;
  begin
    coshyp:= 1/2*(exp(e)+exp(-e));
  end;

function sinhyp(e:real):real;
  begin
    sinhyp:= 1/2*(exp(e)-exp(-e));
  end;

function zx(c,xo,x:real): real;
  begin
    if x < xo then
      begin
        zx:=0;
      end
    else
      begin
        zx:= c*(coshyp((x-xo)/c)-1);
      end;
  end;

function cosphi(cm,xmo,x:real): real;
  begin
    if x < xmo then
      begin
         cosphi:=1;
      end
    else
      begin
         cosphi:=1/(1+sqr(sinhyp((x-xmo)/cm)));
      end;
  end;
{inputsection}
begin
clrscr;
teller :=1;
gotoxy(10,10);
writeln('  input : file (f) or manual (m)?');
gotoxy(45,10);
```

```
d := readkey;
clrscr;
gotoxy(1,2);
clrscr;
gotoxy(5,10);
writeln('Processing data, please wait.....');
assign (datafile,'c:\tpw\integral.dat');
reset (datafile);
assign (results,'c:\tpw\results.doc');
rewrite (results);
for teller :=1 to 50 do
begin
if d = 'm' then
  begin
    gotoxy(1,9);
    writeln(' pos  = ');
    writeln(' line = ');
    writeln(' amp  = ');
    writeln(' xuo  = ');
    writeln(' cu   = ');
    writeln(' xlo  = ');
    writeln(' cl   = ');
    writeln(' xmo  = ');
    writeln(' cm   = ');
    writeln(' xmax = ');
    writeln(' zmax = ');
    gotoxy(10,6 );readln(pos) ;
    gotoxy(10,7 );readln(l  ) ;
    gotoxy(10,8 );readln(amp) ;
    gotoxy(10,9 );readln(xuo) ;
    gotoxy(10,10);readln(cu ) ;
    gotoxy(10,11);readln(xlo) ;
    gotoxy(10,12);readln(cl ) ;
    gotoxy(10,13);readln(xmo) ;
    gotoxy(10,14);readln(cm ) ;
    gotoxy(10,15);readln(xmax);
    gotoxy(10,16);readln(zmax);
  end;
if d = 'f'then
  begin
    read(datafile,pos);
    read(datafile,l);
    read(datafile,amp);
    read(datafile,xuo);
    read(datafile,cu);
    read(datafile,xlo);
    read(datafile,cl);
    read(datafile,xmo);
    read(datafile,cm);
    read(datafile,xmax);
    readln(datafile,zmax);
  end;

        {program-part between xuo & xlo;
        lift-off points in highest and lowest pretension;
        delta z equals the z coordinate of the line in highest pretension}

  x:=xuo;
  h:=(xlo-xuo)/100;
```

```
  i1:=0;
  for i:= 1 to 100 do
     begin
        a  := x;
        b  := x+h;
        ab := (a+b)/2;
        dza := zx(cu,xuo,a );
        dzab:= zx(cu,xuo,ab);
        dzb := zx(cu,xuo,b );
        fa  := cosphi(cm,xmo,a )*sqr(dza )*dza;
        fab := cosphi(cm,xmo,ab)*sqr(dzab)*dzb;
        fb  := cosphi(cm,xmo,b )*sqr(dzb )*dzb;
        i1 :=i1+1/6*(b-a)*(fa+4*fab+fb);
        x  :=b;
     end;

        {programme-part between xlo & xmax-amp; lift-off point in lowest pretension;
        Delta z equals the z coordinate of the line in highest pretension
        minus the z coordinate of the line in lowest pretension }

  x:=xlo;
  h:=(xmax-amp-xlo)/300;
  i2:=0;
  for i:=1 to 300 do
     begin
        a  := x;
        b  := x+h;
        ab  := (a+b)/2;
        dza := abs(zx(cu,xuo,a )-zx(cl,xlo,a ));
        dzab:= abs(zx(cu,xuo,ab)-zx(cl,xlo,ab));
        dzb := abs(zx(cu,xuo,b )-zx(cl,xlo,b ));
        fa  := cosphi(cm,xmo,a )*sqr(dza )*dza;
        fab := cosphi(cm,xmo,ab)*sqr(dzab)*dzb;
        fb  := cosphi(cm,xmo,b )*sqr(dzb )*dzb;
        i2  :=i2+1/6*(b-a)*(fa+4*fab+fb);
        x   :=b;

     end;
{programme-part between xmax-amp & xmax;
Top end region between Xmax + amp & - amp;
delta z equals the z coordinate of the fairlead
minus the z coordinate of the line in highest pretension }

  x:=xmax-amp;
  h:=(amp)/10;
  i3:=0;
  for i:=1 to 10 do
     begin
        a  := x;
        b  := x+h;
        ab  := (a+b)/2;
        dza := abs(zx(cu,xuo,a )-zmax);
        dzab:= abs(zx(cu,xuo,ab)-zmax);
        dzb := abs(zx(cu,xuo,b )-zmax);
        fa  := cosphi(cm,xmo,a )*sqr(dza )*dza;
        fab := cosphi(cm,xmo,ab)*sqr(dzab)*dzb;
        fb  := cosphi(cm,xmo,b )*sqr(dzb )*dzb;
        i3  :=i3+1/6*(b-a)*(fa+4*fab+fb);
        x   :=b;
```

```
      end;
  itot := i1+i2+i3;
  idim:=itot/(sqr(zmax)*sqr(zmax));
  if teller=1 then
    begin
    Writeln(results,' ');
    Writeln(results,' ');
    Writeln(results,' ');
    writeln(results,'    ====================================================');
    writeln(results,'      Pos  Line  Amp (m)  I (Huse m^4)     I/H^4 (-)');
    writeln(results,'    ====================================================');
    end;
  gotoxy(1,4+teller);
  if teller=26 then
    begin
    writeln(results,' ');
    writeln(results,'    ====================================================');
    writeln(results,'      Pos  Line  Amp (m)  I (Huse m^4)     I/H^4 (-)');
    writeln(results,'    ====================================================');
    end;
  if I = 1 then
    begin
        k := 'A';
    end;
  if I = 2 then
    begin
        k := 'B';
    end;
    write(results,pos:9);write(results,k:5);write(results,'    ');write(results,amp:4:3);write(results,'    ');
    write(results,itot:4:10);write(results,'      ');writeln(results,idim:4:10);
  end;
  if d = 'm' then
    begin
      teller := 50
    end;
  if d = 'f' then
    begin
      teller:=teller +1;
   end;
clrscr;
gotoxy(10,10);
writeln('Finished processing.');gotoxy(10,12);
writeln('Close this window.');gotoxy(10,13);
writeln('You can find the results in the output-text-file:');
end.
```

{Pos	Ampl	xuo	cu	xlo	cl	xmo	cm	xmax	zmax }
1	A	0.060	3.219569209	4.367060314	4.100009439	2.279866662	3.725273935	3.100975799	6.579547488	1.409
1	A	0.080	3.009940154	4.945101694	4.203949875	2.069771221	3.725273935	3.100975799	6.579547488	1.409
1	A	0.100	2.773377872	5.634866435	4.299415879	1.883560537	3.725273935	3.100975799	6.579547488	1.409
1	A	0.120	2.504506067	6.467063414	4.387346090	1.717771275	3.725273935	3.100975799	6.579547488	1.409
1	A	0.140	2.196414663	7.483729982	4.468545040	1.569546918	3.725273935	3.100975799	6.579547488	1.409
2	A	0.060	2.953463399	5.106166594	3.956443550	2.582666737	3.533862603	3.558845796	6.604551788	1.409
2	A	0.080	2.709373023	5.828317550	4.072551297	2.336648300	3.533862603	3.558845796	6.604551788	1.409
2	A	0.100	2.431407197	6.702185663	4.178777381	2.119948923	3.533862603	3.558845796	6.604551788	1.409
2	A	0.120	2.112189165	7.773390262	4.276269938	1.928113716	3.533862603	3.558845796	6.604551788	1.409
2	A	0.140	1.742031776	9.106085466	4.366005443	1.757504019	3.533862603	3.558845796	6.604551788	1.409
3	A	0.060	2.609727346	6.135277848	3.778255477	2.978834908	3.292277107	4.173856655	6.632032207	1.409
3	A	0.080	2.317302873	7.076781896	3.910209011	2.683295726	3.292277107	4.173856655	6.632032207	1.409
3	A	0.100	1.980317169	8.237024387	4.030349169	2.424962760	3.292277107	4.173856655	6.632032207	1.409
3	A	0.120	1.587990108	9.689343531	4.140126441	2.197869331	3.292277107	4.173856655	6.632032207	1.409
3	A	0.140	1.125758343	11.540608250	4.240762756	1.997199847	3.292277107	4.173856655	6.632032207	1.409
4	A	0.060	2.209027755	7.440785682	3.580233695	3.445536047	3.018428161	4.921090599	6.658782087	1.409
4	A	0.080	1.854729546	8.690037986	3.730760174	3.088235642	3.018428161	4.921090599	6.658782087	1.409
4	A	0.100	1.440671273	10.262900960	3.867076132	2.778541860	3.018428161	4.921090599	6.658782087	1.409
4	A	0.120	0.950646688	12.281545240	3.991028196	2.508385492	3.018428161	4.921090599	6.658782087	1.409
4	A	0.140	0.362006073	14.931753860	4.104155885	2.271338587	3.018428161	4.921090599	6.658782087	1.409
5	A	0.060	1.712146992	9.217923504	3.348101581	4.028062833	2.689953755	5.887586100	6.686038631	1.409
5	A	0.080	1.272681001	10.935735240	3.521684255	3.588857140	2.689953755	5.887586100	6.686038631	1.409
5	A	0.100	0.749923108	13.157622480	3.677895735	3.211886355	2.689953755	5.887586100	6.686038631	1.409
5	A	0.120	0.118110038	16.101890860	3.819135808	2.885953161	2.689953755	5.887586100	6.686038631	1.409
5	A	0.140	-0.660369537	20.119226560	3.947381232	2.602271236	2.689953755	5.887586100	6.686038631	1.409

{Input data for all positions and amplitudes of Line A}

{Pos	Ampl	xuo	cu	xlo	cl	xmo	cm	xmax	zmax }
1	B	0.060	3.250993542	4.303359481	4.122490799	2.246739032	3.751504539	3.056092150	6.578994752	1.404
1	B	0.080	3.043568000	4.872556329	4.225403718	2.039589932	3.751504539	3.056092150	6.578994752	1.404
1	B	0.100	2.809529993	5.551575100	4.319929826	1.855968710	3.751504539	3.056092150	6.578994752	1.404
1	B	0.120	2.543577054	6.370544684	4.406997062	1.692467321	3.751504539	3.056092150	6.578994752	1.404
1	B	0.140	2.238896977	7.370685896	4.487400915	1.546274274	3.751504539	3.056092150	6.578994752	1.404
2	B	0.060	3.498179482	3.665075121	4.260577958	1.970518919	3.932915780	2.648073224	6.551746574	1.404
2	B	0.080	3.320439030	4.119641358	4.352301195	1.794548776	3.932915780	2.648073224	6.551746574	1.404
2	B	0.100	3.121575054	4.654901731	4.436867847	1.637617676	3.932915780	2.648073224	6.551746574	1.404
2	B	0.120	2.897728746	5.291101653	4.515031293	1.497098816	3.932915780	2.648073224	6.551746574	1.404
2	B	0.140	2.644039675	6.055261522	4.587442331	1.370804311	3.932915780	2.648073224	6.551746574	1.404
3	B	0.060	3.710639205	3.151238761	4.383031938	1.736932278	4.091654869	2.310276140	6.524662570	1.404
3	B	0.080	3.556672133	3.520402706	4.465250104	1.586090112	4.091654869	2.310276140	6.524662570	1.404
3	B	0.100	3.385636433	3.950287747	4.541306362	1.450839888	4.091654869	2.310276140	6.524662570	1.404
3	B	0.120	3.194652297	4.454934167	4.611819400	1.329127699	4.091654869	2.310276140	6.524662570	1.404
3	B	0.140	2.980152742	5.052690875	4.677327340	1.219228022	4.091654869	2.310276140	6.524662570	1.404
4	B	0.060	3.939120243	2.634533079	4.518774383	1.490478833	4.265335548	1.961244182	6.490748994	1.404
4	B	0.080	3.808946750	2.924360700	4.590913940	1.364843178	4.265335548	1.961244182	6.490748994	1.404
4	B	0.100	3.665440959	3.257858974	4.657892357	1.251514320	4.265335548	1.961244182	6.490748994	1.404
4	B	0.120	3.506550129	3.644222223	4.720199333	1.148958362	4.265335548	1.961244182	6.490748994	1.404
4	B	0.140	3.329776634	4.095200697	4.778264094	1.055874087	4.265335548	1.961244182	6.490748994	1.404
5	B	0.060	4.049985696	2.397210966	4.586205155	1.372930753	4.350739584	1.797494570	6.472101190	1.404
5	B	0.080	3.930703248	2.652908316	4.653516343	1.258821066	4.350739584	1.797494570	6.472101190	1.404
5	B	0.100	3.799685522	2.945440441	4.716125000	1.155580134	4.350739584	1.797494570	6.472101190	1.404
5	B	0.120	3.655208668	3.282198381	4.774464136	1.061892408	4.350739584	1.797494570	6.472101190	1.404
5	B	0.140	3.495193161	3.672526702	4.828914754	0.976636448	4.350739584	1.797494570	6.472101190	1.404
0										

{Input data for all positions and amplitudes of Line B}

C.3. Output File

Pos	Line	Amp (m)	I (Huse m^4)	I/H^4 (-)
1	A	0.060	0.0065685983	0.0016665898
1	A	0.080	0.0156379119	0.0039676631
1	A	0.100	0.0308057093	0.0078160484
1	A	0.120	0.0539830084	0.0136966107
1	A	0.140	0.0875120979	0.0222036372
2	A	0.060	0.0089392809	0.0022680813
2	A	0.080	0.0213086066	0.0054064362
2	A	0.100	0.0420537001	0.0106698973
2	A	0.120	0.0738852251	0.0187462165
2	A	0.140	0.1202030519	0.0304980114
3	A	0.060	0.0127428699	0.0032331308
3	A	0.080	0.0304202555	0.0077182508
3	A	0.100	0.0601760577	0.0152679159
3	A	0.120	0.1060900383	0.0269172466
3	A	0.140	0.1734402169	0.0440053861
4	A	0.060	0.0183270954	0.0046499648
4	A	0.080	0.0438257235	0.0111194965
4	A	0.100	0.0869397367	0.0220584173
4	A	0.120	0.1539375757	0.0390571609
4	A	0.140	0.2532400512	0.0642522618
5	A	0.060	0.0271295269	0.0068833246
5	A	0.080	0.0650195302	0.0164968055
5	A	0.100	0.1294762883	0.0328508241
5	A	0.120	0.2306214902	0.0585134630
5	A	0.140	0.3827318949	0.0971070326

Pos	Line	Amp (m)	I (Huse m^4)	I/H^4 (-)
1	B	0.060	0.0063855999	0.0016433621
1	B	0.080	0.0152015931	0.0039121966
1	B	0.100	0.0299450993	0.0077065026
1	B	0.120	0.0524733129	0.0135042371
1	B	0.140	0.0850625678	0.0218912246
2	B	0.060	0.0046281073	0.0011910637
2	B	0.080	0.0110018372	0.0028313710
2	B	0.100	0.0216309927	0.0055668308
2	B	0.120	0.0378089998	0.0097303118
2	B	0.140	0.0610885367	0.0157214027
3	B	0.060	0.0034063489	0.0008766388
3	B	0.080	0.0080842533	0.0020805180
3	B	0.100	0.0158636310	0.0040825750
3	B	0.120	0.0276617381	0.0071188695
3	B	0.140	0.0445606803	0.0114678864
4	B	0.060	0.0023637113	0.0006083115
4	B	0.080	0.0055952257	0.0014399559
4	B	0.100	0.0109485792	0.0028176648
4	B	0.120	0.0190308140	0.0048976634
4	B	0.140	0.0305449496	0.0078608767
5	B	0.060	0.0019507849	0.0005020430
5	B	0.080	0.0046094142	0.0011862530
5	B	0.100	0.0090029088	0.0023169380

Literature

- ***References in this report***

1. **Chakrabarti, S.K.** : *"Hydrodynamics of Offshore Structures"* , Computational Mechanics Publications, Boston & Springer-Verlag Berlin 1987.
2. **Chakrabarti, S.K.** : *"Offshore Structure Modeling"* , Advanced Series on Ocean Engineering - volume 9. World Scientific Publishing Co.,Ltd., 1994.
3. **Ghosh, S. ,Gehring,D.H. & Sember,W.J.** : *"Modern Mooring System in the View of Classification Societies."* , Presented at SNAME Texas Section Annual Meeting februari 1992.
4. **Huse, E** : *" Influence of Mooring Line Damping upon Rig Motions"* , Paper no.5204, Offshore Technology Conference, Houston 1986.
5. **Huse, E** : *" Practical Estimation of Mooring Line Damping"* , Paper no.5676, Offshore Technology Conference, Houston 1988.
6. **Polderdijk, S.H.** : *"Response of Anchor Lines to Excitation at the top."* , Paper in BOSS 1985.
7. **Tiantalfyllou, M.S. ,Yue , D.K.P. & Tein, D.Y.S.** : *"Damping of Floating Structures"* , Paper no. 7489, Offshore Technology Conference 1994.
8. **Wichers, J.E.W. & van Sluijs, M.F.** : *"The influence of waves on the low frequency hydrodynamic coefficients of moored vessels".* Paper no. 3625, Offshore Technology Conference, Houston 1979.

- ***Consulted Literature***

1. **American Petroleum Institute** : *"Recommended Practice for the analysis of spread mooring systems for floating drilling units : RP-2P".*
2. **van den Boom, H.J.J. & van Walree, F.**:*" Hydrodynamic aspects of flexibel risers".* Paper No. 6438, Offshore Technology Conference, Houston 1990.
3. **Huse, E. & Matsumoto, K.** *:" Mooring line damping due to first- and second order vessel motion".* Paper No. 6137, Offshore Technology Conference, Houston 1989.
4. **Huse, E.** *:"New devellopments in prediction of mooring system damping".* Paper No. 6593, Offshore Technology Conference, Houston 1991.
5. **Journee, J.M.J.** : *"Hydromechanische aspecten van drijvende offshore constructies",* rapport nr. 633-K / herdruk.
6. **Larsen, C.M. & Fylling,I.J.** : *"Dynamic behaviour of anchor lines".* Proceedings BOSS conference , Boston 1982.
7. **Larsen, C.M.** : *"Flexible riser analysis - Comparisson of results from computer programs".* Division of marine structures, The Norwegian Institute of Technology, Trondheim, Norway.
8. **O'Brien, P.J. & McNamara, J.F.** *:"Significant characteristics of three dimensional flexibel riser analysis".* Eng. struct. 1989, volume 11, October.
9. **Tein, D.Y.S.** *:"Mooring system low-freqeuncy damping forces: discussion notes".* Proceedings of the workshop on 'Marine Riser Mechanics', Michigan 1992.